

AD-A102 994

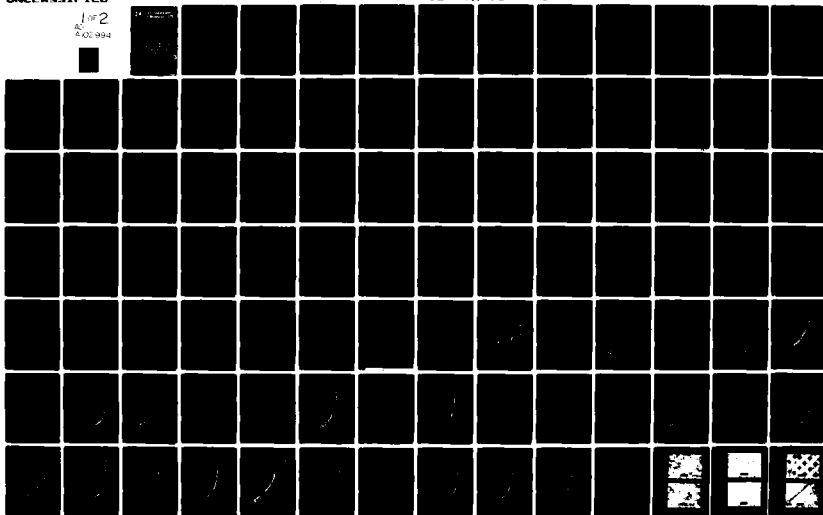
MANCHESTER UNIV/UNIV OF MANCHESTER INST OF SCIENCE AN--ETC F/8 11/4
MEASUREMENT OF THE THERMAL DIFFUSIVITY OF CARBON/CARBON FIBRE C--ETC(U)
JAN 81 R TAYLOR, R N PROCTER AFOSR-77-3449

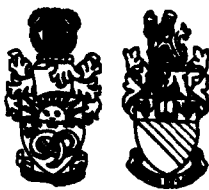
UNCLASSIFIED

AFOSR-TR-81-0638

NL

1 of 2
AL
8 02 994





Joint Department of Metallurgy

LEVEL 11

AD A102994

University of Manchester
University of Manchester
Institute of Science and
Technology

Approved for public release;
distribution unlimited.

DTIC
ELECTE
AUG 14 1981
S D C

81 8 14 0 25

Joint University & UMIST Metallurgy Building
Grosvenor Street Manchester M1 7HS
Telephone 061-236 3311

REF FILE 6024

Unclassified

REPORT DOCUMENTATION PAGE		READ INSTRUCTIONS BEFORE COMPLETING FORM
1. Report Number <i>AFOSR-TR-81-0638</i>	2. Govt Accession No. <i>AD-A102995</i>	3. Recipient's Catalog Number
4. Title (and Subtitle) MEASUREMENT OF THERMAL DIFFUSIVITY OF CARBON FIBRE CARBON COMPOSITES FROM 300-3000K		5. Type of Report & Period Covered FINAL SCIENTIFIC REPORT 1/10/77 - 30/9/80
		6. Performing Org. Report Number
7. Author(s) R. TAYLOR and R.N. PROCTER		8. Contract or Grant Number AFOSR-77-3449.
9. Performing Organization Name and Address DEPARTMENT OF METALLURGY UNIVERSITY OF MANCHESTER/UMIST MANCHESTER ENGLAND.		10. Program Element, Project, Task Area & Work Unit Numbers P.E. 61102F Project Task: 2308B1
11. Controlling Office Name and Address AFOSR BUILDING 410 BOLLING AFB. WASHINGTON D.C. 20332		12. Report Date <i>JAN 81</i>
		13. Number of Pages <i>111</i>
14. Monitoring Agency Name and Address		15. <i>Unclassified</i>
16. & 17. Distribution Statement Approved for public release; distribution unlimited.		
18. Supplementary Notes		
19. Key Words THERMAL DIFFUSIVITY, THERMAL CONDUCTIVITY, CARBON FIBRE, CARBON COMPOSITES, LASER PULSE METHOD, HIGH TEMPERATURES.		
20. <input checked="" type="checkbox"/> Abstract Thermal diffusivity measurements have been made using the heat pulse method on three 3-D carbon fibre carbon composites, three 1-D carbon fibre carbon composites from fibres "F" and "A" and matrix graphite. Thermal conductivity has been calculated from these results and a model outlined which predicts the thermal conductivity of a 3-D composite from the processed conductivities of the constituents.		

Unclassified

GRANT NUMBER / AFOSR-77-3449/

Measurement of the thermal diffusivity of carbon/carbon fibre composites from 300-3000K.

D. R. / Taylor ~~and~~ R.N. / Procter.
Department of Metallurgy
University of Manchester/UMIST
Grosvenor Street,
Manchester
England

January 1981

Final Scientific report, 1st October 1977-30th September 1980,

Approved for public release - distribution unlimited.

Prepared for

A.F.O.S.R.
Building 410
Bolling A.F.B.
Washington D.C. 20332

E.O.A.R.D.
London
England.

A.F.M.L.
Wright-Patterson A.F.B.
Dayton.
Ohio 45433.

Accession For	
NTIS GRA&I	<input checked="checked" type="checkbox"/>
DTIC TAB	<input type="checkbox"/>
Unannounced	<input type="checkbox"/>
Justification	
By_	
Distribution/	
Availability Codes	
Avail and/or	
Dist	Special

A

REC-106 4 1981

AIR FORCE OFFICE OF SCIENTIFIC RESEARCH (AFSC)
NOTICE OF TRANSMITTAL TO DTIC
This technical report has been reviewed and is
approved for public release IAW AFR 190-12.
Distribution is unlimited.
MATTHEW J. KESTER
Chief, Technical Information Division

Tables

1. Materials specification.
2. Specimen data
3. Least squares fit conductivity functions
4. Unit cell constants
5. Calculated conductivity C.F.C.C. "A" X axis upper bound
6. " " " "A" X axis lower bound
7. " " " "A" Z axis upper bound
8. " " " "A" Z axis lower bound
9. " " " "B" X axis upper bound
10. " " " "B" X axis lower bound
11. " " " "B" Z axis upper bound
12. " " " "B" Z axis lower bound
13. " " " "C" X axis upper bound
14. " " " "C" X axis lower bound
15. " " " "C" Z axis upper bound
16. " " " "C" Z axis lower bound

Figures

1. Unit cell of C.F.C.C. "A" and "C"
2. Unit cell of C.F.C.C. "B".
3. Schematic of equipment
4. C.F.C.C. "A" X axis thermal diffusivity
5. C.F.C.C. "A" X axis thermal conductivity
6. C.F.C.C. "A" X axis % deviation of thermal conductivity from least squares function.
7. C.F.C.C. "A" Z axis thermal diffusivity
8. C.F.C.C. "A" Z axis thermal conductivity
9. C.F.C.C. "A" Z axis % deviation of thermal conductivity from least squares function.
10. C.F.C.C. "B" X axis thermal diffusivity
11. C.F.C.C. "B" X axis thermal conductivity
12. C.F.C.C. "B" X axis % deviation of thermal conductivity from least squares function
13. C.F.C.C. "B" Z axis thermal diffusivity
14. C.F.C.C. "B" Z axis thermal conductivity
15. C.F.C.C. "B" Z axis % deviation of thermal conductivity from least squares function
16. C.F.C.C. "C" X axis thermal diffusivity
17. C.F.C.C. "C" X axis thermal conductivity
18. C.F.C.C. "C" X axis % deviation of thermal conductivity from least squares function
19. C.F.C.C. "C" Z axis thermal diffusivity
20. C.F.C.C. "C" Z axis thermal conductivity
21. C.F.C.C. "C" Z axis % deviation of thermal conductivity from least squares function
22. Matrix material thermal diffusivity
23. Matrix material thermal conductivity
24. Fibre "F" 1-D composite thermal diffusivity parallel to fibre axis
25. Fibre "F" 1-D composite thermal conductivity parallel to fibre axis
26. Fibre "F" 1-D composite thermal diffusivity perpendicular to fibre axis
27. Fibre "F" 1-D composite thermal conductivity perpendicular to fibre axis

- 28 Fibre "AP 1-D composite without CVD. Thermal diffusivity parallel to fibre axis
- 29 Fibre "A" 1-D composite without CVD. Thermal conductivity parallel to fibre axis
- 30 Fibre "A" 1-D composite without CVD. Thermal diffusivity perpendicular to fibre axis
- 31 Fibre "A" 1-D composite without CVD. Thermal conductivity perpendicular to fibre axis
- 32 Fibre "A" 1-D composite with CVD - graphitised to 2300°C. Thermal diffusivity parallel to fibre axis
- 33 Fibre "A" 1-D composite with CVD - graphitised to 2300°C. Thermal diffusivity perpendicular to fibre axis
- 34 S.E.M. view of 1-D C.F.C.C. fibre "F" parallel to axis x 3,200
- 35 S.E.M. view of 1-D C.F.C.C. fibre "F" parallel to axis x 3,200 after heating.
- 36 S.E.M. view of 1-D C.F.C.C. fibre "F" to 2900K parallel to axis x 10,200
- 37 S.E.M. view of 1-D C.F.C.C. fibre "F" parallel to axis x 10,200
- 38 S.E.M. view of C.F.C.C. "A" X axis x 33 Virgin sample
- 39 S.E.M. view of C.F.C.C. "A" X axis x 330 Virgin sample
- 40 S.E.M. view of C.F.C.C. "A" X axis x 3200 Virgin sample
- 41 S.E.M. view of C.F.C.C. "A" X axis x 10,200 Virgin sample
- 42 S.E.M. view of C.F.C.C. "A" Z axis x 33 after heating to 2900K
- 43 S.E.M. view of C.F.C.C. "A" Z axis x 320 after heating to 2900K
- 44 S.E.M. view of C.F.C.C. "A" Z axis x 3300 after heating to 2900K
- 45 S.E.M. view of C.F.C.C. "B" X axis x 28
- 46 S.E.M. view of C.F.C.C. "B" X axis x 102
- 47 S.E.M. view of C.F.C.C. "B" Z axis x 30
- 48 S.E.M. view of 1-D composite fibre "A" (CVD'd) x 3,000
- 49 S.E.M. view of 1-D composite fibre "A" (CVD'd) x 10,000
- 50 S.E.M. view of 1-D composite fibre "A" (CVD'd) x 2,000
- 51 S.E.M. view of 1-D composite fibre "A" (CVD'd) x 5,000
- 52 S.E.M. view of 1-D composite fibre "A" (CVD'd) x 10,000
- 53 S.E.M. view of 1-D composite fibre "A" (no CVD) x 2,000
- 54 S.E.M. view of 1-D composite fibre "A" (no CVD) x 5,000

55. S.E.M. view of 1-D composite fibre "A" (no CVD) x 10,000
56. S.E.M. view of 1-D composite fibre "A" (no CVD) x 20,000
57. S.E.M. view of 1-D composite fibre "A" (no CVD) x 1,000
58. S.E.M. view of C.F.C.C. "C" Z axis x 50
59. S.E.M. view of C.F.C.C. "C" X axis x 50
60. S.E.M. view of C.F.C.C. "C" X axis x 3,000
61. S.E.M. view of C.F.C.C. "C" Z axis x 2,000
62. S.E.M. view of C.F.C.C. "C" Z axis x 5,000
63. S.E.M. view of C.F.C.C. "C" X axis x 200
64. S.E.M. view of C.F.C.C. "C" Z axis x 500
65. Schematic model of composite "A". (After AFML-TR-77-46)
66. Thermal conductivity of 1-D C.F.C.C. transverse axis thermal conductivity as a function of constituent conductivity and F.V.F.
67. Conduction channels in 3-D C.F.C.C. unit cell.

1. Introduction

The thermal transport properties of three dimensional carbon-fibre composites (C.F.C.C.) have been measured over the temperature range 300-3000K.

The thermal diffusivity (α) has been measured over this temperature range using the laser pulse technique.^(1,2) Data thus obtained has been converted to thermal conductivity (λ) using the standard expression

$$\lambda = \alpha \rho C_p$$

where ρ is density and C_p is specific heat.

The structure of these materials is such that it is necessary to make measurements along two axes in order to characterise the properties.

Although the experimental data is, in its own right extremely valuable, an additional aim of this investigation has been an attempt to model the C.F.C.C. thermal conductivity in terms of the properties of the constituents. Three different 3-D composites were supplied by the A.F.M.L., Wright-Patterson A.F.B. These were

- a) Material A 3-D orthogonal C.F.C.C. using Fibre "F" material.
- b) Material B 3-D C.F.C.C. using Fibre "F" material using on 8-harness satin weave.
- c) Material C- 3-D orthogonal C.F.C. using Fibre "A" High Modulus(H.M.) fibre material.

Samples of matrix material and 1-dimensional composites to assist modelling were also obtained and measured over the same temperature range.

Although the finished 3-D C.F.C.C. consists only of a porous body containing carbon fibre yarns and graphitised matrix material there are many variables within processing so an accurate description of the finished composite may be much more complex. A fairly simple modelling approach has been adapted since accurately quantifiable information on constituent properties, from 1-D composites and matrix material is not available.

Data for composites, A and B (fibre F) has been detailed in the progress report for the period ending 30/9/79. Consequently this report will concern itself primarily with data for material "C" and comparable 1-D composites and an evaluation of comparisons with data for materials "A" and "B".

2. Characterisation of Materials

Materials "A" and "C" are 3-D orthogonal C.F.C.C. in which the carbon fibres are formed into yarns. In the case of composite "A" this is known as a 2-2-3 composite comprising two yarns of 1440 filament yarns in the X and Y direction and three yarns of 1440 filaments forming the reinforcement in the Z direction. A unit cell of this material is shown in figure 1. Composite "C" is similar but in this case is a 2-2-1 composite. The X and Y reinforcement is composed of two yarns of 1000 filaments/site whereas the Z axis reinforcement is composed of one 3000 filament yarn. Material B is also a 3-D composite, but in this case the yarns are not orthogonal. The X and Y yarns are woven into an 8-harness satin weave to form a reinforcement plane which is pierced by the Z-yarns. This type of construction is shown in figure 2.

The manufacture of a typical composite begins with the construction of a fibre preform. The second stage is to coat the preform with pyrolytic carbon. This infiltration of the preform is done using low pressure, isothermal deposition of vapour phase carbon (C.V.D) prior to densification of the preform by pitch impregnation, and high pressure pyrolysis. The C.V.D. stage is instituted to stiffen the preform and prevent deformation during high pressure pyrolysis. This impregnation process may be typically repeated 5 times. The composite is finally graphitised at 3023K (2750°C). The objective of this processing is to impregnate the fibre bundles and fill crossover pockets and voids with graphitic matrix material.

The following additional specimens were provided by the A.F.M.L. Wright Patterson A.F.B.

- 1) Samples of Fibre "A" and Fibre "F" material used in the composites.
- 2) A sample comprised only of graphitised matrix material.
- 3) A 1-D composite made using fibre "F" material that had not been subject to the C.V.D. process prior to densification and graphitisation.

- 4) A 1-D composite made using Fibre "A" material that had been C.V.D.'d and graphitised to 2573K (2300°C).
- 5) A 1-D composite made using Fibre "A" that had been graphitised to 2973K (2700°C) but not C.V.D.'d.

The basic properties of all materials measured are listed in Table 1.

Table 1. Materials Specification

	Composite A	Composite B	Composite C	Matrix Graphite	1 dimensional composites		
					(a)	(b)	(c)
Fibre type	F	F	A	-	F	A(no CVD)	A(CVD)
Graphitisation temperature ($^{\circ}\text{C}$)	2750	2750	2750	2750	2750	2750	2300
Bulk density gcm^{-3}	1.883	1.917	1.885	1.36	1.915	1.663	1.627
Open Porosity %	6.1	5.95	4.8	-	-	-	-
Fibre volume fraction X & Y axis	0.13	-	0.13	N/A	N/A	N/A	N/A
Fibre volume fraction Z axis	0.22	0.132	0.22	N/A	0.52	0.50	0.50
Thread counts yarns/in X & Y axis	N/A	30	N/A	N/A	N/A	N/A	N/A
Filaments/end X & Y axis	N/A	1400	N/A	N/A	N/A	N/A	N/A
Fibre cross section	Crenulated	Crenulated	Round	N/A	Cren- ulated	Round	Round
Fibre bulk density	1.66	1.66	1.8- 1.88	N/A	1.66	1.8- 1.88	1.8- 1.88
Fibre diameter μm	6.50	6.50	7.0	N/A	6.50	7.0	7.0
Filaments/yarn	1440	1440	1000(X&Y) 3000 (Z)	N/A	1440	1000	1000

3. Measurement Technique

The U.M.I.S.T. apparatus (figure 3) has recently been described in detail⁽³⁾ so will only be briefly described here. The front face of a disc shaped sample is heated instantaneously ($\sim 10^{-3}$ s) using a 100J ruby laser. The specimen is heated to the measurement temperature inside a graphite susceptor heated using an induction coil. The subsequent temperature transient on the rear face of the sample is recorded using an infra-red sensor. Thermal diffusivity is calculated from

$$\alpha = \frac{w}{\pi^2} \frac{L^2}{t_{\frac{1}{2}}} \quad (1)$$

where L is the sample length.

$t_{\frac{1}{2}}$ is the time taken to attain half the maximum temperature rise
 $\frac{w}{\pi^2}$ is a constant, which in the absence of heat losses = 0.139.

The amplified signal is digitally logged by a microcomputer which samples data at 0.001s intervals.

Heat losses are inevitable at high temperatures and necessitate that $\frac{w}{\pi^2}$ decreases. This has been analysed by Cowan⁽⁴⁾. To minimise this correction and avoid overly large corrections for finite pulse time affects⁽⁵⁾ it is desirable to select a sample length such that $0.025s < t_{\frac{1}{2}} < 0.2s$. Suitable programming enables $t_{\frac{1}{2}}$ to be computed to precision better than $10^{-4}s$ (including correction for finite pulse time where necessary). The ratio of transient amplitudes $\Delta T(10t_{\frac{1}{2}}) / \Delta T(t_{\frac{1}{2}})$ or $\Delta T(5t_{\frac{1}{2}}) / \Delta T(t_{\frac{1}{2}})$ is then determined and $\frac{w}{\pi^2}$ calculated using the analysis outlined by Cowan. Finally the sample length is corrected for thermal expansion and the diffusivity computed from these three parameters.

4. Sample Description

Specimens 6.35mm diameter and of length chosen to fit the experimental requirements listed in the preceding section were cored from each material billet provided. Samples were cored from the Z and X directions of the 3-D C.F.C.C. materials since they are symmetrical in the X and Y directions. Specimens perpendicular and transverse were machined from the 1-D composites. For the matrix graphite the isotropy of the material was verified using samples cored from two orthogonal directions. Sample data is presented in Table 2.

Density measurements were obtained using a liquid densitometer and reveal only minor variations between samples. Bulk densities are in general 2-3% lower which indicates a small amount of open porosity.

Table 2. Specimen Details

Composite Type	Orientation	Sample No	Length cm	Density gmcm ⁻³
3D CFCC "A"	X axis	1	0.242	1.926
"		2	0.242	1.920
"	Z axis	1	0.399	1.916
"		2	0.398	1.887
"		3	0.298	1.919
"		4	0.301	1.925
3D CFCC "B"	X axis	1	0.439	1.950
Fibre "F"		2	0.439	1.942
	Z axis	1	0.338	1.936
		2	0.336	1.931
		3	0.338	1.928
1-D CFCC	Parallel to	1	0.454	1.910
Fibre "F"	fibre axis	2	0.458	1.905
(2750°C)	Transverse to	1	0.1995	1.900
	fibre axis	2	0.152	1.897
		3	0.1992	1.910
Matrix	-	1	0.297	1.369
		2	0.3005	1.389
3-D CFCC "C"	X axis	1	0.3068	1.890
		2	0.257	1.876
		3	0.3105	1.886
	Z axis	1	0.3668	1.880
		2	0.3601	1.888
1-D C FCC	Parallel to fibre	1	0.4039	1.622
Fibre "A"	axis	2	0.353	1.626
CVD (2300°C)	Transverse to	1	0.2065	1.629
	fibre axis	2	0.2135	1.624
1-D C FCC	Parallel to	1	0.4086	1.665
Fibre "A"	fibre axis	2	0.3561	1.668
No CVD	Transverse to	1	0.2128	1.701
(2750°C)	fibre axis	2	0.2012	1.665

5. Experimental Procedure

Diffusivity measurements were carried out on all the materials listed in section 2 (except for the Fibre "A" 1-D composite graphitised to 2573K) over the temperature range 300-3000K. It is necessary to make these measurements in four distinct stages as follows.

- a) 350-750K. Transients were recorded using a $\text{Hg}_x\text{Cd}_{1-x}\text{Te}$ detector (cut off wavelength 5.5 μm) and a synchronous (detector) lock-in amplifier. This was an experimental system replacing the earlier InSb detector (used for fibre "F" composites) and was only useable down to approximately 350K at acceptable noise levels.
 - b) 500-1500K. Transients were detected using PbS detector (cut off wavelength 3.0 μm) and the measurement temperature recorded using a Type K thermocouple.
 - c) 1200-2300K. As b) above but temperatures recorded using an optical pyrometer.
 - d) 2000-3000K. A vacuum ($< 10^{-4}$ Torr) was sufficient to protect the samples over the preceding temperature ranges. Above 2300K the vapour pressure of graphite increases so it is necessary to suppress evaporation. This was done by completing measurements in an atmosphere of helium at 20 p.s.i. pressure.
- The above temperature ranges all overlap. This is to confirm that these changes in measurement technique did not yield different diffusivity values.

For modelling purposes it is necessary to convert the measured thermal diffusivity to thermal conductivity. This requires accurate data for specific heat and thermal expansion. The specific heat data used was supplied by A.F.M.L. (6) synthesised from measurements from 350-1000K on POCO graphite (7) and a C.F.C.C. composite "A" (8) from 1500-3000K. This data is fitted to a 5th order polynomial using a least squares function (figure 3).

$$\begin{aligned} C_p = & -5.444 \times 10^{-1} + 5.5076 \times 10^{-3} T - 4.9454 \times 10^{-6} T^2 \\ & + 2.3389 \times 10^{-9} T^3 + 5.5749 \times 10^{-13} T^4 - 5.3241 \times 10^{-17} T^5 \end{aligned} \quad (3)$$

Thermal expansion data supplied by A.F.M.L.⁽⁶⁾ has been used to correct for density changes with temperature.

Specimens for microstructural investigation were prepared by grinding and polishing down to 1/4 μm . These were then etched for 1-5 minutes in a hot solution of potassium dichromate in phosphoric acid. In order to improve resolution in the electron microscope, the etched specimens were then lightly sputtered with gold.

6. Results

At least two specimens were measured for each type of specimen. Conductivity values derived from the diffusivity data were fitted with least squares functions. A number of different functions were tried and the best fit over the whole temperature range was usually a fourth order polynomial. Although data for each specimen type is presented briefly in section 6(A) - 6(G) the coefficients and root mean square errors for the best fit functions are listed in Table 3.

(A) 3-D Composite 'A'

(i) X Axis

The diffusivity of two X axis samples was measured over the complete temperature range. The results are shown in Figure 4. They provide an excellent agreement with AFML flash diffusivity data, ⁽⁶⁾ also shown, which was obtained from a CFCC similar to 'A'.

Figure 5 shows the X axis conductivity together with directly measured data obtained from different billets of 'A' type material by the comparative rod method ⁽⁶⁾. The direct method conductivity is higher at low temperatures, and this may simply be a product of inter-billet variations. However Lee and Taylor ⁽⁹⁾ and Minges ⁽¹⁰⁾ have observed similar discrepancies between direct and diffusivity-derived conductivity.

There is no systematic difference in the properties of the two samples and this is shown more clearly in Figure 6 which is a plot of % deviation from the least squares function.

(ii) Z Axis

Figure 7 shows the diffusivity of four samples, again compared with diffusivity data from a material similar to composite 'A' ⁽⁶⁾. As in the previous case, the agreement of the diffusivity data is good.

Figure 8 shows the resultant conductivity values with comparative rod data for comparison ⁽⁶⁾. As before, the latter data is higher. Billet variations or, as Lee and Taylor ⁽⁹⁾ imply, differences in measurement

Table 3 Least Square Fit Conductivity Functions.

Composite Type and Axis	Best fit polynomial Coefficients						% RMS Error
	Polynomial Order	T ⁰	T ¹	T ²	T ³	T ⁴	
CFCC 'A' X axis	4	0.67531	-5.21149x10 ⁻⁵	-2.1528x10 ⁻⁷	1.2428x10 ⁻¹⁰	-1.921x10 ⁻¹⁴	3.6
CFCC 'A' Z axis	3	1.0463	-3.9355x10 ⁻⁴	6.4192x10 ⁻⁸	2.2071x10 ⁻¹²	-	3.3
CFCC 'B' X axis	4	1.7611	-1.4727x10 ⁻³	7.6701x10 ⁻⁷	-1.8815x10 ⁻¹⁰	1.7153x10 ⁻¹⁴	4.3
CFCC 'B' Z axis	4	0.66092	2.0294x10 ⁻⁵	-3.5184x10 ⁻⁷	2.0619x10 ⁻¹⁰	-3.3782x10 ⁻¹⁴	4.2
CFCC 'C' X axis	4	0.65557	-2.1677x10 ⁻⁵	-2.4127x10 ⁻⁷	1.3431x10 ⁻¹⁰	-2.0871x10 ⁻¹⁴	5.7
CFCC 'C' Z axis	4	0.9093	7.6494x10 ⁻⁵	-4.0977x10 ⁻⁷	1.9416x10 ⁻¹⁰	-2.6723x10 ⁻¹⁴	2.7
1-D CFCC Fibre "f" Parallel to fibre axis	4	4.1192	-2.9682x10 ⁻³	1.1770x10 ⁻⁶	-2.1011x10 ⁻¹⁰	1.0583x10 ⁻¹⁴	3.8
1-D CFCC Fibre "f" Transverse to fibre axis	4	0.27302	6.6837x10 ⁻⁵	-2.1870x10 ⁻⁷	1.1960x10 ⁻¹⁰	-2.0259x10 ⁻¹⁴	3.7
1-D CFCC Fibre "A" CVD (2300°C) Parallel to fibre axis	4	0.346	1.325x10 ⁻³	-1.39x10 ⁻⁶	5.42x10 ⁻¹⁰	-7.4x10 ⁻¹⁴	2.9
1-D CFCC Fibre "A" CVD (2300°C) Transverse to fibre axis	4	0.04685	3.478x10 ⁻⁴	-3.96x10 ⁻⁷	1.69x10 ⁻¹⁰	-2.443x10 ⁻¹⁴	2.0
1-D CFCC Fibre "A" No CVD(2700°C) Parallel to fibre axis	4	2.368	-7.214x10 ⁻⁴	-1.075x10 ⁻⁷	1.186x10 ⁻¹⁰	-2.051x10 ⁻¹⁴	4.0
1-D CFCC Fibre "A" No CVD(2700°C) Transverse to fibre axis	4	0.2018	3.232x10 ⁻⁵	-1.587x10 ⁻⁷	8.808x10 ⁻¹¹	-1.394x10 ⁻¹⁴	4.0
Bulk Matrix	4	0.9020	-1.2206x10 ⁻⁴	-3.9952x10 ⁻⁷	2.4646x10 ⁻¹⁰	-4.1589x10 ⁻¹⁴	4.6

method may be responsible. In this case, however, it seems appropriate to question the validity of the low temperature specific heat data. Over a temperature range of 350-1000K this relies entirely on the specific heat of POCO graphite, whereas there is evidence that the specific heat of fibre 'F' alone is 30% higher at 300K⁽⁹⁾. The law of mixtures would suggest that the composite value should lie between these two limits.

Figure 9 shows the data deviation plot for the least squares function given in Table 3. A systematic relationship between deviation and sample can be seen which may be partly, but not completely, explained by differences in sample density (see Table 2).

(B) 3-D Composite 'B'

(i) X Axis

Diffusivity data and derived conductivity values of two X axis samples are shown in Figures 10 and 11 respectively. No comparative diffusivity data is available. However, comparative rod conductivity data⁽⁶⁾, from a different billet, shows excellent agreement.

Figure 12 shows the deviation from the least squares fit.

(ii) Z Axis

Diffusivity and conductivity results from three samples are shown in Figures 13 and 14 respectively. Comparative rod data⁽⁶⁾, again from a different billet, is higher by a factor of 20-25% over most of the temperature range.

Figure 15 shows that deviation from the least squares fit is broadly sample dependent. Differences in sample densities are insignificant.

(C) 3-D Composite 'C'

(i) X-Axis

Diffusivity data and derived conductivity values for three X-axis samples are shown in figures 16 and 17. No comparative data is available. There was some indication of difference, between sample 1 and samples 2 and 3. This data is very similar to that obtained for composite 'A'.

17.

Figure 18 shows the deviation from the least squares fit given in Table 3.

(ii) Z Axis

Diffusivity data and derived conductivity values for two Z-axis samples are shown in figures 19 and 20 respectively. There is no detectable sample difference and again similarity to the data obtained for composite 'A'.

Figure 21 shows the deviation from the least squares fit given in Table 3.

(D) Matrix Material

Diffusivity and conductivity results from two bulk matrix samples are shown in Figures 22 and 23 respectively.

The samples were cut orthogonally to determine the degree of anisotropy, if any. The data indicate an essentially isotropic material.

The high porosity of the bulk matrix (~40%) contrasts with the high density of the composites and, by inference, with the low porosity of the matrix material within the composite. Evidence suggests in general that the density of carbon composite phases in situ is higher than when processed individually⁽¹¹⁾. However, the matrix 'crossover' pockets (see Figure 1) are known to have porosity values of between 10-50%⁽⁶⁾.

The matrix conductivity is very similar to that of POCO graphite type AXM-5Q1, as well documented reference material⁽¹⁰⁾. With an average density of 1.75 grms/cm³, the POCO porosity is considerably lower, however. Whilst radiative and gaseous conduction modes may become important in high porosity, low conductivity materials⁽¹²⁾ no enhancement of the matrix thermal properties was observed in a helium atmosphere both at low and high temperatures. Similarly, such expressions as are available to quantify radiative conduction in porous materials suggest that this too would be insignificant in the present case.

(E) Fibre "F" 1-D Composite. No CVD -2700°C Graphitisation

(i) Axis Parallel with Fibres

Diffusivity and conductivity results from two parallel (//) axis

samples are shown in Figures 24 and 25. No comparative data is available.

The 1-D composite was unique in that its properties change significantly after heating to temperatures $> 2300\text{K}$. Spot measurements, at temperatures of $600\text{--}700\text{K}$, were made after the principal measurements had been completed. These revealed that the diffusivity of both samples was reduced to 50% or less of its original value. In addition there was a permanent change in sample length and diameter of $+1\text{--}1.5\%$ respectively.

Since there are no orthogonal yarn influences, it is expected that the 1-D composite thermal expansion be higher than that of the 3-D materials⁽⁶⁾. However, no permanent offsets have been reported before. Significantly, it is now known that the processing of the 1-D material differs from that of the other composites⁽⁶⁾ reported here.

Typically, the high temperature ($2000\text{--}3000\text{K}$) measurement runs lasted 2-3 hours. Oxygen contamination has been ruled out since other sample types were not effected.

Subsequent liquid densitometer measurements showed a density increase of about 1%. Compared with the nominal decrease in bulk density, this indicates a decrease in closed porosity and microstructural changes.

The high conductivity of the 1-D parallel axis is another surprising feature. The room temperature value of approximately 3.0 W/cmK must be compared with available data on Fibre 'F' conductivity which indicates a value of $\approx 0.6\text{ W/cmK}$ along the fibre axis^(9,6,13). This large difference in the properties of the 1-D composite and fibres has important implications and will be discussed more fully when composite modelling techniques are examined.

Doubts have been raised concerning the efficacy of diffusivity measurements on highly orientated composites where the integrity of conduction paths is preserved. A good example of this is the parallel axis of the 1-D composite. Arguably, an effective composite diffusivity does not exist for such materials in which event the rear face temperature analysis (see Equation 2) will give meaningless results, except in two extreme cases.

These are:

$$1) \alpha_1 \approx \alpha_2$$

$$\alpha_1 \gg \alpha_2$$

where α_1 and α_2 are the diffusivities of the phases.

Case 2) has been used by Lee and Taylor⁽⁹⁾ to measure the diffusivity of carbon fibres.

The rear face temperature analysis enables the calculation of diffusivity with any value of x ($0 < x < 1$) in t_x provided the appropriate value of w/π^2 is used in Equation 2. Calculation of diffusivity for different values of x gives a check on how closely the observed transient conforms to its theoretical form and thus may provide information as to the nature of the sample.

The rear face temperature transients of several 1-D composite samples were recorded over a temperature range where heat losses would not distort the transient. The difference in diffusivity values calculated from t_x values in the range $0.2 < t_x < 0.8$ was less than $\pm 4\%$. It may be concluded therefore that the parallel axis does have a meaningful effective diffusivity.

(ii) Axis Transverse to Fibres

Diffusivity and conductivity results for the transverse fibre (TF) axis from three samples are shown in Figures 26 and 27.

The samples transverse to the fibre axis also showed irreversible dimensional changes after heating to 2400K. Increases in sample length were higher being in the range 2.6-4.9%. Fibre thermal expansion is known to be higher in the transverse direction^(6,14).

(F) 1-D Composite Fibre "A". No CVD - Graphitised at 2750°C

(i) Axis parallel to fibres

Measured thermal diffusivity and derived thermal conductivity data for two samples are shown in figures 28 and 29. The diffusivity is some 30% lower than the data obtained for the fibre "F" - 1-D composite. The density is also significantly lower (1.7 gm cm^{-3} compared to 1.89 gm cm^{-3})

and the derived conductivity values lie some 37% lower.

(ii) Axis transverse to fibres

In similar fashion the thermal diffusivity data obtained for this direction (figure 30) are also some 30% lower and the thermal conductivity values (figure 31) are likewise 37% lower.

(G) 1-D Composite Fibre "A" + CVD Graphitised at 2300°C

(i) Axis parallel to fibres

Thermal diffusivity data for 2 samples are shown in figure 32.

These data are much lower than those for the 1-D composite of Fibre "A" without CVD by a scaling factor of 0.3-0.5. The influence of CVD is almost impossible to ascertain since the difference is almost certainly due primarily to the difference in graphitisation temperature. An attempt was made to graphitise one sample by heating to 3000K. However the diffusivity decreased and subsequent examination revealed cracks between fibres and between fibres and matrix.

(ii) Axis transverse to fibres

Thermal diffusivity data are presented in figure 33 obtained for this direction showed values exhibiting a different temperature dependence to the values obtained for fibre "A" with no CVD. At $T > 1000K$ values are similar but at 300K values are only 70% of the non CVD'd samples.

7. Microstructural Investigation.

Figures 34 and 35 show scanning electron microscope (S.E.M.) views across the fibre axis of two 1-D composite samples, made from fibre "F" material. The latter is sample Z after measurements up to 2900K whereas the former has undergone no heating. There were no obvious microstructural changes which could explain the large transverse offset. Fibre/matrix interfaces appeared very similar with no evidence of increased separation, as higher magnification shows (figures 36 and 37).

Figure 38 shows a general view across the X axis of an unheated specimen of C.F.C.C. "A". The fibre yarns running from bottom left to top right are Y axis reinforcement, the other fibre yarns are Z axis. Pores of up to 100µm were visible in the matrix "cross over" pockets.

Broken yarn/yarn interfaces were a common feature of the 3-D composites as illustrated in figure 39 whereas yarn/matrix interfaces were generally intact. The X axis reinforcement is composed of two yarns but there was little evidence of yarn splitting in the unheated composite.

Figure 40 shows greater separation between fibres and matrix than was visible in the 1-D composite. In some regions the volume between adjacent fibres was completely filled with material of an apparently different form to the rest of the matrix (see figure 41). This quite possibly is CVD material⁽⁶⁾.

A general view across the Z axis of a C.F.C.C. "A" specimen that had been measured up to 2900K is shown in figure 42. Splitting within the Z axis yarns could be seen and the pattern of broken yarn/yarn interfaces repeated but more clearly marked than in the unheated specimen (figure 43). However spot diffusivity measurements taken during cooling had revealed no measurable change in thermal properties. No evidence could be seen of changes in the fibre/matrix interface (figure 44).

A general view across the X axis of C.F.C.C. "B" is shown in figure 45, illustrating the different method of fabricating this composite. The

X-reinforcements were not easy to distinguish individually because of the apparent absence of matrix "cross over" pockets. The area between the Z yarns appeared very homogeneous a feature further illustrated in figure 46. Presumably this is a result of using a weave instead of orthogonal fibres held in place before CVD by a jig⁽⁶⁾. The X and Y reinforcements are therefore able to expand into the cross over pockets, otherwise filled by the matrix. The vertical cracks, both major and minor were regularly spaced and probably mark the boundary between adjacent X-Y reinforcement planes which are nominally 0.254mm (254µm thick).

Broken Z yarn/X-Y interfaces were quite prominent and the fibre/matrix microstructure was very similar to that of C.F.C.C. "A". Figure 47 shows a general view across the Z axis illustrating the fine weave pierced fabric construction. Broken yarn/yarn interfaces are clearly visible.

However when we examine the composites nominally made from fibre "A" then discrepancies become evident. Some very good micrographs were obtained of the two 1-D fibre "A" composites which clearly show a circular fibre shape. In figure 48 for the 1-D composite that has been CVD'd can be distinctly seen a number of spherical fibres of about 6µm diameter. At higher magnification in a more heavily etched region of the specimen (figure 49) can be seen two fibres which have clearly visible around them a sheath, presumably of CVD graphite. In figures 50, 51 and 52 at magnifications of x 2,000, x 5,000 and 10,000 are three more regions of the CVD'd 1-D composite. Again the graphite sheath around each individual fibre is evident but more significantly the structure of the in-fill graphite, presumably matrix appears to orient itself transverse (TOG) with respect to the sheath of CVD graphite around each fibre which appears to be parallel oriented graphite (P.O.G.)

By way of contrast the non CVD unidirectional composite has a markedly different microstructure. In figure 53 is shown a micrograph at x 2,000 which may be compared with figure 50. Again whilst the cylindrical nature of the fibres is clearly evident there is a relative lack of detail regarding

the microstructure of the matrix. Progression to higher magnification figure 54 (x 5,000) and figure 55 (x 10,000) which are to be compared with figures 51 and 52, reveal little more detail. At x 20,000 magnification (figure 56) some detail is revealed with slight evidence that matrix graphite does form a sheath around the fibres. However no further detail can be drawn regarding the nature of the microstructure. When a longitudinal section of the non CVD'd 1-D fibre "A" composite is examined a little more detail is apparent. In figure 57 there is clear evidence that the matrix graphite surrounding the fibre is transversely oriented.

If we now consider the 3-D composite supplied as being made of fibre "A" material then a disconcerting difference becomes apparent. In figures 58 and 59 are electron micrographs of the Z axis direction and X axis direction respectively. Higher magnifications however clearly show that the fibres are crenulated (figure 60). This specimen has been heavily etched to show the relief. Even on more lightly etched samples figures 61 (x 5,000) and 62 (x 10,000) the fibre shape can clearly be seen. In these two specimens can also be seen some outcrops of matrix graphite which has obvious structural features of similarity with the CVD'd 1-D composite (figure 50).

Figures 63 (x 200) and 64 (x 1,000) exhibit evidence of cracks at yarn/yarn interfaces whereas there is a better continuity between the interfaces between matrix and yarns. There is evidence of substantial porosity in the matrix graphite in figure 64.

It is clear that the 3-D composite is not made from fibre "A" unless some extremely unusual etching effect is evident in the 3-D composite that is not apparent in the 1-D composite. We must therefore conclude that the wrong composite has been supplied and moreover is most probably made from fibre "F" material. This does not appear to be composite "A", although the diffusivity results are very similar. Analysis of figures 58 and 59 suggests that the unit cell dimensions in the Z and X directions are 0.685mm and 590mm respectively which is substantially less than the unit cell dimensions

of composite "A" (0.84×0.76 mm). This is a scaling factor of 0.8 and it is extremely unlikely that the electron microscope calibration could be in error by 20%.

8. Modelling of C.F.C.C. Thermal Conductivity

The intended approach of determining the thermal transport properties of the individual fibre and matrix phases and combining this data in the appropriate 3-D geometry is clearly invalidated by the lack of suitable specimens from which 1-D composites and matrix graphite experimental data may be analysed, and by the fact that composite "C" does not appear to be made from fibre "A" material.

The thermal conductivity of a composite will be a function of the thermal conductivities of the matrix material and of the fibres. These will be affected by processing variables; matrix graphite by the presence of porosity and the fibres by preform stiffening by carbon vapour deposition. To that extent none of the back-up materials; the three 1-D composites and the matrix graphite, can be said to be representative of the 3-D composites.

The bulk density of the matrix graphite is only 1.36 gcm^{-3} whereas the bulk densities of the composites are much higher. This implies that some scaling factor is required to predict the conductivity of the matrix material of the composites. Again whilst composites A and B and the 1-D fibre "F" composite have comparable densities, that for composite C and the two fibre "A" 1-D composites differ significantly. Additionally the fibre F and fibre A composites graphitised to 2750°C did not have CVD treatments and cannot be considered typical of the 3-D composites whereas the only 1-D composite that did have CVD treatment was only graphitised to 2300°C . Hence it is not possible to take into account the influence of processing upon the properties of the constituent phases.

This may be qualitatively summarised as follows:

- 1) Constituent densities tend to be significantly higher within the CFCC ^(6,11). Increases of 20% and more have been reported in both matrix and fibres ⁽¹¹⁾. In the case of the fibres, some of this density increase is due to the filling of pores in the fibre bundles ⁽¹⁴⁾.
- 2) If used, the CVD process produces a sheath-like coating around the

individual fibres (see Figure 51). The form of the coating varies with fibre type and in the case of fibre 'F' is isotropic^(14,15,16) or transverse⁽¹⁷⁾. Where fibres are closely packed (separation less than $1\frac{1}{2}$ fibre diameters) the inter-fibre space may be entirely filled with CVD material⁽¹⁷⁾.

3) The elastic modulus, thermal conductivity and bulk density of CVD CFCC are lower than when CVD is absent. The CVD process tends to seal off the fine porosity of the fibres, preventing infiltration by the matrix (14,15,16).

4) The matrix crystallites in the vicinity of fibres with isotropic CVD coatings are transversely oriented (TOG) w.r.t. the fibre axes⁽¹⁴⁾. In other regions e.g. cross-over pockets and where spacing between fibres is large, the matrix is isotropic.

5) Matrix crystallites in the vicinity of non CVD'd 'F' fibres are parallel oriented (POG) with the fibre axes⁽¹⁷⁾.

It is clear that the properties of CFCC materials result from a complex interaction of the individual phases. In the case of non CVD'd yarns, the matrix must not only increase fibre conductivity by infill of fibre defects, but also with its POG structure contribute very significantly to axial conductivity.

In the case of CVD'd material, it is more likely that CVD infill is the major influence on axial conductivity with that of the matrix less prominent. In all examples however the matrix properties themselves will be influenced by FVF since this is a factor in determining the proportions of POG/TOG and isotropic matrix. A schematic model of composite A⁽¹⁷⁾ is reproduced in figure 65.

8.1 Matrix Graphite

The large difference in density between the as supplied matrix graphite and the fibre composites raises doubts as to whether the measured values are appropriate for use in composite modelling.

It has been conclusively shown that the conductivity of graphite is dominated by conduction along layer planes and that the thermal conductivity of polycrystalline graphite may be represented by⁽¹⁸⁾

$$\frac{1}{\lambda} = \epsilon \beta \frac{1}{\lambda_a} = \alpha \frac{1}{\lambda_a} \quad (2)$$

where λ_a is the thermal conductivity along layer planes and the parameters ϵ and β represent a tortuosity factor and a porosity factor respectively. Taylor et al⁽¹⁸⁾ have analysed a number of graphites using this form of analysis and consider that three scattering processes contribute to the thermal resistivity.

$$\frac{1}{\lambda} = \alpha \left(\frac{1}{\lambda_u} + \frac{1}{\lambda_B} + \frac{1}{\lambda_I} \right) \quad (3)$$

where λ_u , λ_B , and λ_I represent the contribution to thermal conductivity due to Umklepp scattering, grain boundary and isotope scattering.

Taylor et al have shown that that isotope scattering will contribute some 2-3% to the total thermal resistance so, in view of the assumptions to be made, this will be neglected. An empirical relationship for the mean free path has been derived by Taylor⁽¹⁹⁾

$$\lambda_u = 8.75 \times 10^{-7} \exp 1130/T \quad (4)$$

from which the thermal conductivity $\lambda_u = 1/3 CVL_u$ may be calculated.

(Values are listed up to 1000K by Taylor). Explicit equations for boundary scattering have been derived by Kelly⁽²⁰⁾

$$\lambda_B = K_1 + K_2 + K_3 \quad (5)$$

$$K_1 + K_2 = \frac{1}{2} N_0 k L_a T^2 \left\{ \frac{V_L}{\theta_L^2} J_3 \left(\frac{\theta_L}{T} \right) + \frac{V_T}{\theta_T^2} J_3 \left(\frac{\theta_T}{T} \right) \right\}$$

$$K_3 = 16 k \left(\frac{h}{kT} \right)^2 L_a \int_0^{\sigma_m} \int_{-d/2}^{+d/2} \pi^2 \delta^2 \sigma_a^4 w_3 \frac{\exp(hw_3/kT)}{[\exp(hw_3/kT) - 1]^2} d\sigma_a d\sigma_2 \quad (7)$$

where the symbols $N_0, V_L, V_T, h, \delta, \sigma_a, \sigma_L, \sigma_T$ and w_3 are as used previously by Kelly.

At high temperatures it is reasonable to assume that Umklapp scattering will dominate and that boundary scattering will contribute < 10% to the total thermal conductivity. Data for matrix graphite can be fitted by a curve for which $\alpha = 9.0$ and $L_a = 2,750^\circ \text{A}$. to an accuracy of $\pm 8\%$ over all the curve. This value of crystallite size is slightly higher than those derived by Taylor for a range of polycrystalline graphites but similar to a value determined by Kelly and Gilchrist⁽²¹⁾ for pyrolytic graphite graphitised at 2750°C . The value of 9.0 for the porosity/tortuosity factor is higher than those noted by Taylor; however the low density (40% porosity) of the bulk matrix graphite is probably a prime contributory factor.

This matrix graphite with a bulk density of 1.36 gm cm^{-3} has to be compared with bulk densities in the range $1.88\text{--}1.92 \text{ gm cm}^{-3}$ for the two 1-dimensional fibre "A" composites. Hence to use the raw

derived thermal conductivity data is probably unrealistic. A fully dense isotropic graphite would have zero porosity factor and a tortuosity factor of $\sqrt{2}$. A line of interpolation between $\alpha = 1.41$ at zero porosity and $\alpha = 9.0$ at 40% porosity should however permit an evaluation of α for any value of density. Although there is no justification for this, it is perhaps a reasonable assumption in view of the complex interaction of variables and lack of any available data.

8.2. 1-D Composites

The thermal conductivity of a unidirectionally reinforced composite in a direction parallel to the fibres λ_c^{11} is usually expressed in terms of the volume weighted conductivities of the constituents using an Ohm's law approach

$$\lambda_c^{11} = V_f \lambda_f^{11} + (1-V_f) \lambda_m \quad (8)$$

where λ_f^{11} is the conductivity of the fibres

λ_m is the matrix conductivity

V_f is the fibre volume fraction

Applying the results for the three unidirectional composites should in principle permit the calculation of the thermal conductivity λ_f^{11} of the fibres. However the significantly higher densities of the 1-D composites suggests that it would be inappropriate to use the measured matrix conductivity in equation 8. Certainly the composite conductivity of the 1-D fibre "F" composite ($3.0 \text{ W cm}^{-1} \text{ K}^{-1}$ at 300K) cannot be accounted for in terms of the measured matrix conductivity ($0.85 \text{ W cm}^{-1} \text{ K}^{-1}$ at 300K) and the reported conductivity of fibre "FP" ($0.6 \text{ W cm}^{-1} \text{ K}^{-1}$ at 300K ^(9,13)).

The conductivity anisotropy ratios of the 1-D composites graphitized at 2750°C are approximately 11-12 at room temperature, decreasing to about 8 at 2300K. These are high values and irrespective of whether the bulk matrix properties are representative of the composite matrix, the implication must be that fibre anisotropy is also high. It has been reported ⁽²²⁾ that matrix conductivity is usually below both axial and transverse fibre conductivity. This is a surprising observation and are variance with our measured data.

Various models have been put forward in an attempt to explain the transverse thermal conductivity of a unidirectional composite in terms of the thermal conductivities of the matrix and included fibres. Some of these have been critically assessed by Pilling et al ⁽²³⁾ for fibre/epoxy composites. We adopt a modified Ohm's law approach, the

in-phase shear field analogy, using a model and analysis developed by Springer and Tsai ⁽²⁴⁾. This yields a generalised equation for the 1-D transverse thermal conductivity λ_c^\perp

$$\frac{\lambda_c^\perp}{\lambda_m} = \left(1 - \frac{d}{2b}\right) + \frac{a}{b} \int_0^d \frac{dy}{(2a-\beta) + (\beta\lambda_m/\lambda_f)} \quad (9)$$

where $\beta = f(y)$, a function relating fibre width at any given y and λ_f is the fibre transverse conductivity. The solution of Equation (9) is shown graphically in Figure 66, for a fibre of circular cross-section and square packing, as a function of fibre volume fraction (FVF) and λ_f/λ_m . Equation 5 assumes good contact between fibre and matrix but Figures 34-37, 48-57 have shown this assumption to be quite appropriate for the 1-D composite.

The fibre volume fraction of the 1-D composites of fibre "A" is 50%, that for the 1-D composite of fibre "F" is 52%. Using values for matrix conductivity calculated from diffusivity measurements and values determined for thermal conductivity in a direction perpendicular to fibre orientation λ_c^\perp we deduce, using data at 350K and 1000K.

TABLE 3

Temperature	350K		1000K	
spec type	$\lambda_c^\perp/\lambda_m$	λ_f/λ_m	$\lambda_c^\perp/\lambda_m$	λ_f/λ_m
Fibre "F" no CVD	0.33	0.1	0.38	0.15
Fibre "A" CVD	0.12	<0.01	0.21	0.01
Fibre "A" no CVD	0.23	0.03	0.26	0.05

There are indications that the ratio $\lambda_c^\perp/\lambda_m$ is temperature dependent for all 1-D composites.

If we now considered this data in more detail then three factors can affect the thermal conductivity of the 1-D composites.

- a) The density of matrix graphite in the 1-D composite is higher than that of the matrix graphite as supplied.

b) The fibres within the composites will have been graphitised to a temperature of 2750°C .

c) Bonding of matrix graphite to the fibre preform can confer some directionality on thermal properties for the composite.

Matrix crystallites in the vicinity of non CVD'd type "F" fibres are oriented parallel to the fibre axis.⁽¹⁷⁾

9. 3-D Composites

With the present state of knowledge and lack of suitably relevant data the modelling of C.F.C.C. can only succeed if the problem of quantifying the influence of processing can be avoided. This is possible if the 3-D C.F.C.C. is considered to be a two phase material comprising

- a) Processed fibre yarns representing the axial reinforcement
- b) Isotropic matrix pockets filling the rest of the space in

the unit cell geometry.

9 (i) C.F.C.C.'s A and C

The method rests on the assumption that the yarns and matrix pockets are arranged either in series or in parallel and that the resulting thermal model is analogous to series and parallel connected electrical circuits. Essentially, it extends the method used by Knappe and Martinez-Freire ⁽²⁶⁾ to three dimensions.

Along the axis under consideration, the composite unit cell is subdivided into four parallel conduction channels (see Figure 67). It is then required that:

- a) The temperature difference ΔT along the heat flow direction is constant.
- b) The total heat flow Q may be divided into four parts i.e.

$$Q = Q_1 + Q_2 + Q_3 + Q_4 \quad (10)$$

The thermal conductivity of each channel is calculated using an Ohm's law approach. Thus, for the Z axis channels indicated in Figure 67:

$$\frac{2a}{\lambda_{1Z}} = \frac{s}{\lambda_m} + \frac{2a-s}{\lambda_{1x}} \quad (11)$$

giving

$$\lambda_{1Z} = \frac{2a\lambda_m\lambda_{1x}}{(s\lambda_{1x} + g\lambda_m)} \quad (12)$$

where λ_{1x} is the transverse conductivity of the X axis yarn.

Similarly,

$$\lambda_{2Z} = \frac{2a\lambda_{1x}\lambda_{1y}}{(s\lambda_{1x} + g\lambda_{1y})} \quad (13)$$

$$\lambda_{3Z} = \frac{2a\lambda_m \lambda_{\perp y}}{(s\lambda_m + g\lambda_{\perp y})} \quad (14)$$

Lastly,

$$\lambda_{4Z} = \lambda_{//Z} \quad (15)$$

where $\lambda_{//Z}$ is the parallel conductivity of the Z axis yarn.

The conductivities of the individual channels are then area-weighted and added to obtained the total conductivity of the unit cell. For the Z axis, the following result is obtained:

$$\lambda_Z = \frac{\lambda_{1Z}(2b-h)r + \lambda_{2Z}hr + \lambda_{3Z}(2c-r)h + \lambda_{4Z}(2c-r)(2b-h)}{4bc} \quad (16)$$

And for the X axis:

$$\lambda_X = \frac{\lambda_{1X}rs + \lambda_{2X}(2c-r)s + \lambda_{3X}(2c-r)g + \lambda_{4X}rg}{4ac} \quad (17)$$

$$\text{where } \lambda_{1X} = \frac{2b\lambda_m \lambda_{\perp y}}{[h\lambda_m + (2b-h)\lambda_{\perp y}]}, \quad \lambda_{2X} = \frac{2h\lambda_{\perp Z} \lambda_{\perp Y}}{[h\lambda_{\perp Z} + (2b-h)\lambda_{\perp Y}]}$$

$$\lambda_{3X} = \frac{2b\lambda_m \lambda_{\perp Z}}{[h\lambda_{\perp Z} + (2b-h)\lambda_m]}, \quad \lambda_{4X} = \lambda_{//X}$$

In the real composite, these results must represent only the upper bound of channel and unit cell conductivities. Account must also be taken of the effect of structural defects i.e. split yarns, broken interfaces and porosity, though the latter may already be adequately represented within the 1-D composite and bulk matrix data.

For split yarns and broken interfaces perpendicular to heat flow, the lower bound to individual channel conductivity will be zero and from this the unit cell lower bound for the particular defect type can be found. A value between the bounds can then be determined from the frequency with which the defect appears in the composite structure.

(ii) C.F.C.C. 'B'

and perpendicular to the weave of a 2-D CRCC, using a method due to Bruggeman. However, this approach uses the separately measured properties of the individual fibres and matrix. Our investigation shows that these properties are considerably affected by the CVD process and fibre bundle densification.

Analyses of 2-D woven composites have agreed the weave structure has little influence on the conductivity perpendicular to the reinforcement plane^(23,26). Although the non orthogonal FWPF construction increases conduction path length, this is balanced by increased conductivity⁽²³⁾.

Figure 45 has shown that the X-Y weave is not significantly distorted by the Z axis yarns. It seems appropriate, therefore, to retain the orthogonal unit cell analysis for the Z axis conductivity of CFCC 'B'.

The case of the parallel or in-plane (X axis) conductivity is more complex. The weave also results in increased in-plane conductivity paths, but Kessler⁽²³⁾ has estimated that the effect is negligible for the particular weave used in CFCC 'B' (eight-harness satin weave). Figures 45 and 46 have shown the absence of clearly defined matrix cross-over pockets in the X-Y weave, the yarns tending to fill the whole volume available.

The reduced incidence of the relatively high porosity matrix pockets may explain the higher density of CFCC 'B'. Given that the yarn axial conductivity is considerably greater than that of the bulk matrix, the orthogonal analysis must represent a lower bound to the X axis conductivity of this composite.

A simple upper bound can be determined from the assumption that the heat flow paths within the X-Y weave are confined to the X axis yarns. The low conductivity transverse paths through the Y axis yarns are then effectively 'short circuited'. Using the orthogonal analysis, this may be implemented by expanding the X axis yarn into the volume normally occupied by the Y yarn-matrix conduction channel. Although this implies a reduction in yarn FVF, because of processing complications it is not clear that there must be a concomitant reduction in yarn conductivity such as would be implied by

Equation 4. Equation 17 then becomes:

$$\lambda_X = \frac{\lambda_{2X}(2c-r)s + \lambda_{3X}(2c-r)g + 2\lambda_{4X}ar}{4ac} \quad (18)$$

10. Analysis of Data

10.1 1-D C.F.C.C. Composites

If we follow the approach suggested in 8.1 to deduce thermal conductivity values for the matrix graphite within the 1-D composite then a matrix density of $\sim 1.9 \text{ gm cm}^{-3}$ would be appropriate for the 1-D fibre "F" composite and 1.67 gm cm^{-3} for the fibre "A" composites. This would suggest porosity/tortuosity factors of 4.25 and 6.5 respectively and imply weighting factors of 2.1 and 1.4 for values of matrix conductivity to be used in equations 8 and 9. Applying this to equation 8 yields room temperatures values of $\lambda_f^{11} = 4.1 \text{ Wcm}^{-1}\text{K}^{-1}$ for fibre "F" and $\lambda_f^{11} = 3.0 \text{ W cm}^{-1}\text{K}^{-1}$ for fibre "A" after graphitisation at 2750°C . It is not realistic to apply this approach to the CVD'd composite of fibre "A" since we have no value for matrix graphite graphitised to only 2300°C .

Considering the perpendicular direction however and using these estimated values for matrix graphite conductivity of $1.8 \text{ Wcm}^{-1} \text{ K}^{-1}$ for the fibre "F" composite and $1.2 \text{ Wcm}^{-1} \text{ K}^{-1}$ for the fibre "A" composite yields values of $\lambda_c^{\perp} / \lambda_m$ of 0.15 and 0.167 for the two composites respectively. The limiting value of $\lambda_f / \lambda_m < 0.01$ would in turn suggest values for $\lambda_m = 1.35 \text{ Wcm}^{-1} \text{ K}^{-1}$ in the fibre "F" composite and $\lambda_m = 1.0 \text{ Wcm}^{-1} \text{ K}^{-1}$ in the Fibre "A" composite.

It must firstly be asked if these values are reasonable. We have concentrated on data at low temperatures because the only data available for comparison is low temperature data (90-270 K) obtained for carbon fibre/epoxy resin composites (24,27,28). It is reasonable to suppose that the orientation of the "a" axis crystallites of a carbon fibre will be directly related to its thermal history. The data of Volga and Pilling et al (24) clearly shows this to be the case. Data by Volga (28) show a dramatic increase in thermal conductivity of carbon fibres with graphitisation temperature. The fibre thermal conductivity λ_f^{11} at 270 K, increases from $1.6 \text{ Wcm}^{-1} \text{ K}^{-1}$ after graphitisation for 1 hour

at 2600°C to $3.0 \text{ Wcm}^{-1} \text{ K}^{-1}$ after 1 hour at 2800°C. Hence our derived values for λ_f^{11} are very much in agreement with these observations. Likewise Pilling et al have determined the transverse thermal conductivity of HTS carbon fibres manufactured from polyacrylonitrile precursor similar to fibre "A" to be $0.06 \text{ Wcm}^{-1} \text{ K}^{-1}$ at 270K. This is again in accord with our conclusion, that the transverse conductivity of both fibre "A" and fibre "F" is at least one, and more nearly two orders of magnitude lower than the parallel conductivity.

The one remaining uncertainty is why the ratio $\lambda_c^\perp / \lambda_m$, using assumed matrix conductivity values, is less than the limiting value of 0.2 predicted by the model for a F.V.F. circa 50%. Hitherto we have concentrated on using bulk properties and neglected the influence of processing. Stover et al⁽¹⁵⁾ have shown that matrix crystallites in the vicinity of non C.V.D.'d fibre "F" composites are parallel oriented (P.O.C.) with respect to the fibre axis. Our electron microscopy observations neither prove nor disprove this observation. However if true this will result in an increase in effective fibre diameter and a concomitant reduction in the amount of randomly oriented matrix graphite in the 1-D composite which would adequately explain the low $\lambda_c^\perp / \lambda_m$ ratio.

10.2 3-D C.F.C.C. Composites

A necessary prerequisite is to establish the compositional similarity between the 1-D composites and the 3-D yarns. In the case of the 1-D fibre a composite and composite "C" this is patently inappropriate since the fibres in composite "C" are clearly of a different type. Nonetheless since we have no accurate data for this composite we will proceed, for reasons that will be made clear later on the assumption that we can apply fibre "A" 1-data to composite "C"

For the general case the yarn fibre volume fraction is calculated from the cross sectional area, the number of filaments/yarn and the affective filament area. This yields a F.V.F. of 0.60 - 0.64⁽⁶⁾ which is higher than the F.V.F. of either 1-D composite. However the difference in processing will

result in a significant difference in properties thereby complicating any attempt to model the results. Since no experimental information is available to quantify the differences between CVD versus non CVD on fibre "F" composites, any attempt to determine the conductivity of a CVD'd yarn from the 1-D composite data can have doubtful merit only. However, since there are no 1-D composites with fibre "F", CVD and standard process available ⁽⁶⁾ there is no alternative. Similar arguments do not now apply to composite "C".

For fibre "F" 3-D composites it has been shown that

- a) Sheath zones primarily of P.O.G. can form around the fibres.
- b) Where filaments are closer together than about $1\frac{1}{2}$ diameters the space may be entirely filled with C.V.D. graphite.
- c) For distances greater than this up to 7 fibre diameters the space is filled with transversely oriented pitch.
- d) At distances greater than approximately 7 diameters the orientation becomes random.

It is further noted that where sheath zones predominate the matrix tends to align the crystallographic planes normal to the filaments. This presents a somewhat idealised concept of the unit cell of a 3-D composite as shown in Figure 65. Broken yarns are likely to be matrix filled.

Our observations on the 1-D fibre composites indicate that the non CVD'd composites of fibre "A" and "F" show fairly dense composites with little evidence of preferred orientation in the matrix graphite. However the electron micrographs of the CVD'd composite of fibre "A" shows the formation of a distinct sheath around individual fibres and evidence for the formation of transversely oriented graphite in the region between fibres. The density of fibres is too high to determine whether the orientation of the matrix graphite would randomise at increased fibre separation.

It therefore seems logical that the change of orientation from P.O.G. to T.O.G. should significantly increase the transverse matrix conductivity. Again our arguments demonstrate that, although the

thermal conductivity of matrix graphite is higher than that of the fibres in the transverse direction the latter will predominate. For example figure 66 shows that a 100% increase in matrix conductivity will result in a 35% increase in transverse conductivity of a composite with a similar F.V.F. A further complication concerns cracks, the density of which is higher in the 3-D composites than in the 1-D composite. The majority of these run parallel to the fibre axis. They should have little effect on the transverse thermal conductivity which is dominated by the matrix but have a significant affect on the axial thermal conductivity.

On the basis of the foregoing discussion, the 1-D composite conductivity data is modified in the following way for use in the 3-D composite model.

- a) Axial conductivity reduced by a factor of 0.66
- b) Transverse conductivity increased by a factor of 2.0.

No additional correction has been made for the difference in FVF noted earlier. The bulk matrix is used unmodified as its porosity is of a similar order to that of the cross- over pockets⁽⁶⁾.

d) Modelling Results

The appropriate unit cell constants are given in Table 4.

Composite Type	Unit Cell dimensions mm						
	a	b	c	g	h	r	s
"A"	0.42	0.38	0.38	0.42	0.32	0.32	0.42
"B"	0.127	0.625	0.625	0.127	0.71	0.71	0.127
"C" *	0.38	0.43	0.43	0.38	0.34	0.34	0.38

* Used as supplied by AFML although this is known to be incorrect.

Table 4

Unit Cell Constants

The predicted upper and lower bounds of C.F.C.C. "A" X axis conductivity are shown in Tables 5 and 6 together with the experimental data as defined

by the least squares function. The rms errors are 27% and 11% respectively. Clearly the lower bound, representing the case of one broken yarn/yarn interface per unit cell, provides the best fit with the experimental data. It was apparent from the microstructural investigation (see Figures 38 and 39) that the lower bound assumptions more closely reflected the real material.

The predicted upper and lower bounds of the CFCC "A" Z axis is shown in Tables 7 and 8. The rms errors are 12% and 9% respectively. The results are very similar to those of the X axis with the greatest error, in the case of the lower bound, occurring at the extremes of the temperature range.

The predicted conductivity of CFCC "B" X axis is shown in Tables 9 and 10. As discussed earlier, the upper and lower bounds of this material are different from those of CFCC "A". The rms errors are 10% and 20% respectively.

As expected the lower bound, which represents the orthogonal unit cell geometry, consistently underestimates the X axis conductivity. The upper bound, which though exaggerating the weave influence, is in much closer agreement with the experimental data.

The calculated upper and lower bounds of CFCC "B" Z axis conductivity are shown in Tables 11 and 12. The rms errors are 24% and 14% respectively. The lower bound chosen is again that of one broken yarn/yarn interface per unit cell and this seems reasonable in view of the evidence provided by the microstructural investigation (See figures 45 and 46).

For C.F.C.C. "C" we have used in the model data for fibre "A" composites although it is clear that the fibres in composite "C" are not fibre "A" but more probably fibre "F". In Tables 13 and 14 the calculated upper and lower bounds are shown for the X axis. The rms errors are 6.6% and 22.8% respectively. The calculated conductivities for the Z axis are presented in Tables 15 and 16 respectively and show r.m.s errors of 17.5% and 23.8% respectively.

Not surprisingly the modelling results for composite "C" are poorer than those for composites "A" and "B". The lower bound which is arguably the most reliable, in view of the microstructural evidence, and certainly gives a better prediction for composite "A" and the Z axis of composite "B", consistently underpredicts the thermal conductivity. Clearly higher conductivities particularly parallel to fibre orientation would be appropriate. Comparison of data for non CVD'd 1-D fibre "F" composites (figures 24-27) and fibre "A" 1-D composites (figures 28-31) show the former to be clearly higher by some 50% at 350K decreasing to 25% at 1500K. If as we believe composite "C" is also a fibre "F" composite data based on figures 24-27 would be more appropriate in the model and lead to better predictions.

6. Conclusions

Modelling of C.F.C.C. thermal properties can only succeed if accurately quantifiable information is available on the properties of the individual phases. In this case it has not been possible to rigorously test the present CFCC model because of the unavailability of any suitably processed 1-D composites. However, in spite of its basic simplicity and the limitations of the 1-D composite data, the predictions of the CFCC model have shown a reasonable agreement with the experimental data.

For composites manufactured from fibre "F" material, with the exception of the X axis of composite "B" which is a special case CFCC conductivities are reflected more closely by the lower bound solutions. It is believed that the microstructural investigation has shown that these in turn reflect most accurately the structural state of the real composites. In the case of composite "C" microstructural evidence comparing this with 1-D composites from fibre "A" leads to the conclusion that fibres are not type "A" but more likely fibre "F". This is reflected in modelling values which consistently under predict and it is suggested that better values might be obtained by using fibre "F" 1-D composite data.

References

1. Parker W.J., Jenkins R.J., Butler C.P. and Abbott Gil (1961)
"Flash method of determining thermal diffusivity, heat capacity and thermal conductivity" J. Appl. Phys. 32 1679-84.
2. Watt D.A. (1966) "Theory of thermal diffusivity by pulse technique" Brit. J. Appl. Phys. 17 231-40.
3. Taylor R. (1980) "Construction of apparatus for heat pulse thermal diffusivity measurements" J. Phys. E. Sci. Inst. 13 1193-99.
4. Cowan R.D. (1963) "Pulse method of measuring thermal diffusivity at high temperatures". J. Appl. Phys. 34 926-7.
5. Taylor R.E. and Clark L.M. III (1974) "Finite pulse time affects in flash diffusivity method" High Temp-High Press 6 65-72.
6. Theibert L.S. (1978) private communication.
7. Taylor R.E. and Groot H. (1978) "Thermophysical properties of POCG graphite " AFOSR-77-3280
8. Cezeirliyen A. and Miller A.P. (1981). "Specific heat capacity and electrical resistivity of a carbon-carbon composite in the range 1500-3000K by a pulse heating method". Int. J. Thermophysics 1 (3) 317-30 (supplied by A.F.M.L. - 1979).
9. Lee H.J. and Taylor R.E. "Thermophysical properties of Carbon/graphite fibres and MOD-3 Fibre reinforced graphite" (1975) Carbon 13 521-7.
10. Minges M.L. (1975) AFML-TR-74-96
11. J. Joriner, A.A. Kelton and P.C. Hopkins (1978) "In situ densities of fibres and matrices in carbon-carbon composites" MDC G 7385.
12. Taylor R. (1972) High Temp-High Press 4 649-658.
13. I.L. Kalnin (1975) "Thermal conductivity of high modulus fibres" composite reliability ASTM STP 580 p.460-73.

14. J.J. Gebhardt (1979) "Influence of fibre coatings on carbon-carbon composite properties" SAMPE conference BOSTON, Massachusetts.
15. Stover E.R., D'Andrea J.F., Bolinger P.N. and Gebhardt J.J.
"Development of interfilament matrix structures in CVD infiltrated carbon/carbon". (1977) 13th Conference on Carbon.Irvine , California.
16. Gebhardt J.J. "Surface effects on pyrolytic Infiltration of carbon fibre preforms" (1979) 14th Conference on Carbon. State College Pennsylvania.
17. AFML TR-77-48.
18. Taylor R., Gilchrist K.E. and Poston L.J. (1968) Carbon 6 537-44.
19. Taylor R. (1966) Phil Mag. 13 157-64.
20. Kelly B.T. Carbon 5 247 (1967)
 ibid 6 71 (1968)
 ibid 6 485 (1969)
21. Kelly B.T. and Gilchrist K.E. Carbon I 355.8 (1969).
23. Kessler W. private communication.
24. Pilling M.W.,Yates B., Black M.A. and Tattersall P. (1979)
 J. Met Sci.14 1326-38.
25. Springer G.S. and Tsai S.W. (1967) J. Comp. Met. 1 166.
26. Knappe W. and Martinez-Friere P. (1965) Kunststoffe 55 776.
27. Knibbs R.H., Baker D.J. and Rhodes G. "Thermal and electrical properties of carbon fibre unidirectionally reinforced composites" (1971) Soc. Plastics Ind. Inc. 24th Annual Tech. Conf.
28. Volga V.I.,Frolov, V.I. and Kusov V.K. (1973) Inorg. Met. 9 643.

THERMAL CONDUCTIVITY MODELING OF CFCO A
A X AXIS
UPPER HOHN

TEMPERATURE (K)	EXP. DATA	CAL. DATA	ERROR
300.0	.643	.943	46.5
350.0	.636	.922	45.1
400.0	.627	.902	43.7
450.0	.619	.881	42.4
500.0	.610	.861	41.1
550.0	.600	.840	39.9
600.0	.591	.819	38.7
650.0	.581	.799	37.5
700.0	.571	.779	36.4
750.0	.561	.759	35.3
800.0	.552	.740	34.2
850.0	.542	.721	33.1
900.0	.532	.703	32.1
950.0	.522	.685	31.1
1000.0	.513	.668	30.1
1050.0	.504	.651	29.2
1100.0	.495	.635	28.3
1150.0	.486	.619	27.4
1200.0	.478	.605	26.6
1250.0	.470	.590	25.7
1300.0	.462	.577	24.9
1350.0	.455	.564	24.2
1400.0	.448	.552	23.4
1450.0	.441	.541	22.7
1500.0	.435	.530	22.0
1550.0	.429	.520	21.3
1600.0	.424	.511	20.6
1650.0	.419	.502	19.9
1700.0	.415	.494	19.2
1750.0	.411	.487	18.5
1800.0	.407	.480	17.8
1850.0	.404	.473	17.2
1900.0	.401	.467	16.4
1950.0	.399	.461	15.7
2000.0	.397	.456	14.9
2050.0	.395	.451	14.1
2100.0	.394	.446	13.3
2150.0	.393	.441	12.4
2200.0	.392	.437	11.4
2250.0	.392	.432	10.3
2300.0	.391	.427	9.2
2350.0	.391	.422	8.0
2400.0	.391	.417	6.6
2450.0	.391	.411	5.2
2500.0	.391	.405	3.6

RMS ERROR= 27.0

Table 5

THERMAL CONDUCTIVITY MODELING OF CFCC A
A X AXIS
LOWER BOUND

TEMPERATURE (K)	EXP. DATA	CAL. DATA	DEPRD
300.0	.643	.779	21.1
350.0	.636	.760	19.5
400.0	.627	.741	18.1
450.0	.619	.722	16.7
500.0	.610	.703	15.4
550.0	.600	.685	14.1
600.0	.591	.667	12.9
650.0	.581	.649	11.7
700.0	.571	.632	10.6
750.0	.561	.615	9.5
800.0	.552	.598	8.5
850.0	.542	.582	7.5
900.0	.532	.567	6.5
950.0	.522	.552	5.6
1000.0	.513	.537	4.7
1050.0	.504	.523	3.8
1100.0	.495	.510	3.0
1150.0	.486	.497	2.2
1200.0	.478	.484	1.4
1250.0	.470	.473	.7
1300.0	.462	.462	-.1
1350.0	.455	.451	-.8
1400.0	.448	.441	-1.5
1450.0	.441	.431	-2.2
1500.0	.435	.422	-2.9
1550.0	.429	.414	-3.5
1600.0	.424	.406	-4.2
1650.0	.419	.399	-4.8
1700.0	.415	.392	-5.5
1750.0	.411	.385	-6.1
1800.0	.407	.379	-6.8
1850.0	.404	.374	-7.5
1900.0	.401	.368	-8.2
1950.0	.399	.363	-8.9
2000.0	.397	.359	-9.6
2050.0	.395	.354	-10.4
2100.0	.394	.350	-11.2
2150.0	.393	.346	-12.0
2200.0	.392	.342	-12.8
2250.0	.392	.338	-13.7
2300.0	.391	.334	-14.7
2350.0	.391	.330	-15.7
2400.0	.391	.325	-16.8
2450.0	.391	.321	-18.0
2500.0	.391	.316	-19.2

RMS ERROR= 10.8

Table 6

THERMAL CONDUCTIVITY MODELING OF CFCC 6
A Z AXIS
UPPER BOUND

TEMPERATURE (K)	EXP. DATA	CAL. DATA	REPROP
300.0	.934	1.186	26.8
350.0	.916	1.153	25.9
400.0	.899	1.123	24.9
450.0	.882	1.093	23.9
500.0	.866	1.064	22.9
550.0	.849	1.035	21.9
600.0	.833	1.007	20.8
650.0	.818	.980	19.8
700.0	.803	.953	18.7
750.0	.788	.927	17.6
800.0	.773	.902	16.6
850.0	.759	.877	15.5
900.0	.745	.854	14.5
950.0	.732	.831	13.5
1000.0	.719	.809	12.5
1050.0	.706	.788	11.6
1100.0	.694	.768	10.7
1150.0	.682	.748	9.8
1200.0	.670	.730	9.0
1250.0	.659	.712	8.2
1300.0	.648	.696	7.4
1350.0	.637	.680	6.7
1400.0	.627	.665	6.1
1450.0	.617	.651	5.5
1500.0	.607	.638	5.0
1550.0	.598	.625	4.5
1600.0	.590	.613	4.0
1650.0	.581	.602	3.6
1700.0	.573	.592	3.2
1750.0	.566	.582	2.9
1800.0	.558	.573	2.6
1850.0	.552	.564	2.3
1900.0	.545	.556	2.1
1950.0	.539	.549	1.8
2000.0	.533	.541	1.5
2050.0	.528	.534	1.2
2100.0	.523	.528	.9
2150.0	.518	.521	.6
2200.0	.514	.515	.2
2250.0	.511	.509	-.3
2300.0	.507	.503	-.9
2350.0	.504	.496	-1.6
2400.0	.502	.490	-2.4
2450.0	.499	.483	-3.3
2500.0	.498	.476	-4.4

RMS ERROR= 12.4

Table 7

THERMAL CONDUCTIVITY MODELING OF CFC-2
A 7 AXIS
LOWER ROUND

TEMPERATURE (K)	EXP. DATA	CAL. DATA	PERIOD
300.0	.934	1.092	14.9
350.0	.916	1.042	15.9
400.0	.899	1.032	14.8
450.0	.882	1.004	13.8
500.0	.866	.975	12.7
550.0	.849	.949	11.6
600.0	.833	.921	10.5
650.0	.818	.895	9.5
700.0	.803	.870	8.4
750.0	.788	.846	7.3
800.0	.773	.822	6.3
850.0	.759	.799	5.3
900.0	.745	.777	4.3
950.0	.732	.756	3.3
1000.0	.719	.736	2.3
1050.0	.706	.716	1.4
1100.0	.694	.697	.5
1150.0	.682	.680	-.3
1200.0	.670	.662	-1.1
1250.0	.659	.646	-1.9
1300.0	.648	.631	-2.6
1350.0	.637	.616	-3.3
1400.0	.627	.602	-3.9
1450.0	.617	.589	-4.5
1500.0	.607	.577	-5.0
1550.0	.598	.565	-5.5
1600.0	.590	.554	-6.0
1650.0	.581	.544	-6.4
1700.0	.573	.534	-6.8
1750.0	.566	.525	-7.2
1800.0	.558	.516	-7.5
1850.0	.552	.508	-7.8
1900.0	.545	.501	-8.1
1950.0	.539	.493	-8.4
2000.0	.533	.487	-8.7
2050.0	.528	.480	-9.1
2100.0	.523	.474	-9.4
2150.0	.518	.468	-9.8
2200.0	.514	.462	-10.2
2250.0	.511	.456	-10.7
2300.0	.507	.450	-11.3
2350.0	.504	.444	-11.9
2400.0	.502	.438	-12.6
2450.0	.499	.432	-13.5
2500.0	.498	.426	-14.5

RMS ERROR= 8.9

Table 8

THERMAL CONDUCTIVITY MODELING OF CFCC R
R X AXIS
UPPER BOUND

TEMPERATURE (K)	EXP. DATA	CAL. DATA	*ERROR
300.0	1.383	1.529	10.5
350.0	1.332	1.483	11.4
400.0	1.283	1.438	12.1
450.0	1.237	1.395	12.8
500.0	1.194	1.354	13.4
550.0	1.153	1.313	13.9
600.0	1.115	1.274	14.3
650.0	1.079	1.237	14.6
700.0	1.045	1.201	14.9
750.0	1.014	1.166	15.0
800.0	.984	1.132	15.1
850.0	.957	1.100	15.0
900.0	.931	1.070	14.9
950.0	.907	1.040	14.7
1000.0	.884	1.012	14.4
1050.0	.863	.985	14.1
1100.0	.844	.959	13.7
1150.0	.825	.935	13.2
1200.0	.808	.911	12.7
1250.0	.793	.889	12.2
1300.0	.778	.868	11.6
1350.0	.764	.848	10.9
1400.0	.752	.829	10.3
1450.0	.740	.811	9.6
1500.0	.729	.794	8.9
1550.0	.719	.778	8.2
1600.0	.710	.763	7.5
1650.0	.701	.749	6.8
1700.0	.693	.735	6.2
1750.0	.685	.723	5.5
1800.0	.678	.711	4.8
1850.0	.671	.699	4.2
1900.0	.664	.688	3.6
1950.0	.658	.678	3.0
2000.0	.653	.668	2.4
2050.0	.647	.659	1.8
2100.0	.642	.650	1.2
2150.0	.637	.641	.7
2200.0	.632	.632	.1
2250.0	.627	.624	-.4
2300.0	.622	.616	-1.0
2350.0	.617	.607	-1.6
2400.0	.612	.599	-2.2
2450.0	.608	.590	-2.9
2500.0	.603	.581	-3.6

RMS ERROR= 10.1

Table 9

THERMAL CONDUCTIVITY MODELING OF CFCC B
B X AXIS
LOWER BOUND

TEMPERATURE (K)	EXP. DATA	CAL. DATA	ERROR
300.0	1.383	1.082	-21.8
350.0	1.332	1.055	-20.7
400.0	1.283	1.029	-19.8
450.0	1.237	1.003	-18.9
500.0	1.194	.978	-18.1
550.0	1.153	.952	-17.4
600.0	1.115	.927	-16.8
650.0	1.079	.903	-16.3
700.0	1.045	.879	-15.9
750.0	1.014	.856	-15.6
800.0	.984	.833	-15.4
850.0	.957	.811	-15.2
900.0	.931	.790	-15.2
950.0	.907	.769	-15.2
1000.0	.884	.749	-15.3
1050.0	.863	.730	-15.5
1100.0	.844	.711	-15.7
1150.0	.825	.694	-16.0
1200.0	.808	.677	-16.3
1250.0	.793	.661	-16.7
1300.0	.778	.645	-17.1
1350.0	.764	.631	-17.5
1400.0	.752	.617	-17.9
1450.0	.740	.604	-18.4
1500.0	.729	.592	-18.8
1550.0	.719	.581	-19.3
1600.0	.710	.570	-19.7
1650.0	.701	.560	-20.1
1700.0	.693	.550	-20.5
1750.0	.685	.542	-20.9
1800.0	.678	.533	-21.3
1850.0	.671	.526	-21.7
1900.0	.664	.518	-22.0
1950.0	.658	.512	-22.3
2000.0	.653	.505	-22.6
2050.0	.647	.499	-22.9
2100.0	.642	.493	-23.2
2150.0	.637	.487	-23.4
2200.0	.632	.482	-23.7
2250.0	.627	.476	-24.0
2300.0	.622	.471	-24.3
2350.0	.617	.465	-24.7
2400.0	.612	.459	-25.1
2450.0	.608	.452	-25.6
2500.0	.603	.446	-26.1

RMS ERROR= 19.9

Table 10

THERMAL CONDUCTIVITY MODELING OF CFC-113
R Z AXIS
UPPER BOUND

TEMPERATURE (K)	EXP. DATA	CAL. DATA	PERPDR
300.0	.641	.904	41.0
350.0	.633	.885	39.7
400.0	.625	.866	38.5
450.0	.616	.847	37.4
500.0	.607	.828	36.4
550.0	.597	.808	35.4
600.0	.587	.789	34.5
650.0	.576	.770	33.6
700.0	.565	.751	32.8
750.0	.555	.732	32.0
800.0	.544	.714	31.3
850.0	.533	.696	30.6
900.0	.522	.678	29.8
950.0	.512	.661	29.1
1000.0	.502	.645	28.5
1050.0	.492	.629	27.8
1100.0	.483	.613	27.1
1150.0	.474	.598	26.4
1200.0	.465	.584	25.6
1250.0	.457	.571	24.9
1300.0	.449	.558	24.1
1350.0	.442	.546	23.3
1400.0	.436	.534	22.5
1450.0	.430	.523	21.7
1500.0	.425	.513	20.8
1550.0	.420	.503	19.8
1600.0	.416	.494	18.9
1650.0	.413	.486	17.8
1700.0	.410	.478	16.8
1750.0	.407	.471	15.7
1800.0	.406	.465	14.6
1850.0	.404	.458	13.4
1900.0	.404	.453	12.2
1950.0	.403	.447	10.9
2000.0	.403	.442	9.6
2050.0	.404	.437	8.3
2100.0	.405	.433	6.9
2150.0	.406	.428	5.5
2200.0	.407	.424	4.1
2250.0	.409	.419	2.7
2300.0	.410	.415	1.2
2350.0	.412	.410	-.4
2400.0	.413	.405	-1.9
2450.0	.414	.400	-3.5
2500.0	.415	.394	-5.2

RMS ERROR= 24.1

Table 11

THERMAL CONDUCTIVITY MODELING OF CICC R
B Z AXIS
LOWER BOUND

TEMPERATURE (K)	EXP. DATA	CAL. DATA	ERROR
300.0	.641	.720	12.4
350.0	.633	.703	11.0
400.0	.625	.686	9.7
450.0	.616	.668	8.5
500.0	.607	.651	7.4
550.0	.597	.635	6.3
600.0	.587	.618	5.4
650.0	.576	.602	4.5
700.0	.565	.586	3.6
750.0	.555	.570	2.8
800.0	.544	.555	2.1
850.0	.533	.540	1.3
900.0	.522	.526	.6
950.0	.512	.512	-.0
1000.0	.502	.498	-.7
1050.0	.492	.485	-1.4
1100.0	.483	.473	-2.0
1150.0	.474	.461	-2.7
1200.0	.465	.449	-3.3
1250.0	.457	.439	-4.0
1300.0	.449	.428	-4.7
1350.0	.442	.418	-5.4
1400.0	.436	.409	-6.1
1450.0	.430	.400	-6.9
1500.0	.425	.392	-7.7
1550.0	.420	.384	-8.5
1600.0	.416	.377	-9.4
1650.0	.413	.370	-10.3
1700.0	.410	.364	-11.2
1750.0	.407	.358	-12.2
1800.0	.406	.352	-13.2
1850.0	.404	.347	-14.2
1900.0	.404	.342	-15.3
1950.0	.403	.337	-16.4
2000.0	.403	.333	-17.5
2050.0	.404	.329	-18.6
2100.0	.405	.325	-19.7
2150.0	.406	.321	-20.9
2200.0	.407	.317	-22.0
2250.0	.409	.314	-23.2
2300.0	.410	.310	-24.4
2350.0	.412	.306	-25.6
2400.0	.413	.302	-26.8
2450.0	.414	.298	-28.0
2500.0	.415	.294	-29.3

RMS ERROR= 13.6

Table 12

THERMAL CONDUCTIVITY MODELING OF CFCC C
C X AXIS
UPPER BOUND

TEMPERATURE (K)	EXP. DATA	CAL. DATA	%ERROR
350.0	.624	.658	5.5
400.0	.616	.647	5.0
450.0	.608	.636	4.6
500.0	.600	.625	4.1
550.0	.591	.613	3.6
600.0	.582	.600	3.1
650.0	.573	.588	2.6
700.0	.563	.575	2.1
750.0	.554	.562	1.6
800.0	.544	.550	1.0
850.0	.534	.537	.5
900.0	.525	.524	-.1
950.0	.515	.512	-.6
1000.0	.506	.500	-1.2
1050.0	.497	.488	-1.7
1100.0	.488	.477	-2.3
1150.0	.479	.466	-2.8
1200.0	.471	.455	-3.4
1250.0	.463	.445	-3.9
1300.0	.455	.435	-4.4
1350.0	.448	.426	-4.9
1400.0	.441	.417	-5.3
1450.0	.434	.409	-5.8
1500.0	.428	.401	-6.2
1550.0	.422	.394	-6.6
1600.0	.417	.388	-7.0
1650.0	.412	.381	-7.3
1700.0	.407	.376	-7.6
1750.0	.403	.371	-7.9
1800.0	.399	.366	-8.2
1850.0	.396	.362	-8.4
1900.0	.393	.359	-8.6
1950.0	.390	.356	-8.8
2000.0	.388	.353	-9.0
2050.0	.386	.350	-9.2
2100.0	.384	.348	-9.3
2150.0	.383	.346	-9.4
2200.0	.381	.345	-9.6
2250.0	.380	.343	-9.7
2300.0	.380	.342	-9.9
2350.0	.379	.341	-10.1
2400.0	.378	.339	-10.3
2450.0	.377	.338	-10.5
2500.0	.377	.336	-10.7

RMS ERROR= 6.6

TABLE 13

THERMAL CONDUCTIVITY MODELING OF CFCC C
C X AXIS
LOWER BOUND

TEMPERATURE (K)	EXP. DATA	CAL. DATA	ERROR
350.0	.624	.539	-13.7
400.0	.616	.530	-14.1
450.0	.608	.520	-14.5
500.0	.600	.511	-14.9
550.0	.591	.501	-15.3
600.0	.582	.491	-15.7
650.0	.573	.480	-16.1
700.0	.563	.470	-16.5
750.0	.554	.460	-17.0
800.0	.544	.450	-17.4
850.0	.534	.439	-17.8
900.0	.525	.429	-18.2
950.0	.515	.419	-18.6
1000.0	.506	.410	-19.1
1050.0	.497	.400	-19.5
1100.0	.488	.391	-19.9
1150.0	.479	.382	-20.3
1200.0	.471	.373	-20.7
1250.0	.463	.365	-21.1
1300.0	.455	.357	-21.6
1350.0	.448	.349	-22.0
1400.0	.441	.342	-22.4
1450.0	.434	.335	-22.8
1500.0	.428	.329	-23.1
1550.0	.422	.323	-23.5
1600.0	.417	.317	-23.9
1650.0	.412	.312	-24.3
1700.0	.407	.307	-24.6
1750.0	.403	.302	-25.0
1800.0	.399	.298	-25.3
1850.0	.396	.294	-25.7
1900.0	.393	.291	-26.0
1950.0	.390	.287	-26.3
2000.0	.388	.284	-26.7
2050.0	.386	.282	-27.0
2100.0	.384	.279	-27.3
2150.0	.383	.277	-27.7
2200.0	.381	.275	-28.0
2250.0	.380	.273	-28.4
2300.0	.380	.271	-28.7
2350.0	.379	.269	-29.1
2400.0	.378	.267	-29.5
2450.0	.377	.265	-29.9
2500.0	.377	.262	-30.4

RMS ERROR= 22.8

TABLE 14

THERMAL CONDUCTIVITY MODELING OF CFCC C
C Z AXIS
UPPER BOUND

TEMPERATURE (K)	EXP. DATA	CAL. DATA	%ERROR
350.0	.894	.825	-7.7
400.0	.886	.811	-8.5
450.0	.877	.797	-9.2
500.0	.868	.782	-9.9
550.0	.857	.767	-10.5
600.0	.846	.752	-11.2
650.0	.834	.736	-11.7
700.0	.822	.721	-12.3
750.0	.810	.706	-12.8
800.0	.797	.690	-13.3
850.0	.784	.675	-13.8
900.0	.770	.660	-14.3
950.0	.757	.646	-14.7
1000.0	.743	.631	-15.1
1050.0	.730	.617	-15.5
1100.0	.717	.603	-15.9
1150.0	.704	.590	-16.2
1200.0	.691	.577	-16.5
1250.0	.679	.564	-16.8
1300.0	.666	.552	-17.1
1350.0	.655	.541	-17.4
1400.0	.643	.530	-17.6
1450.0	.632	.519	-17.9
1500.0	.622	.509	-18.1
1550.0	.612	.500	-18.3
1600.0	.603	.491	-18.5
1650.0	.594	.483	-18.7
1700.0	.586	.475	-18.9
1750.0	.578	.468	-19.1
1800.0	.571	.461	-19.3
1850.0	.565	.455	-19.5
1900.0	.559	.449	-19.7
1950.0	.554	.443	-19.9
2000.0	.549	.438	-20.1
2050.0	.545	.434	-20.4
2100.0	.541	.429	-20.7
2150.0	.538	.425	-21.0
2200.0	.536	.421	-21.4
2250.0	.534	.418	-21.7
2300.0	.532	.414	-22.2
2350.0	.531	.411	-22.7
2400.0	.530	.407	-23.2
2450.0	.530	.404	-23.8
2500.0	.529	.400	-24.5

RMS ERROR= 17.5

TABLE 15

THERMAL CONDUCTIVITY MODELING OF CFCC C
C Z AXIS
LOWER BOUND

TEMPERATURE (K)	EXP. DATA	CAL. DATA	%ERROR
350.0	.894	.763	-14.6
400.0	.886	.750	-15.3
450.0	.877	.737	-16.0
500.0	.868	.723	-16.7
550.0	.857	.709	-17.3
600.0	.846	.695	-17.9
650.0	.834	.681	-18.4
700.0	.822	.667	-18.9
750.0	.810	.653	-19.4
800.0	.797	.639	-19.8
850.0	.784	.625	-20.3
900.0	.770	.611	-20.7
950.0	.757	.598	-21.0
1000.0	.743	.584	-21.4
1050.0	.730	.571	-21.7
1100.0	.717	.559	-22.1
1150.0	.704	.546	-22.4
1200.0	.691	.535	-22.7
1250.0	.679	.523	-22.9
1300.0	.666	.512	-23.2
1350.0	.655	.501	-23.4
1400.0	.643	.491	-23.7
1450.0	.632	.481	-23.9
1500.0	.622	.472	-24.1
1550.0	.612	.463	-24.4
1600.0	.603	.455	-24.6
1650.0	.594	.447	-24.8
1700.0	.586	.439	-25.0
1750.0	.578	.432	-25.2
1800.0	.571	.426	-25.5
1850.0	.565	.419	-25.7
1900.0	.559	.414	-26.0
1950.0	.554	.408	-26.3
2000.0	.549	.403	-26.6
2050.0	.545	.398	-26.9
2100.0	.541	.394	-27.3
2150.0	.538	.389	-27.7
2200.0	.536	.385	-28.1
2250.0	.534	.381	-28.6
2300.0	.532	.377	-29.1
2350.0	.531	.373	-29.7
2400.0	.530	.369	-30.3
2450.0	.530	.366	-31.0
2500.0	.529	.362	-31.7

RMS ERROR= 23.8

TABLE 16.

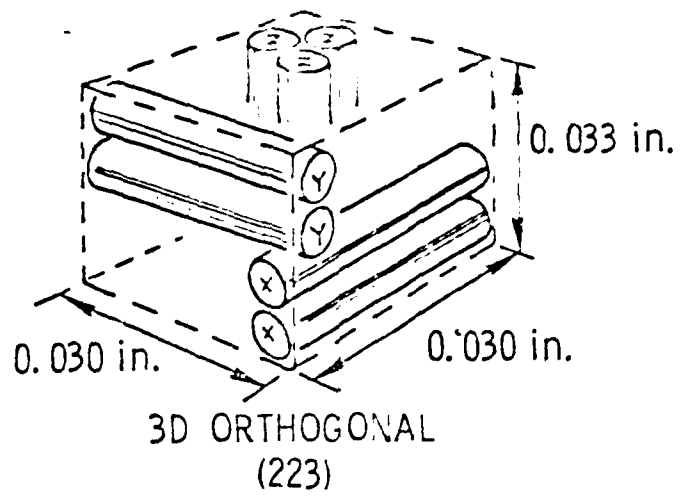


Figure 1

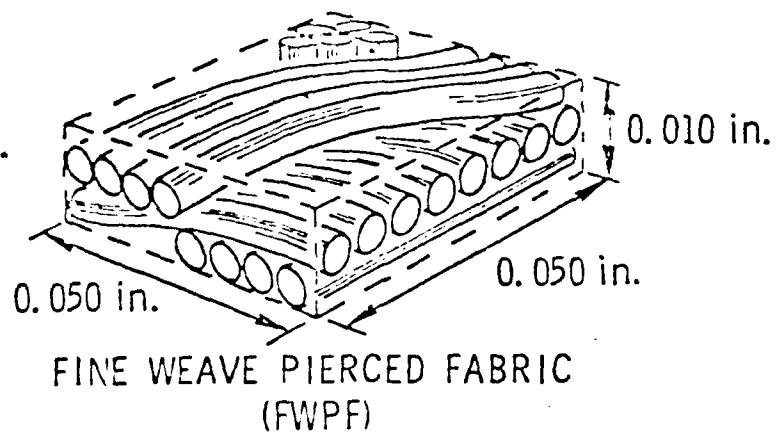


Figure 2

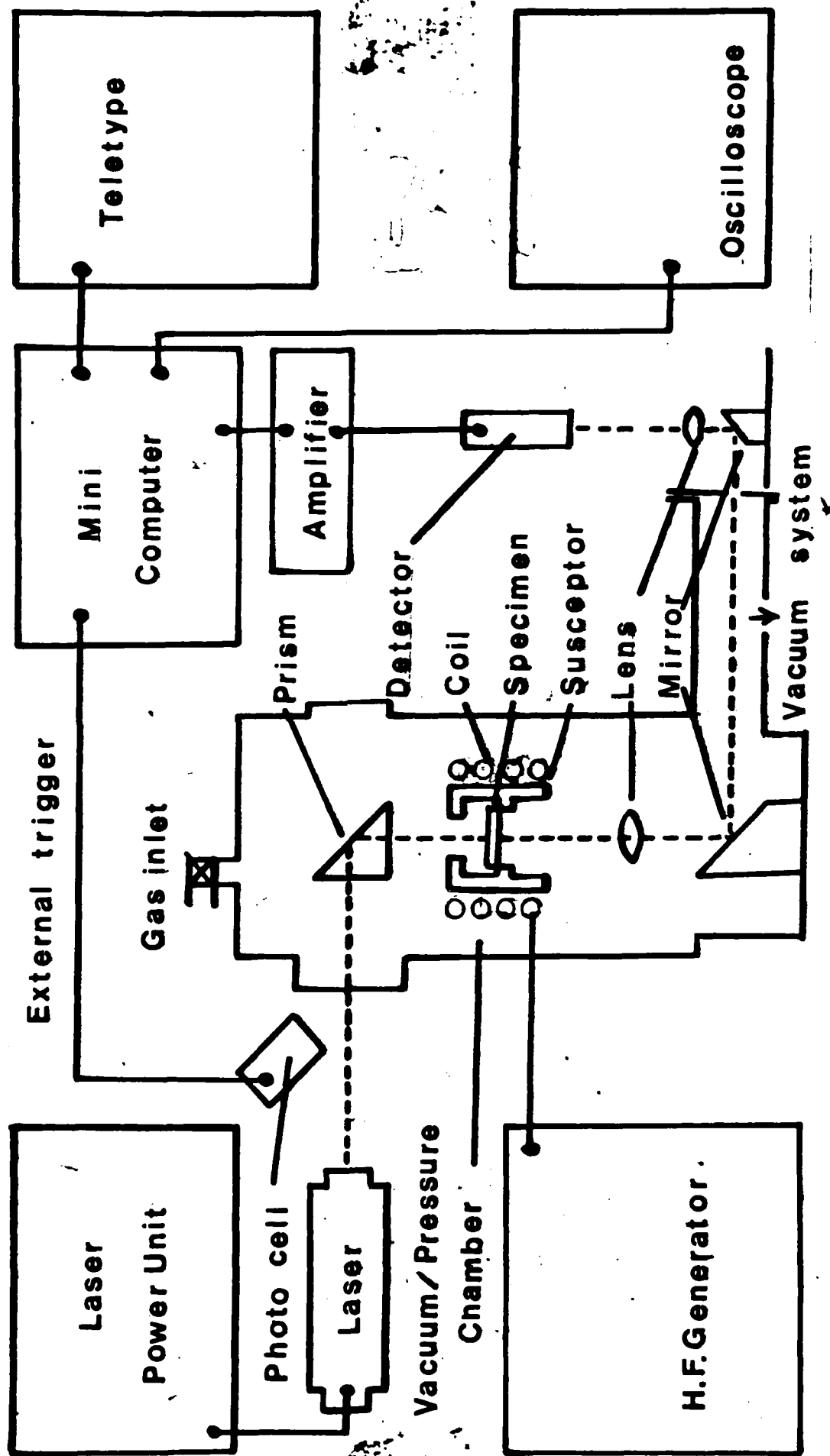


FIGURE 3

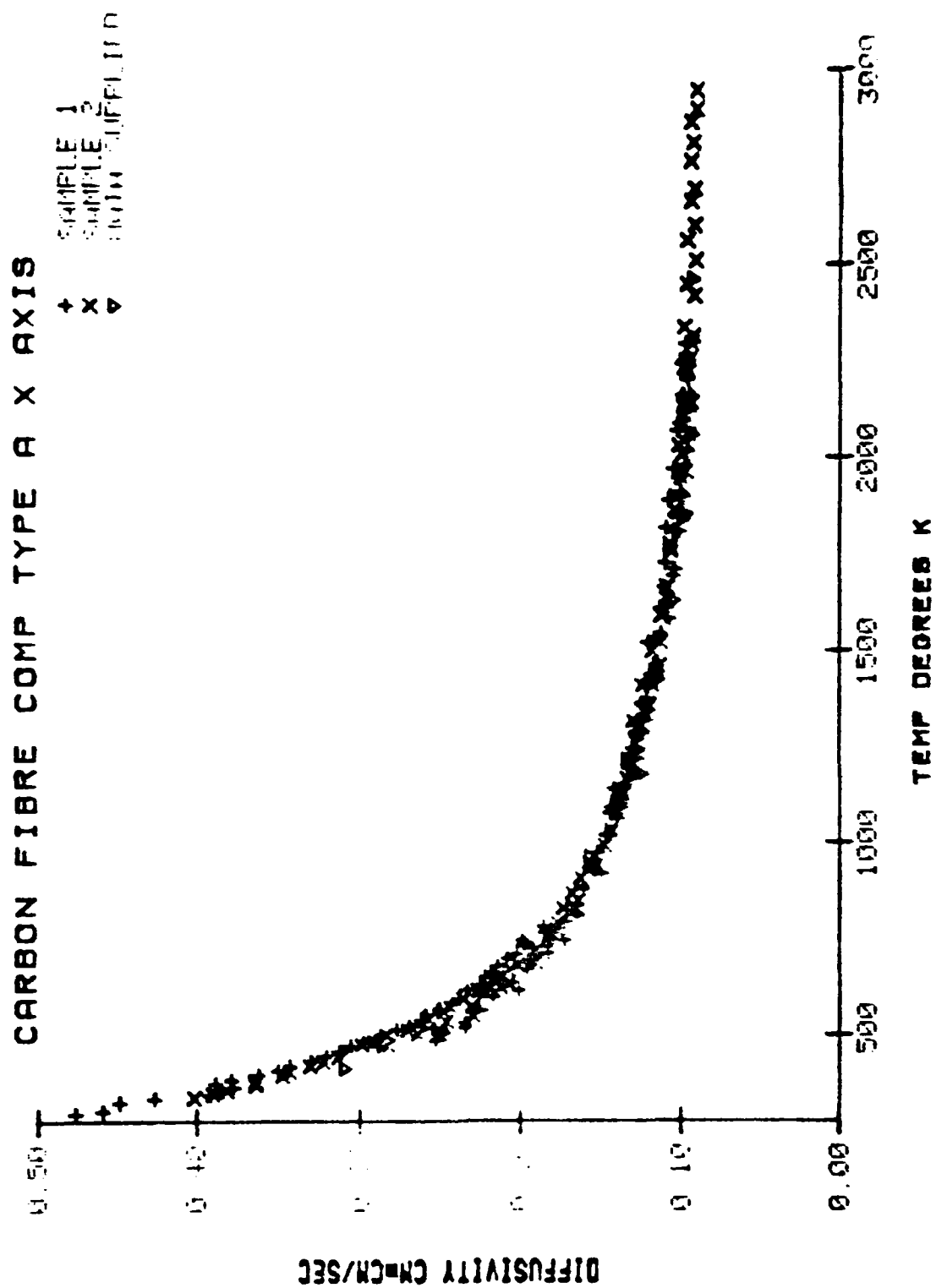
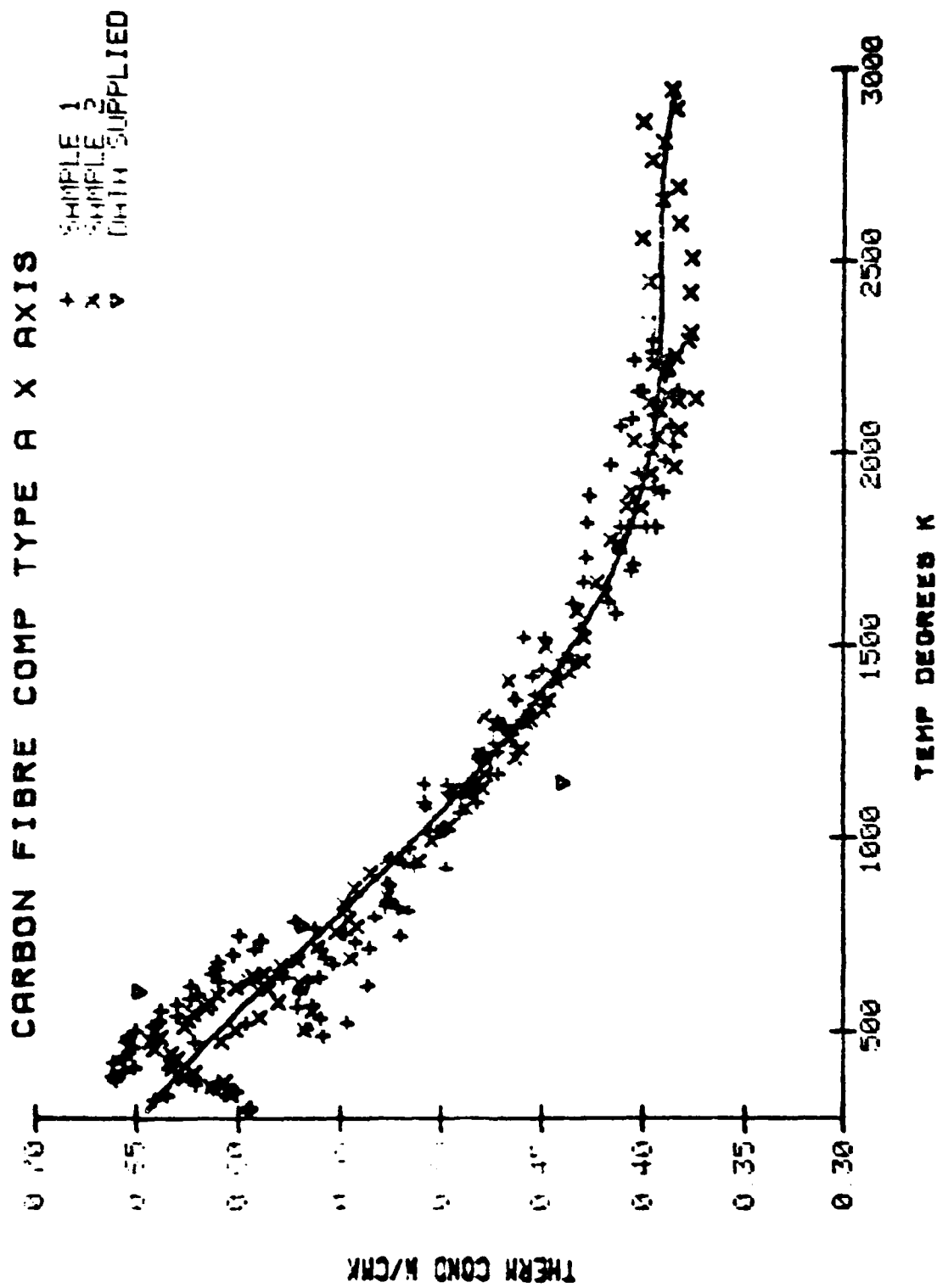
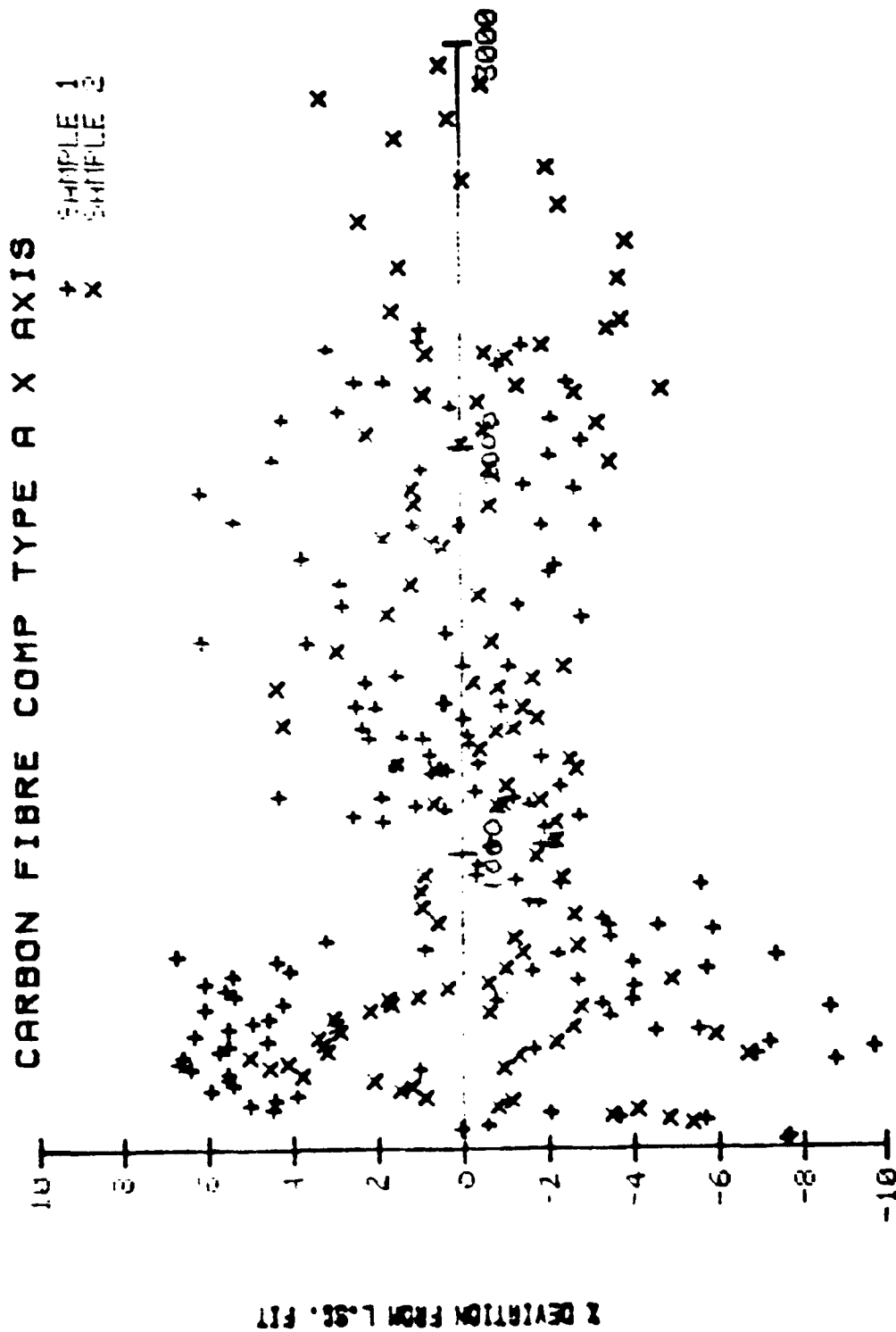


Figure 4





TEMP DEGREES K

Figure 6

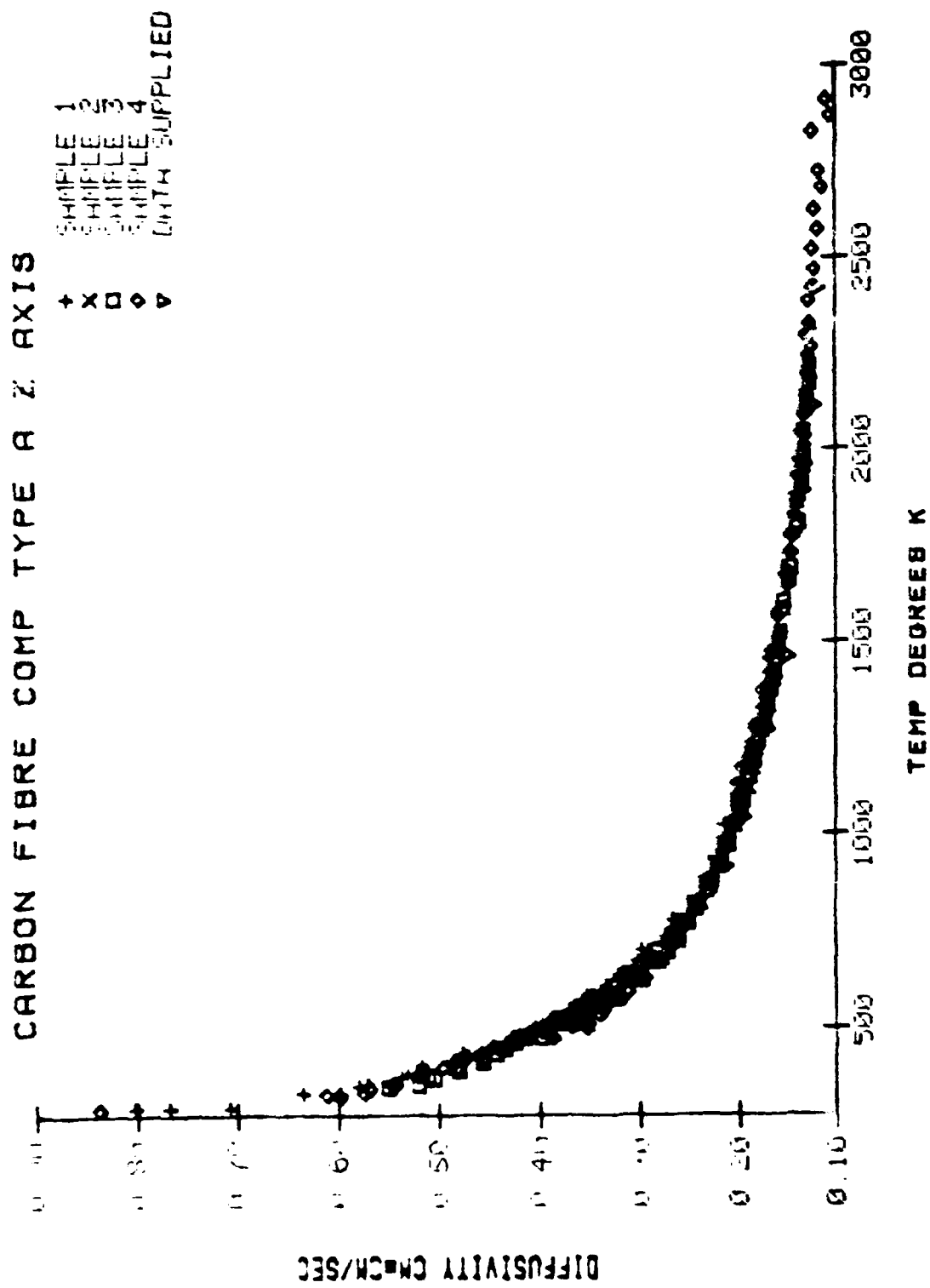
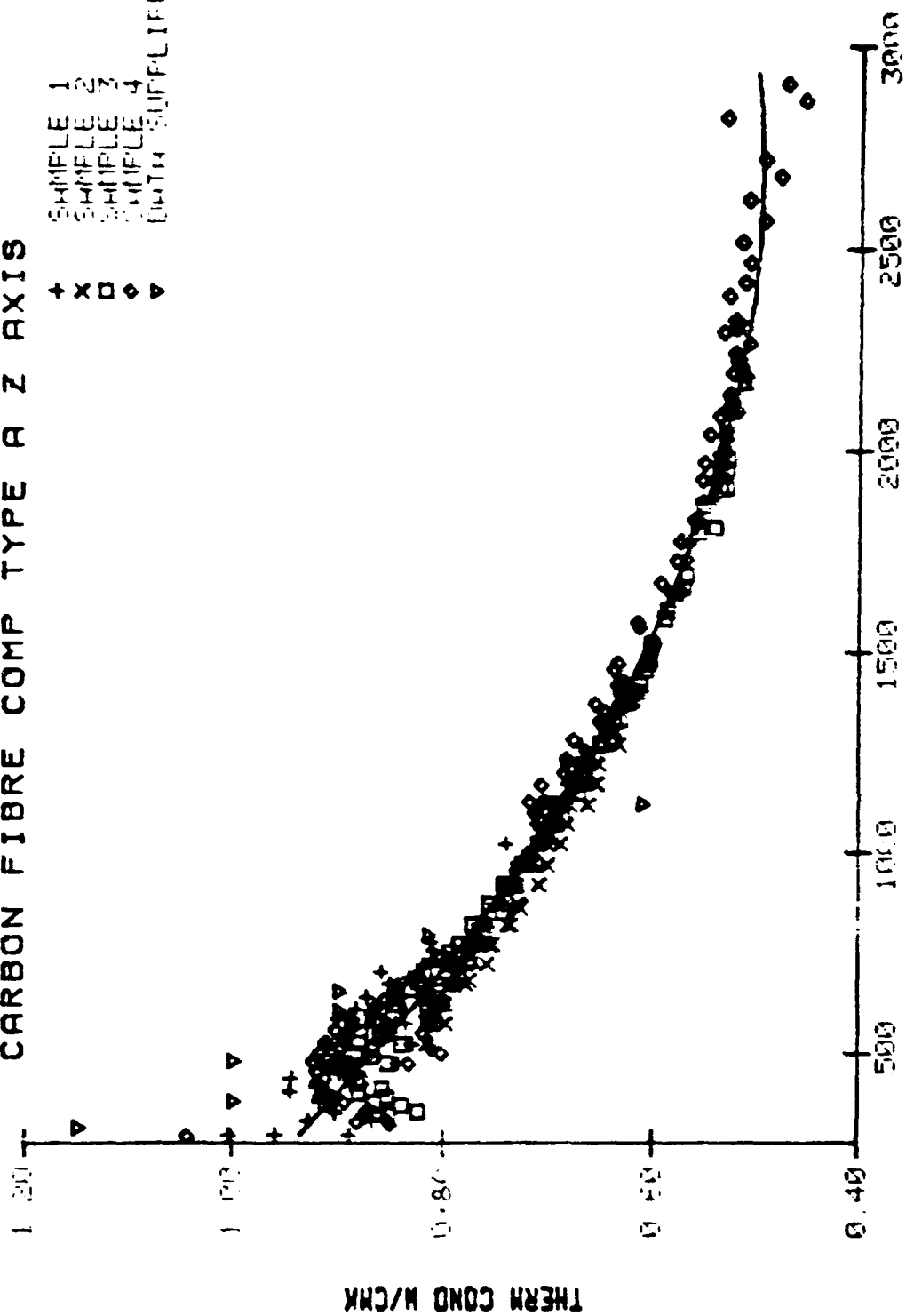


Figure 7

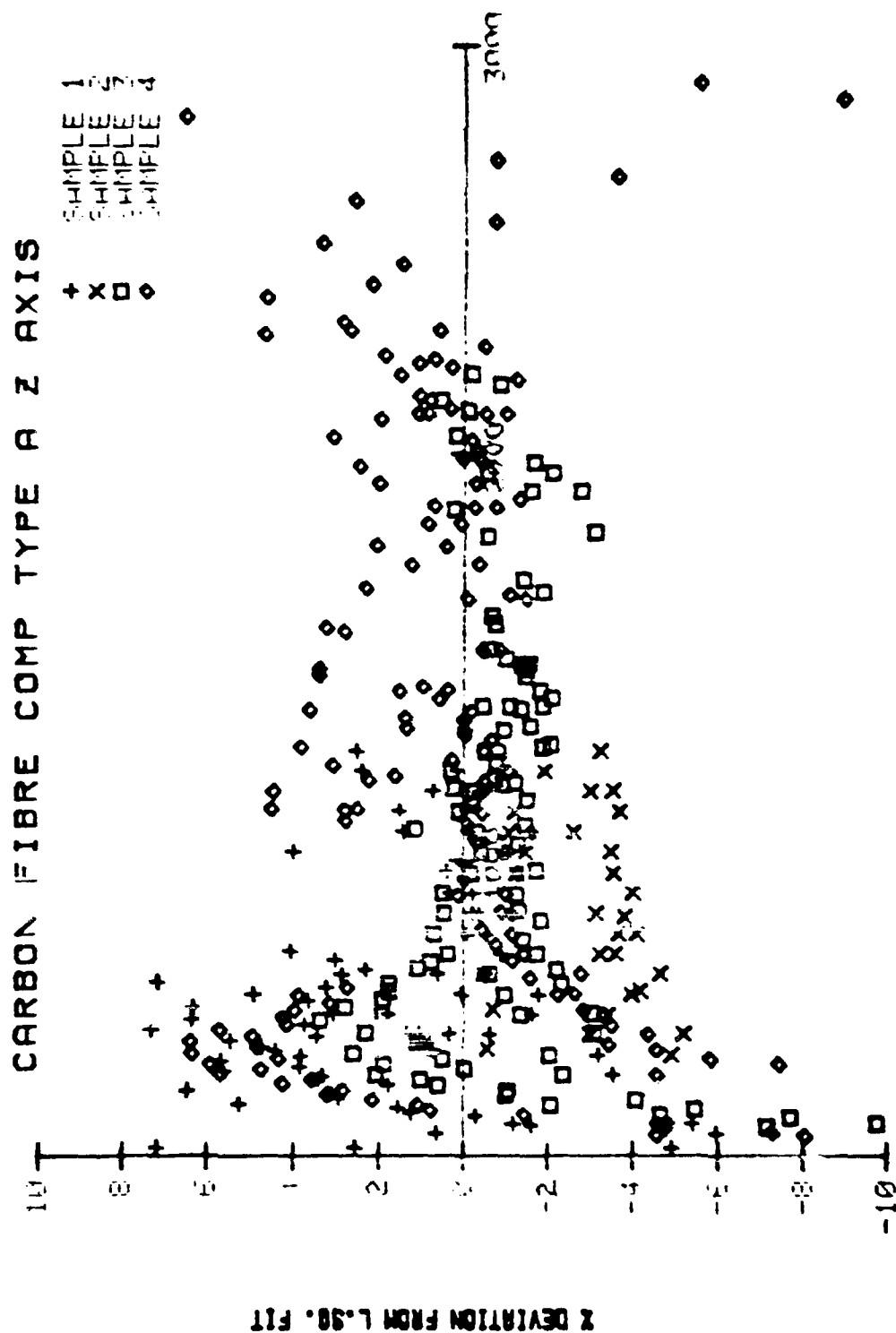
CARBON FIBRE COMP TYPE A Z AXIS

+ SAMPLE 1
 x SAMPLE 2
 o SAMPLE 3
 o SAMPLE 4
 v DATA SUPPLIED



TEMP DEGREES K

Figure 6



TEMP DEGREES K

Figure 9

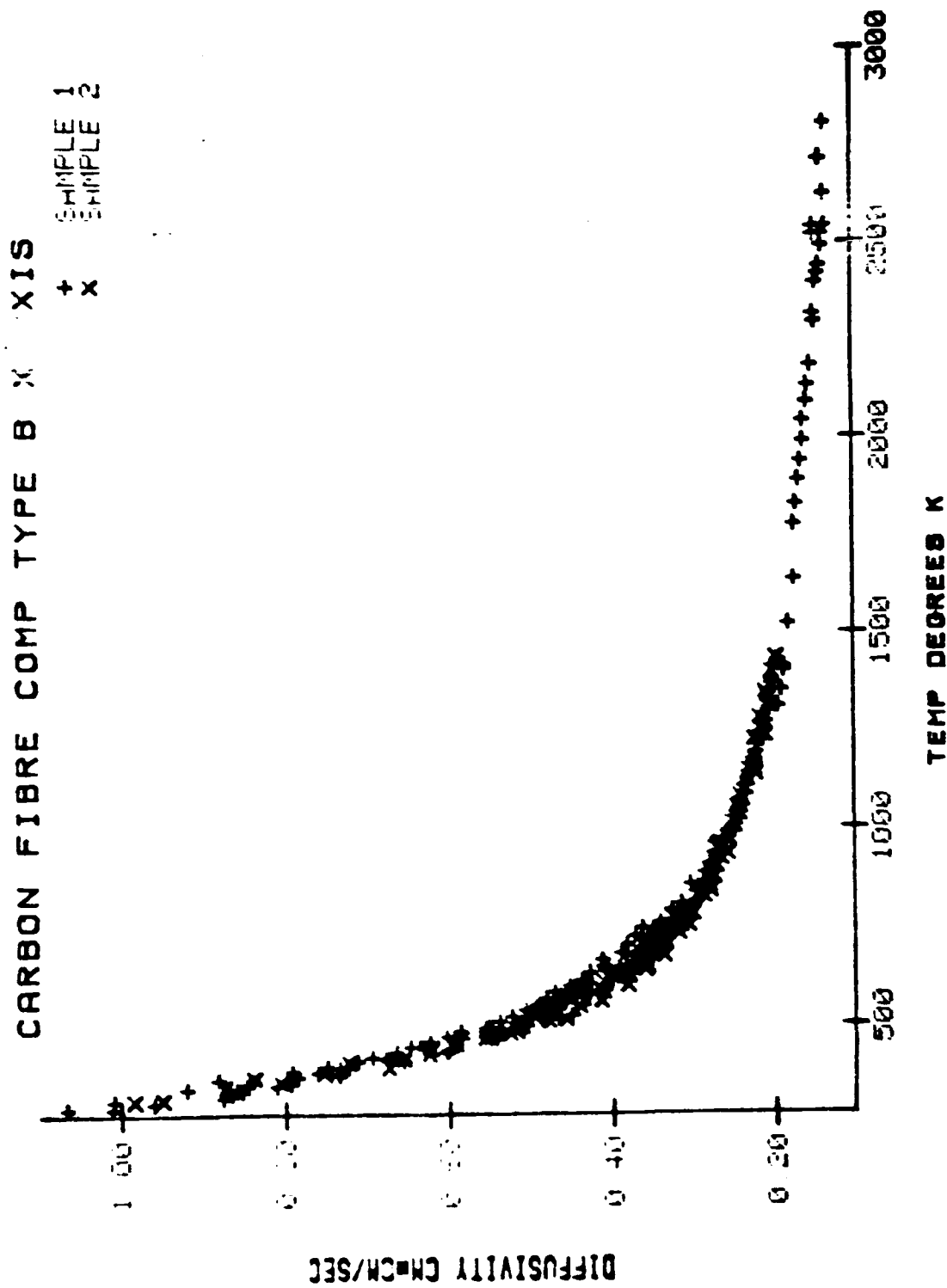


Figure 10

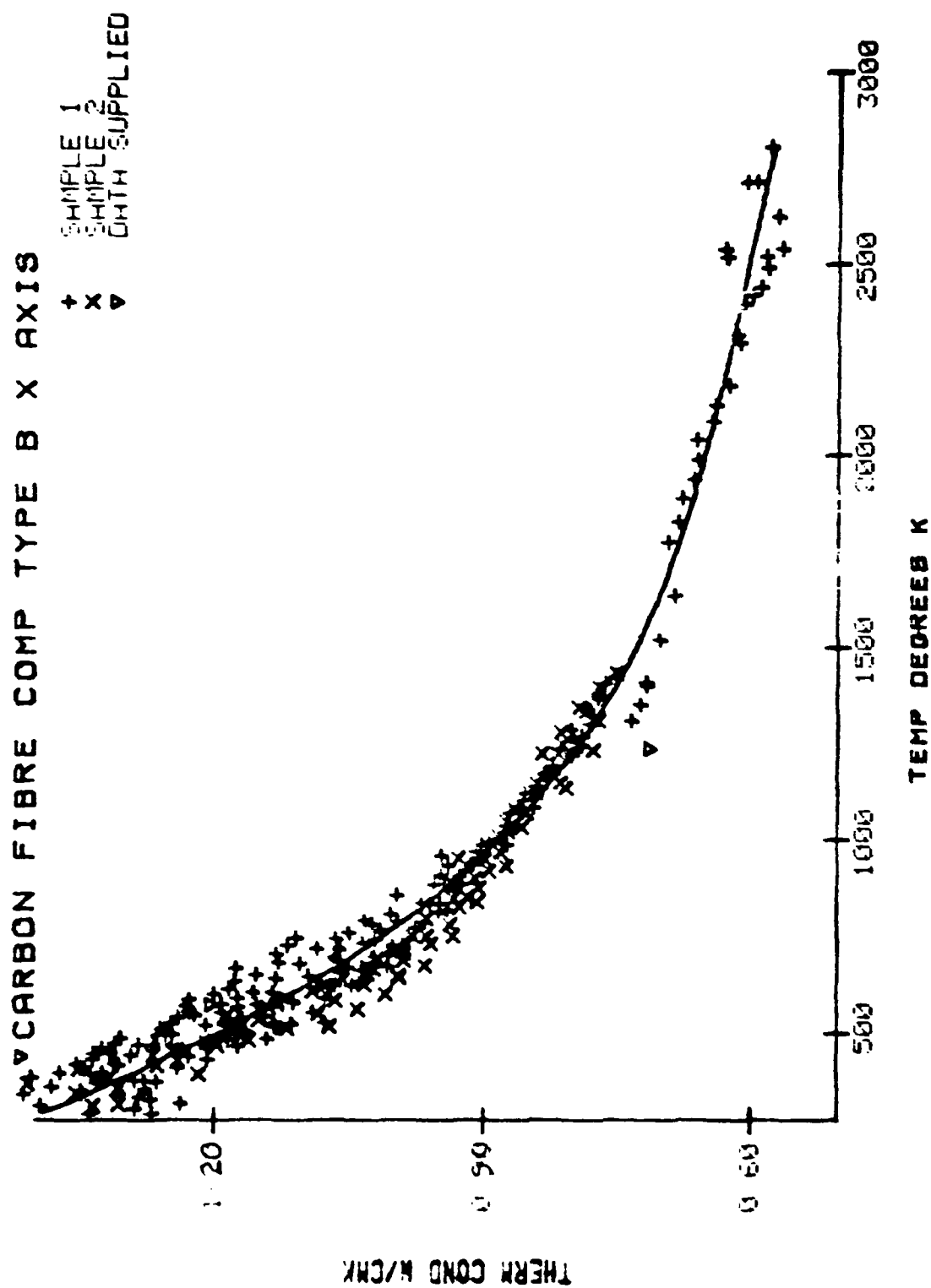
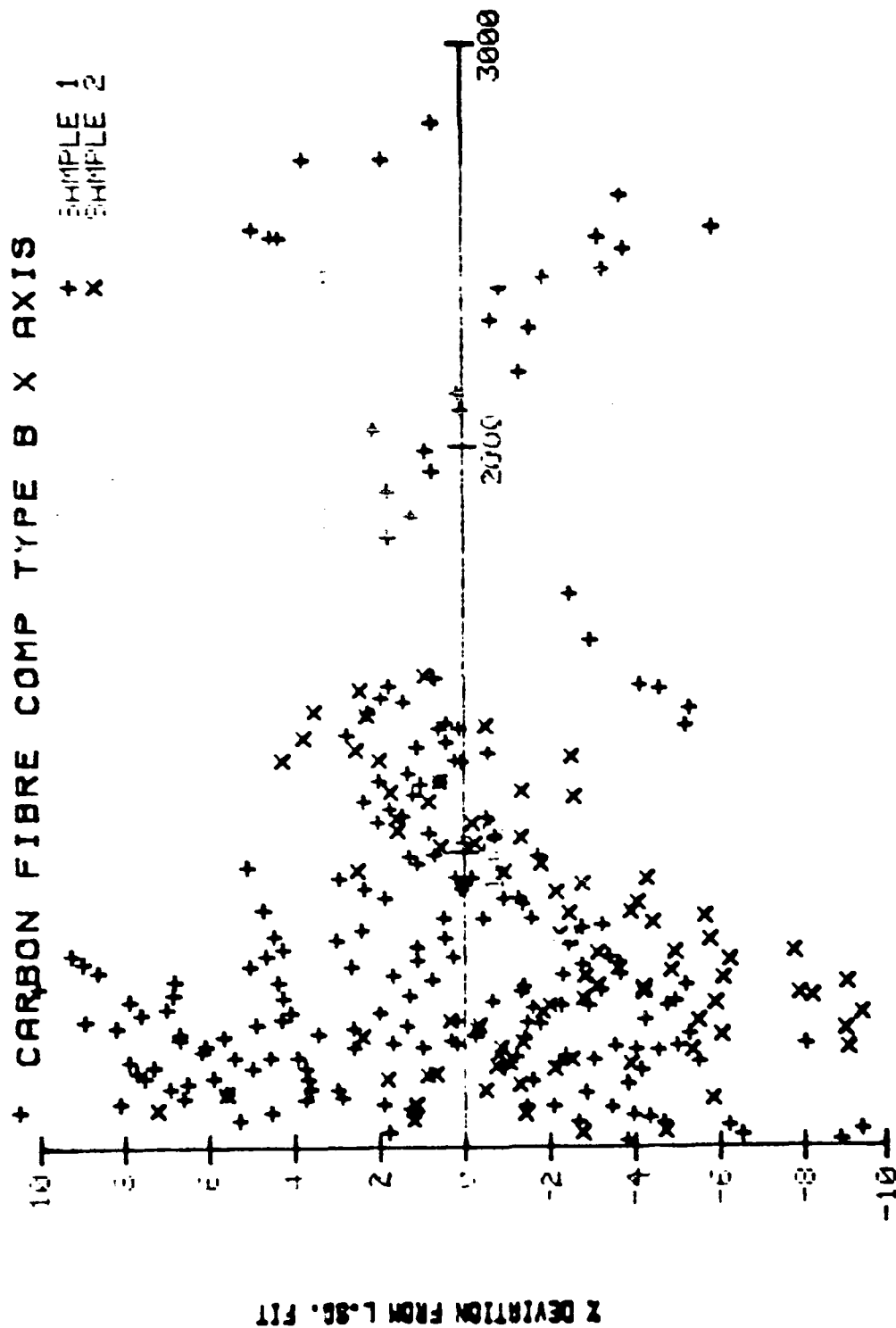


Figure 11



TEMP DEGREES K

Figure 12

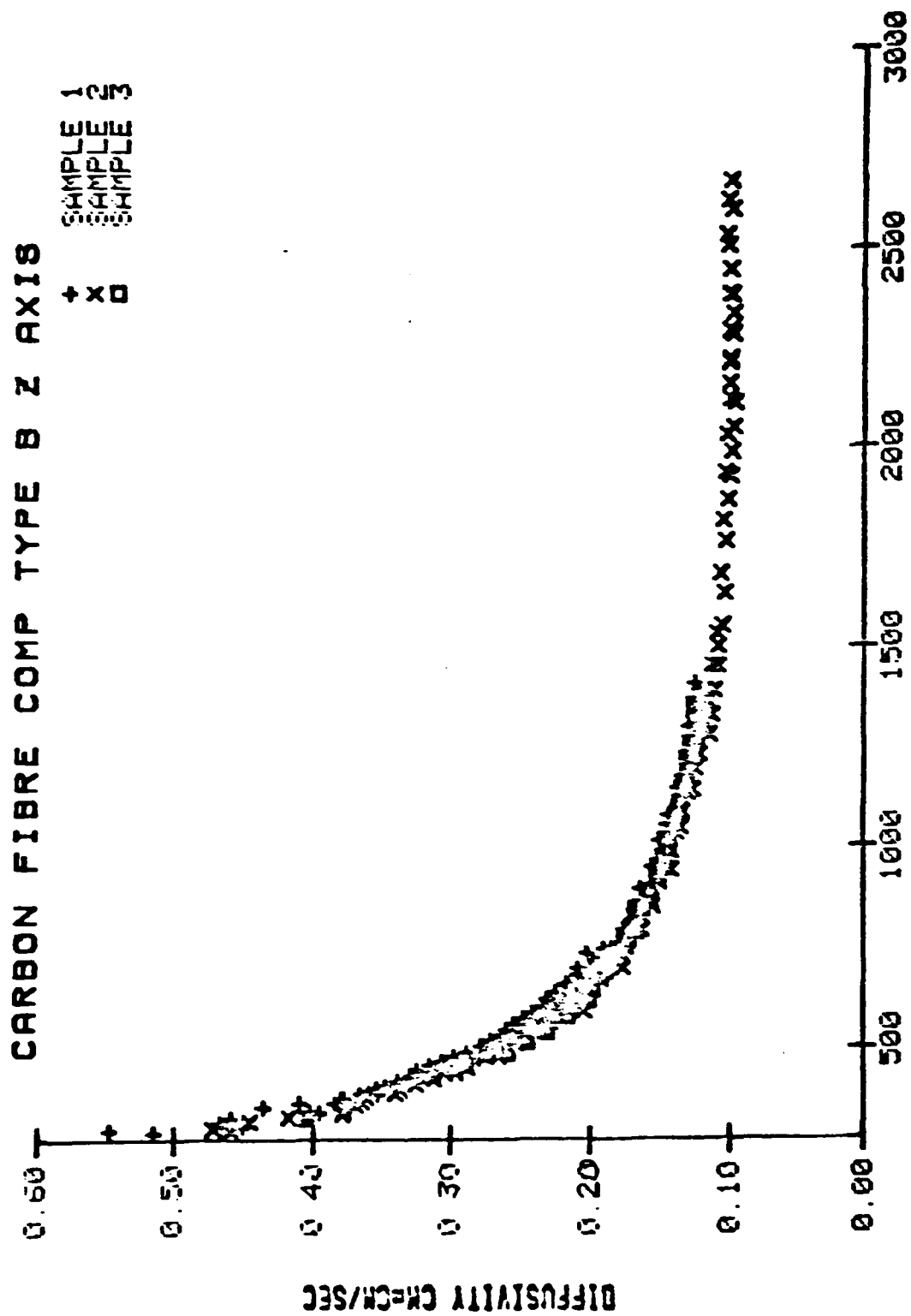


Figure 13

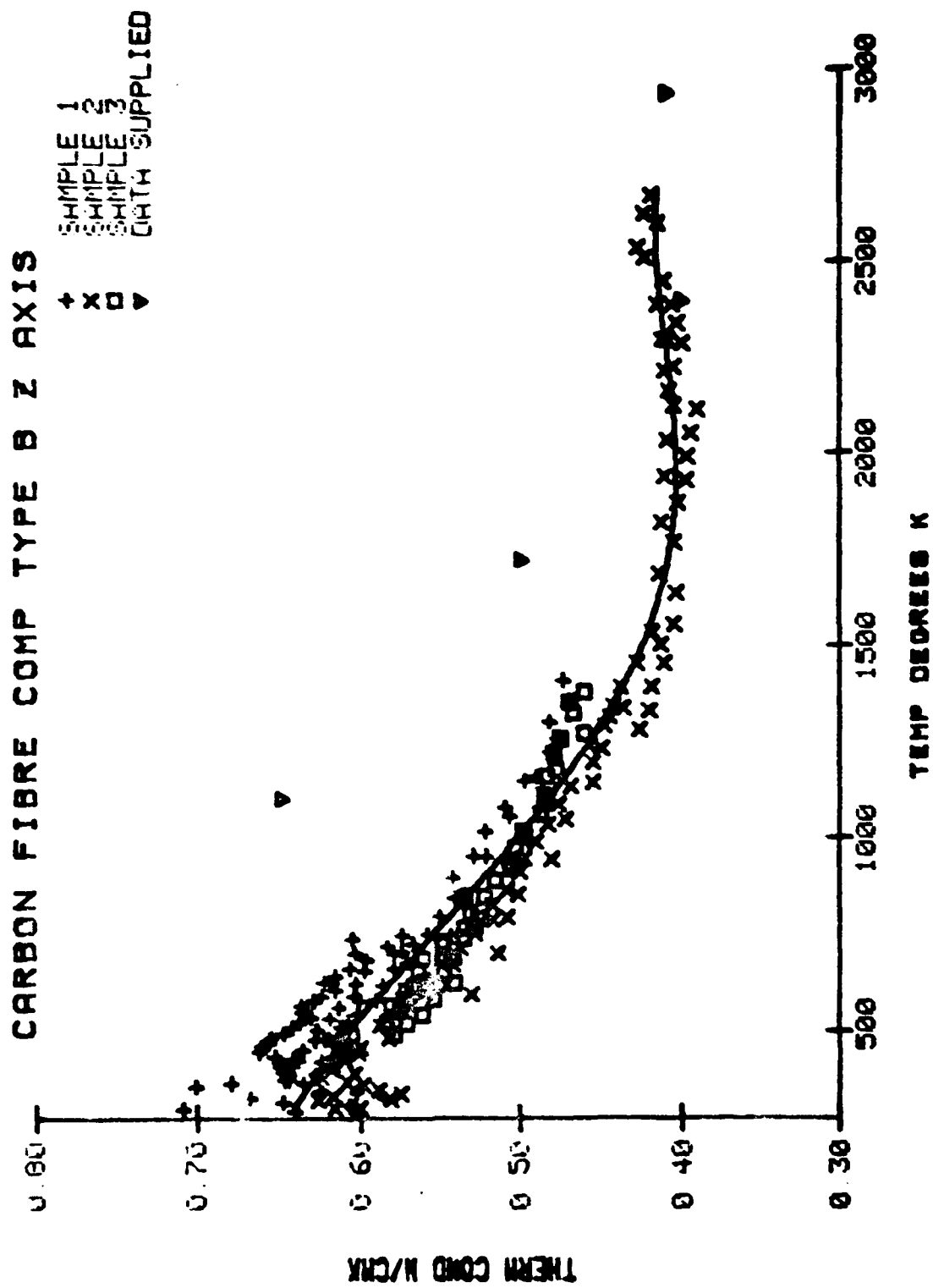
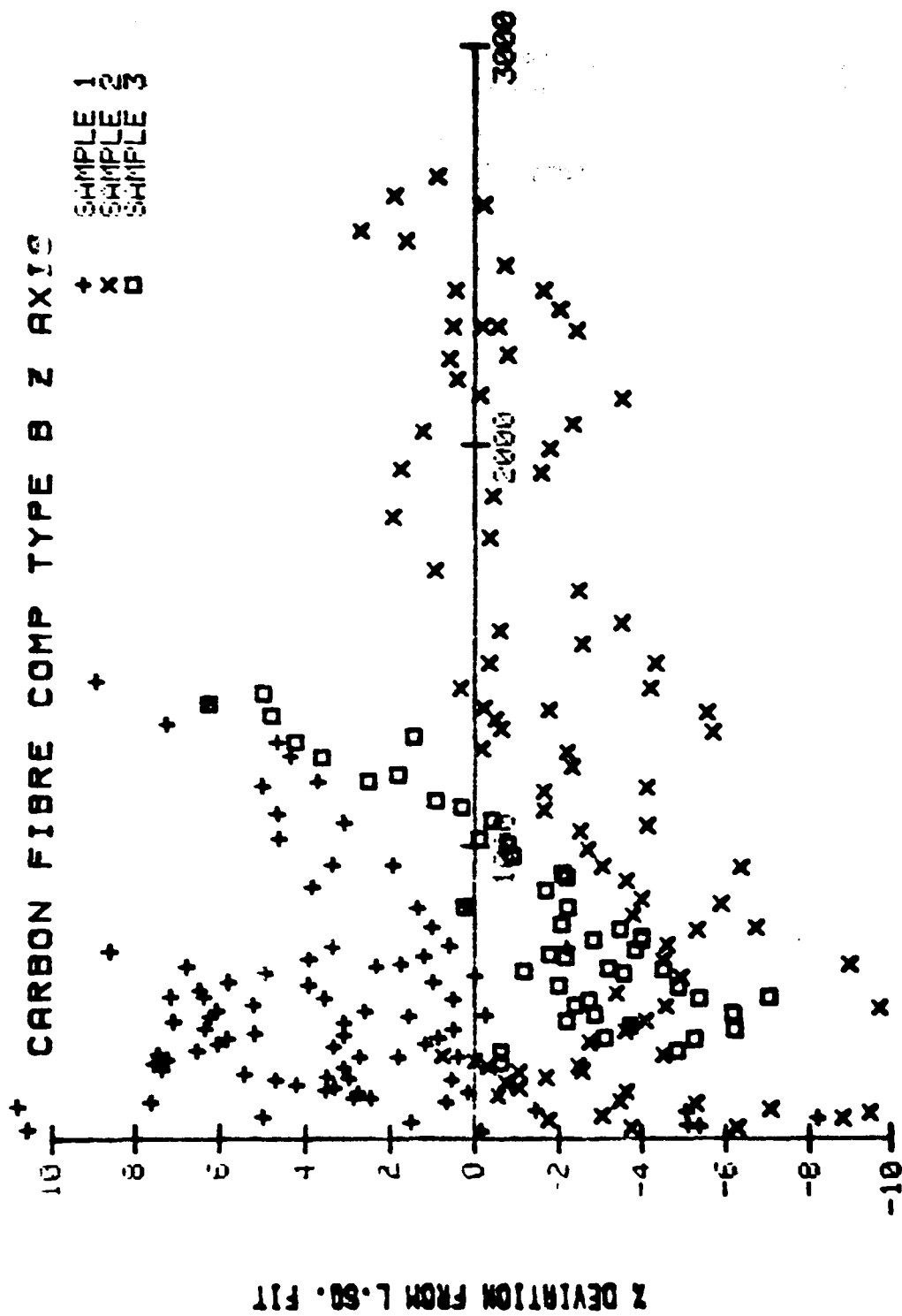


Figure 14



TEMP DEGREES K

Figure 15

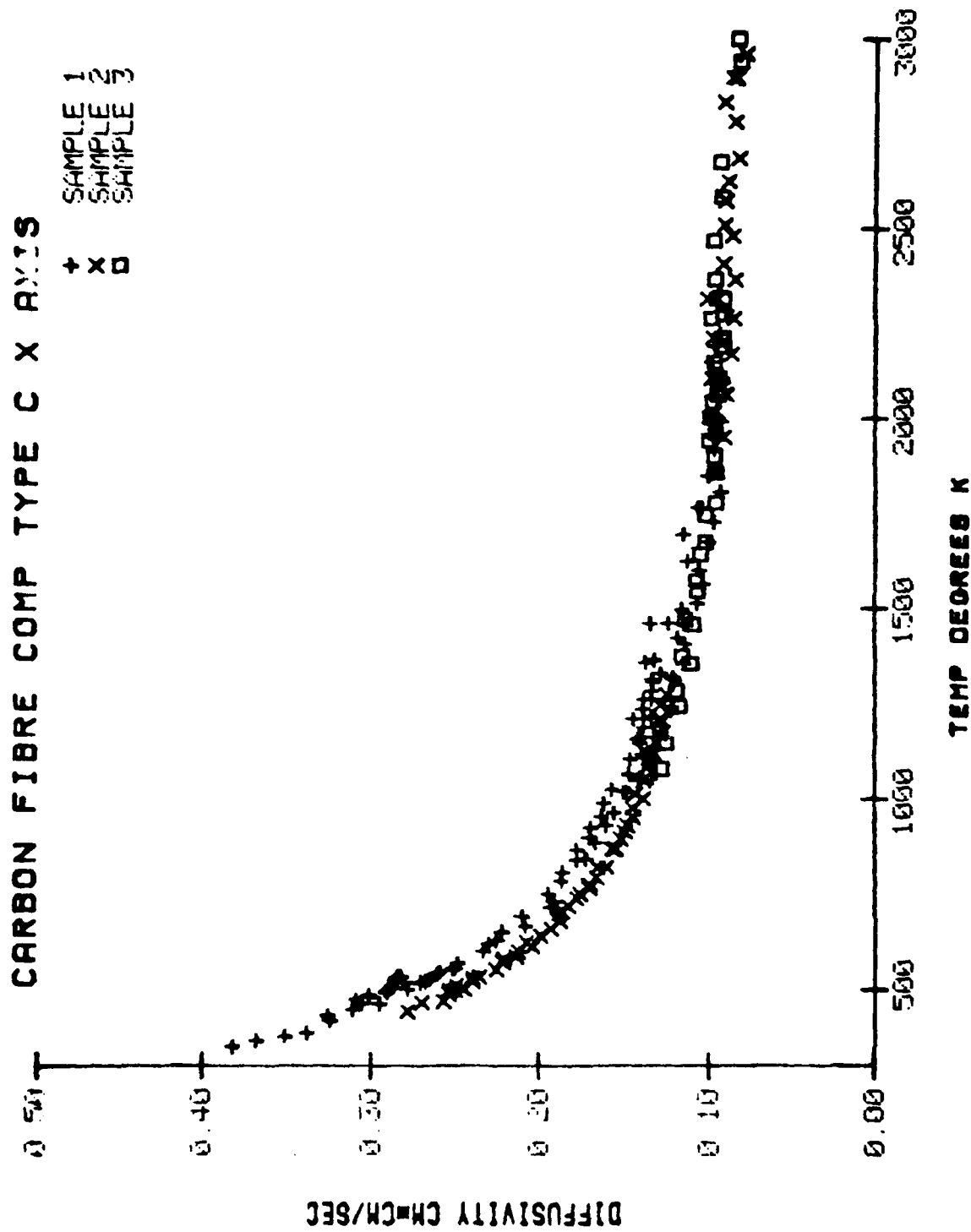


Figure 16

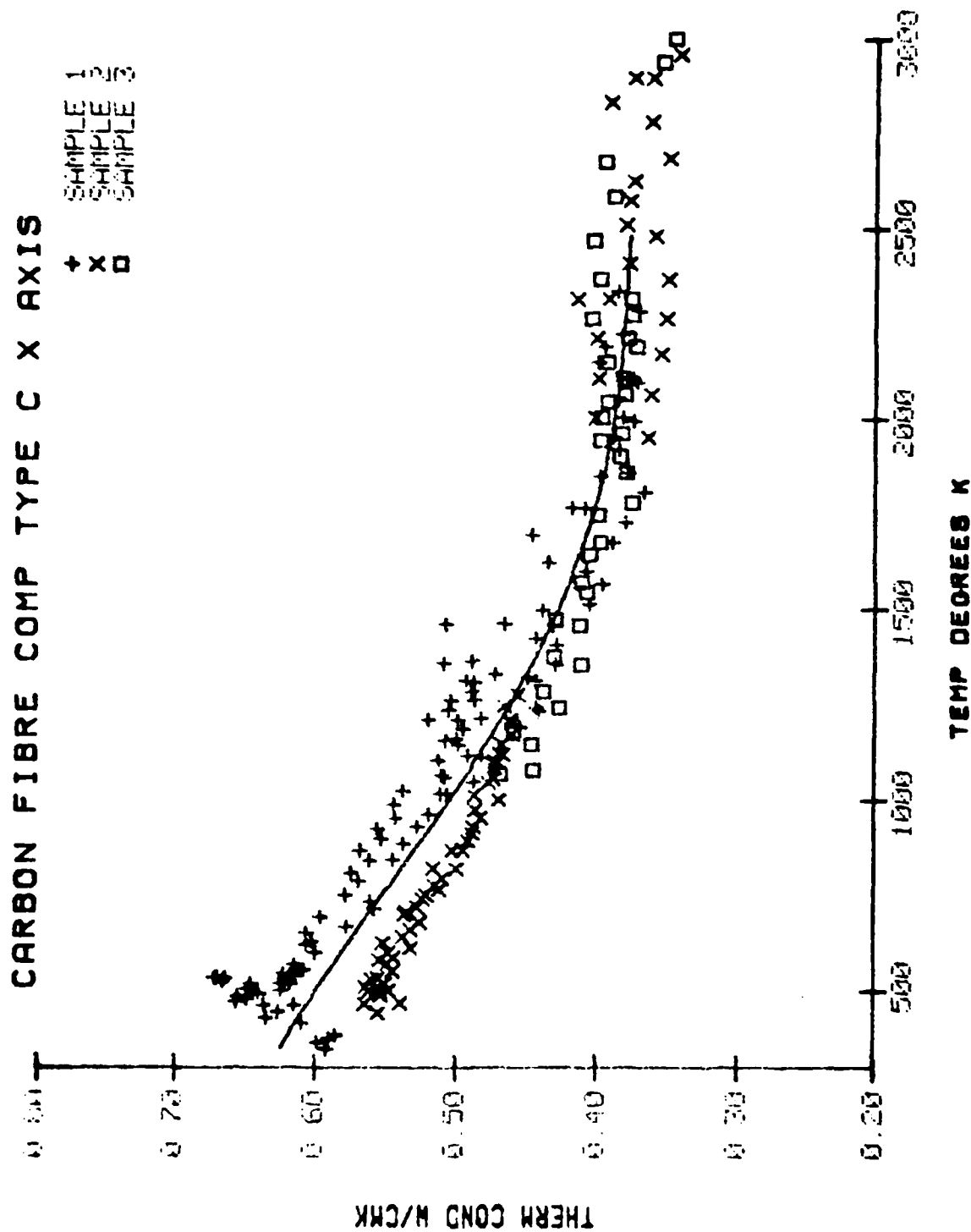


Figure 17

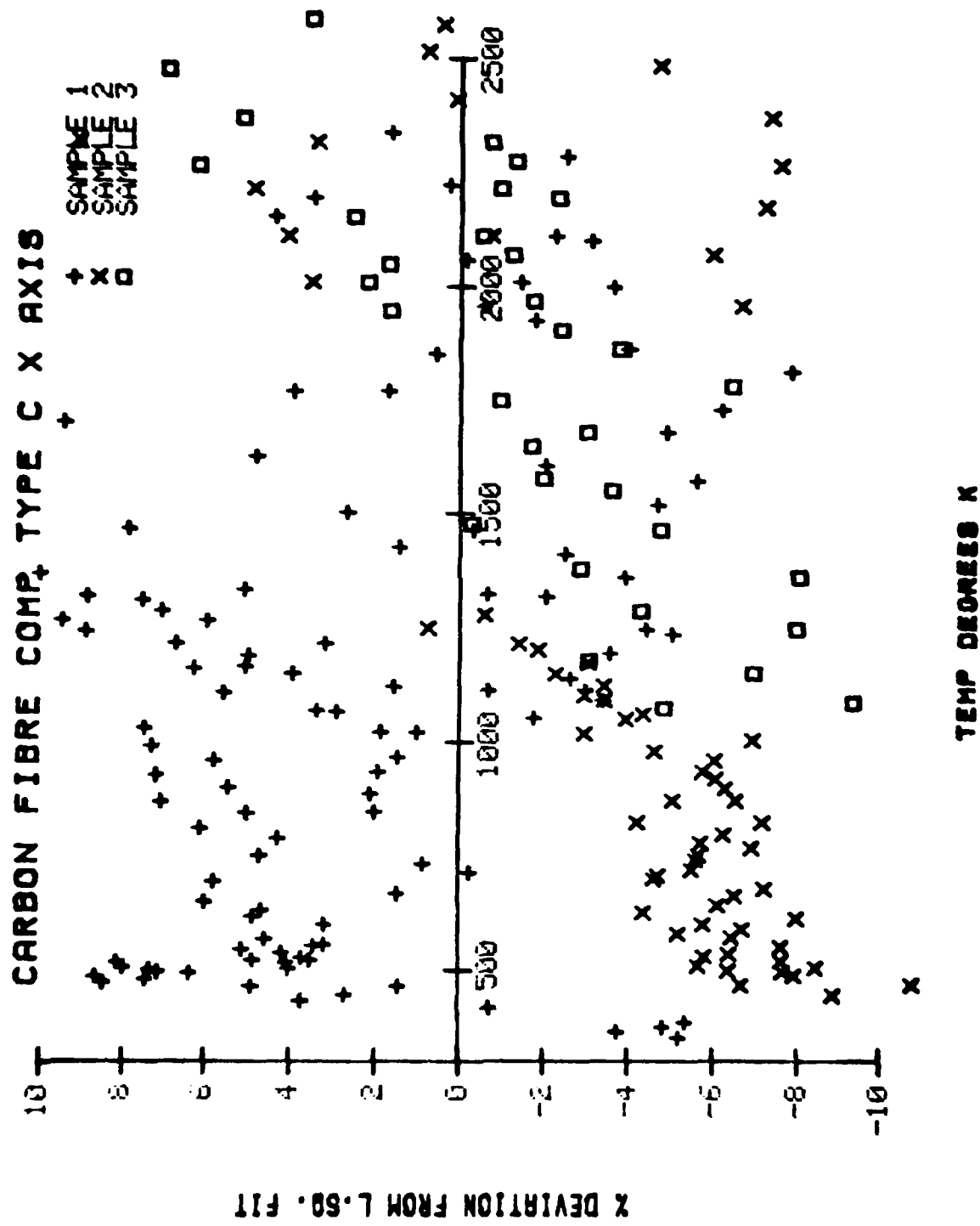


Figure 18

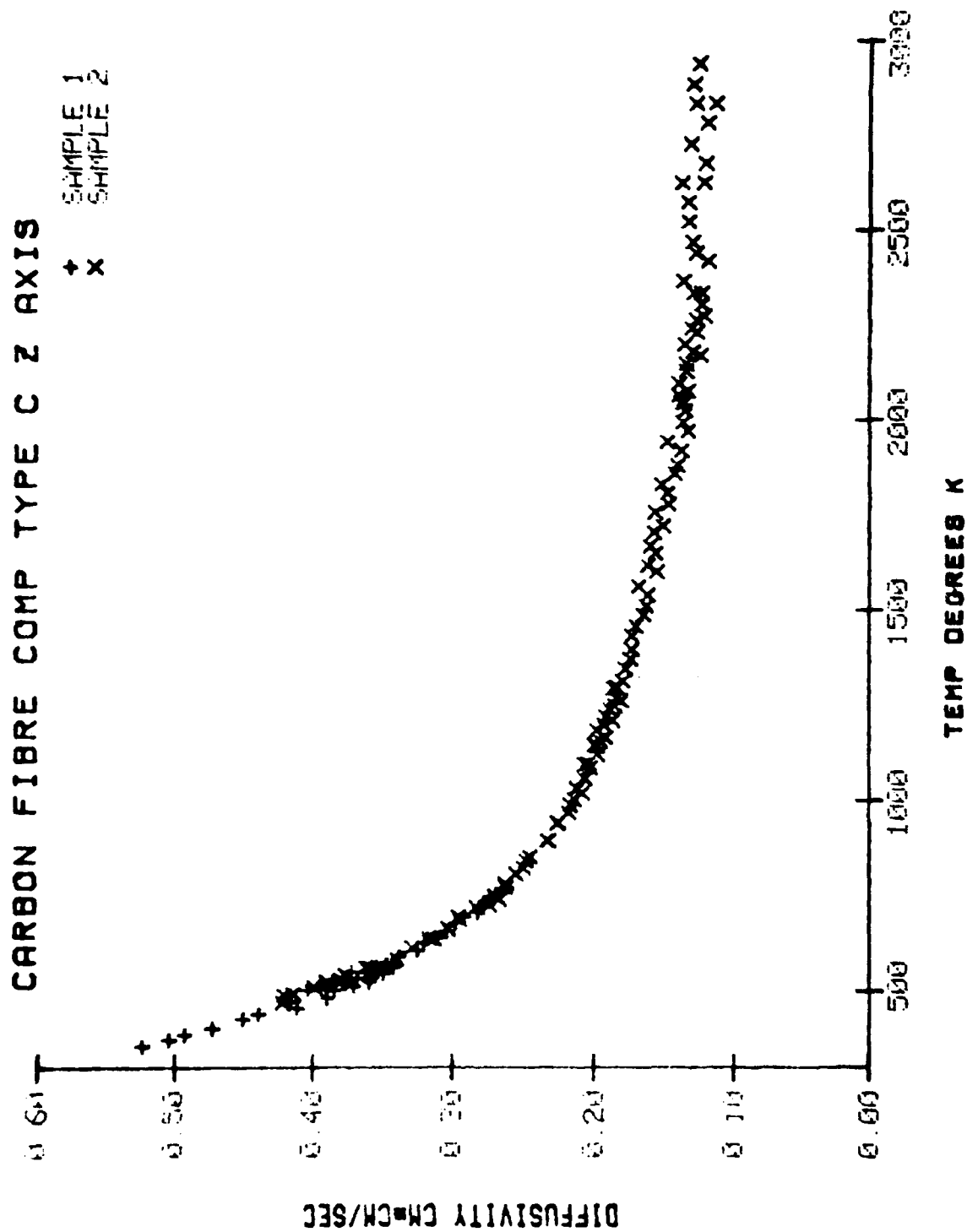


Figure 19

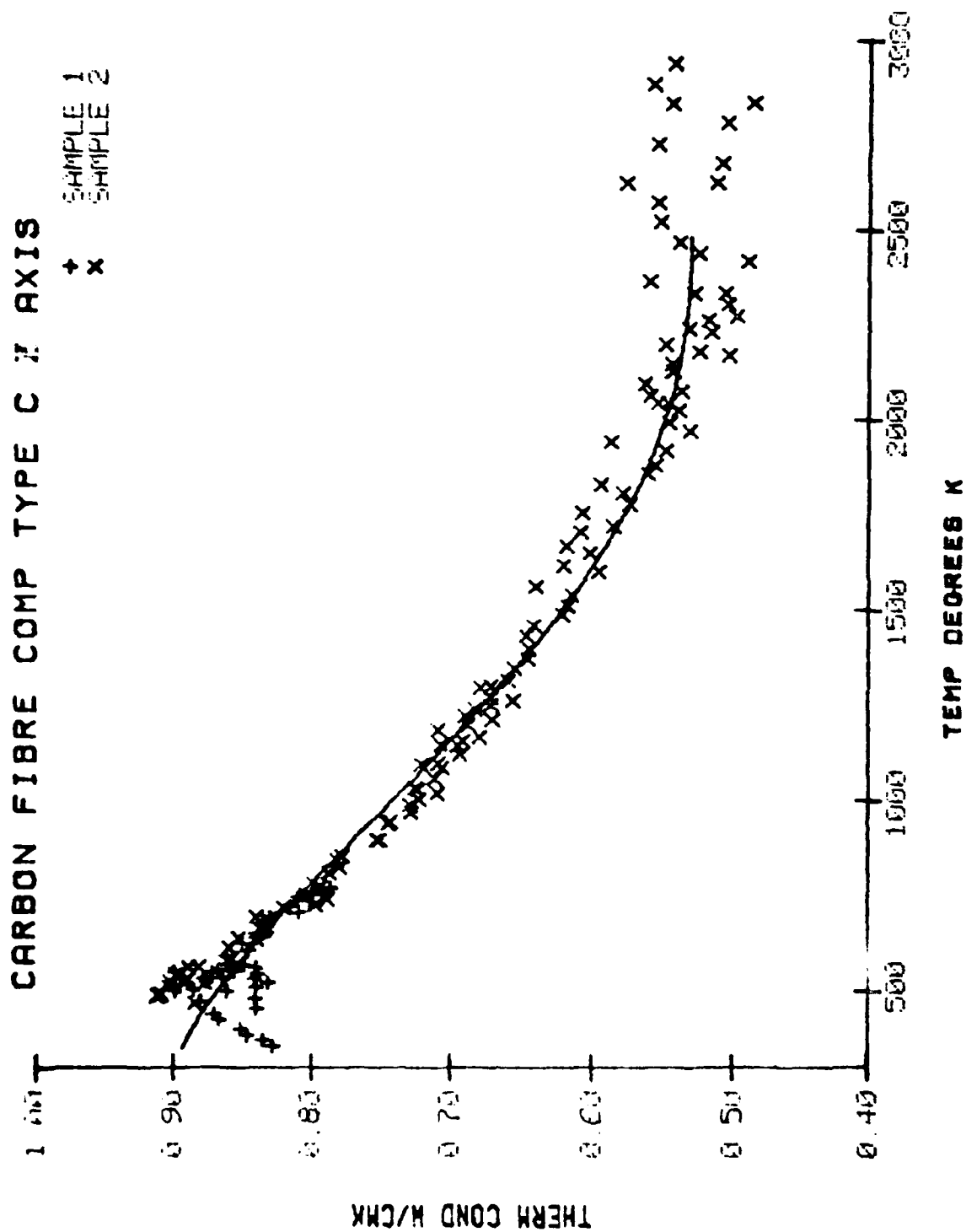


Figure 20

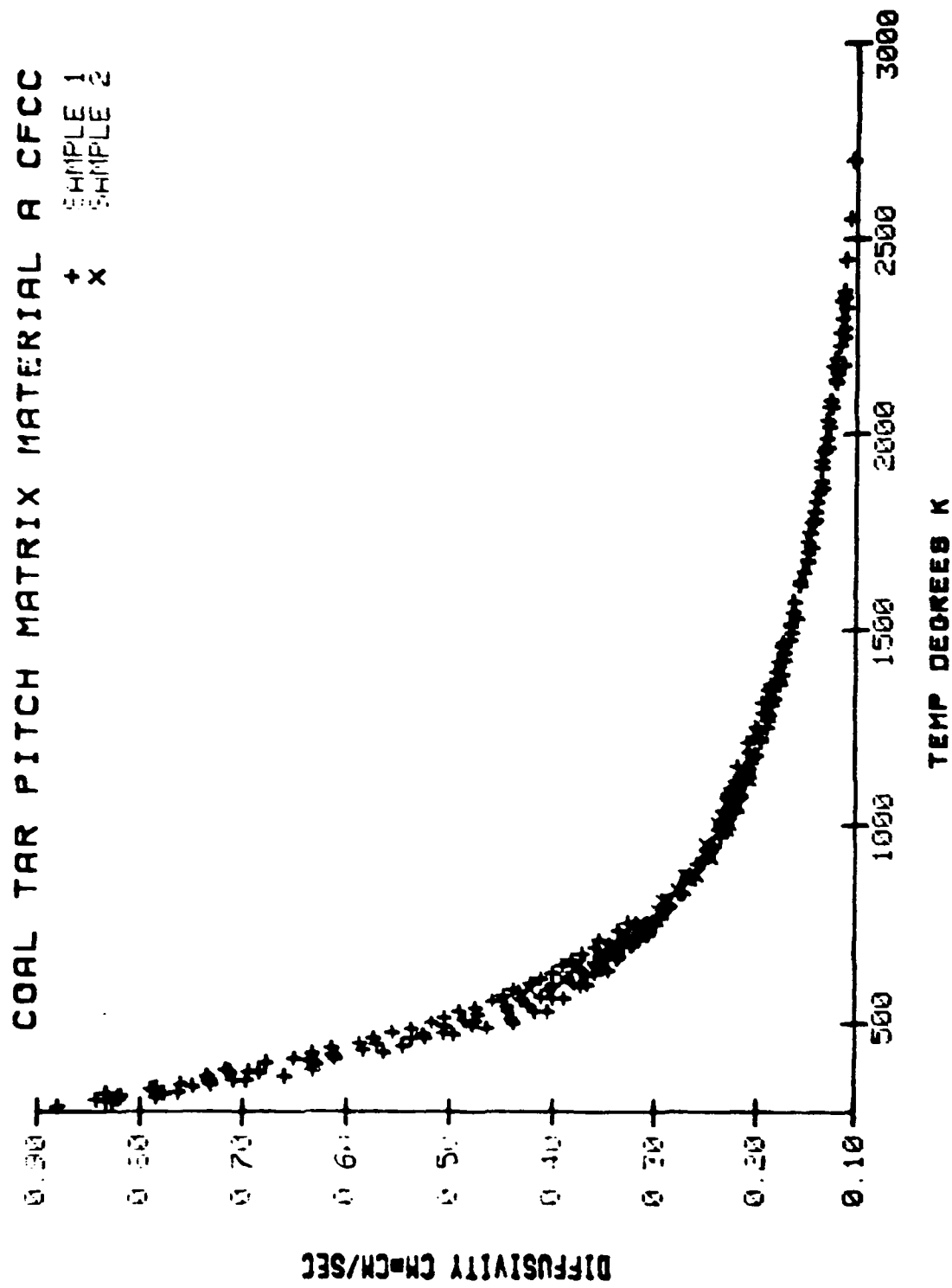


Figure 22

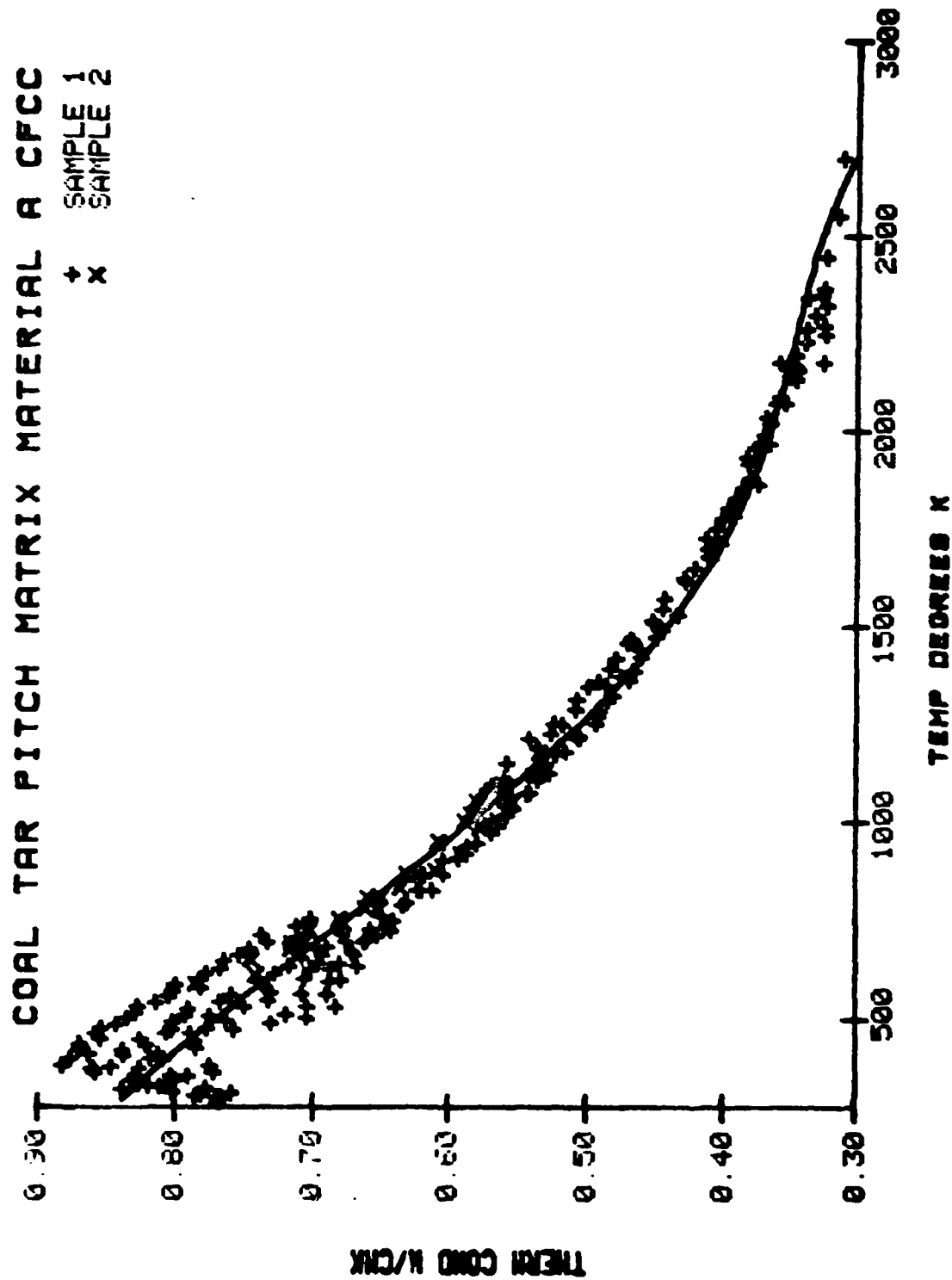


Figure 23

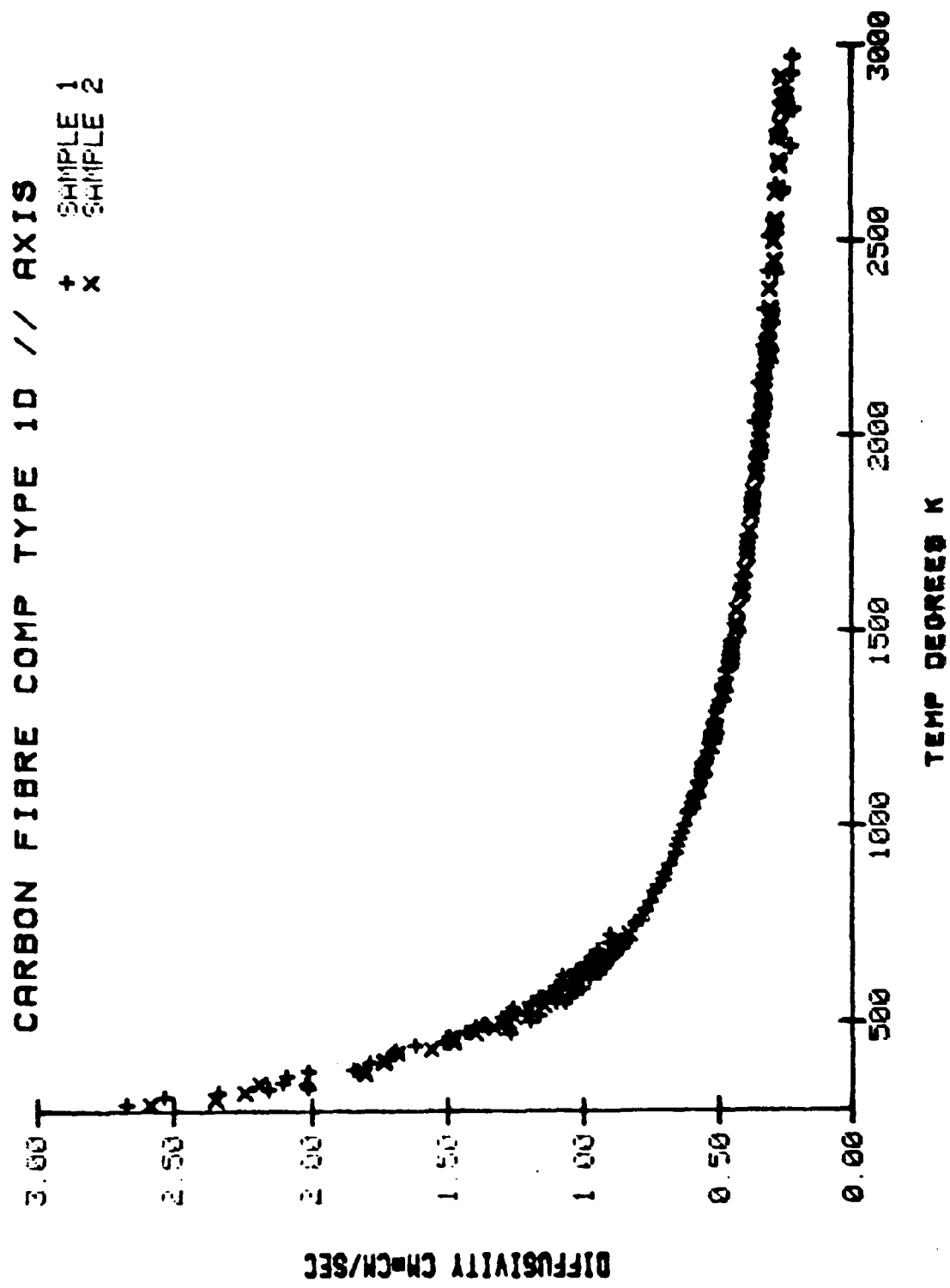


Figure 24

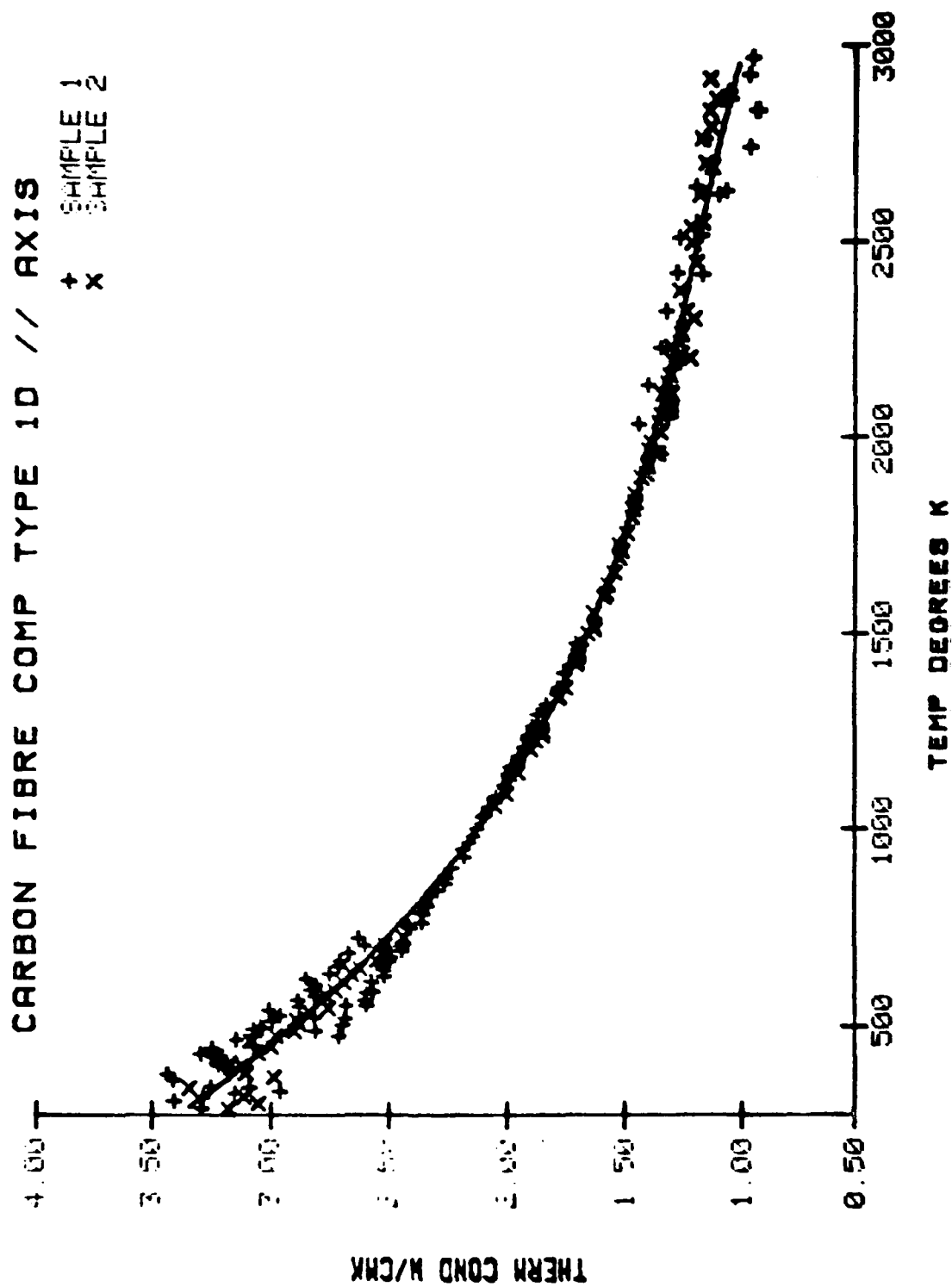


Figure 25

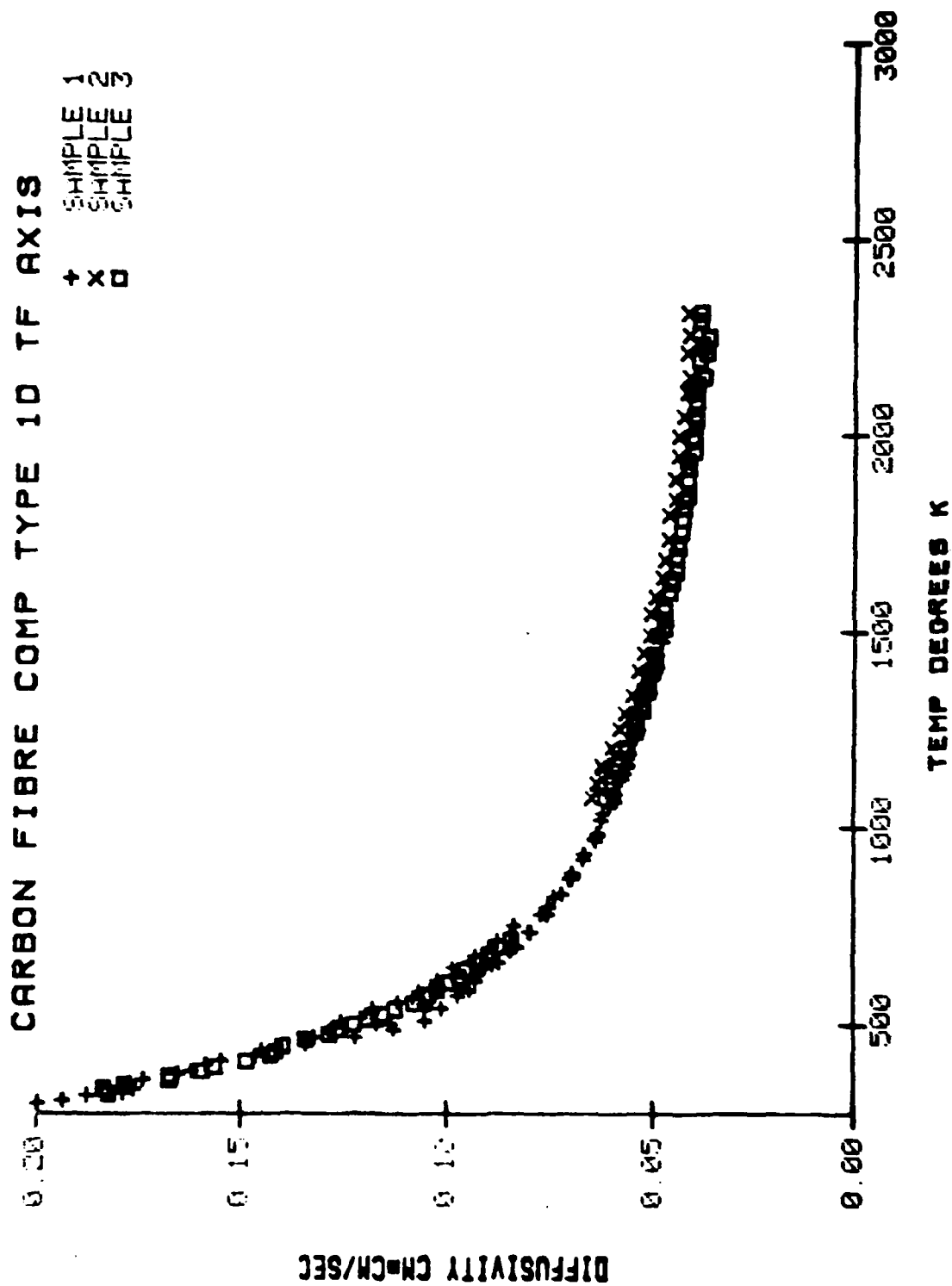


Figure 26

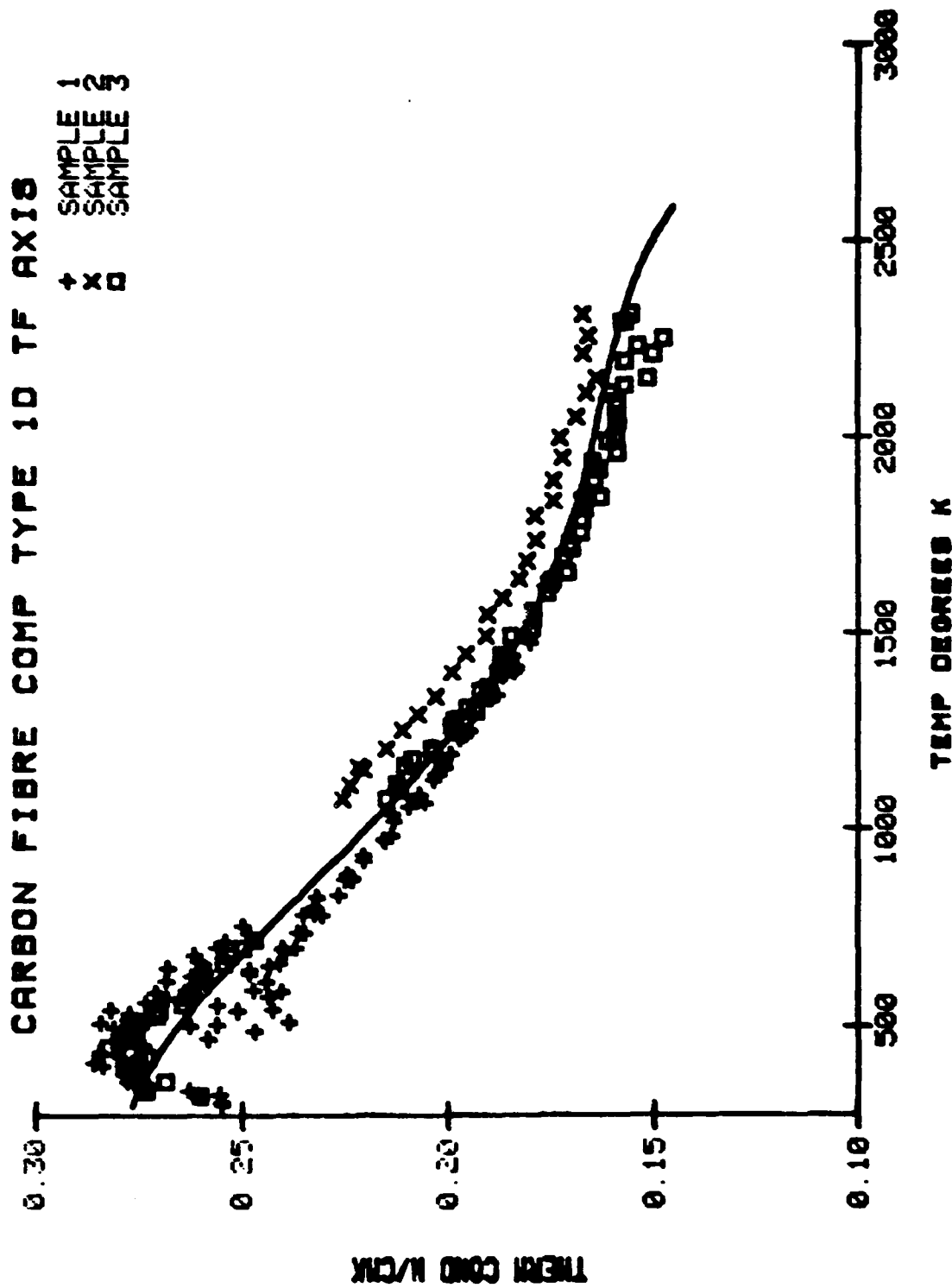


Figure 27

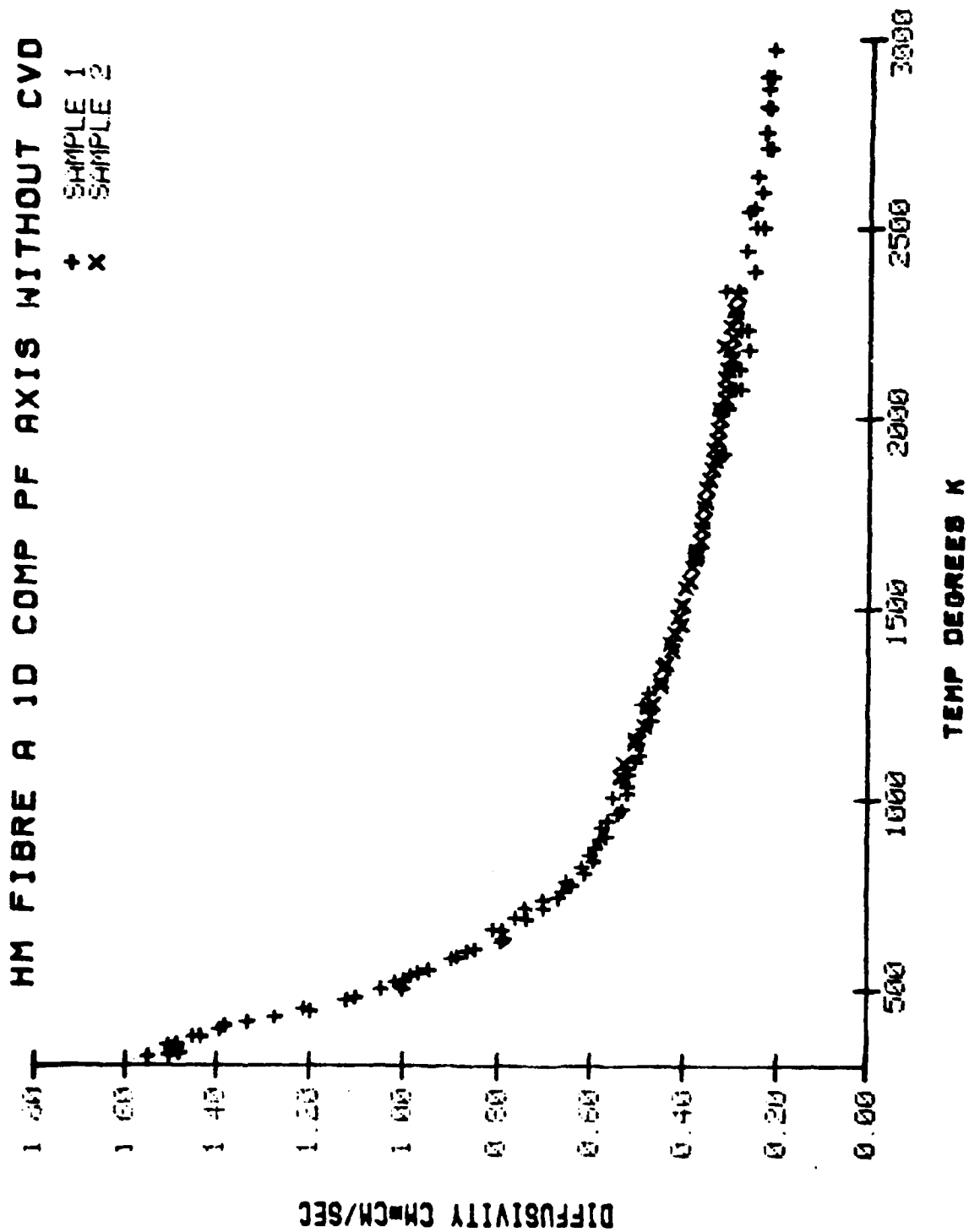


Figure 28

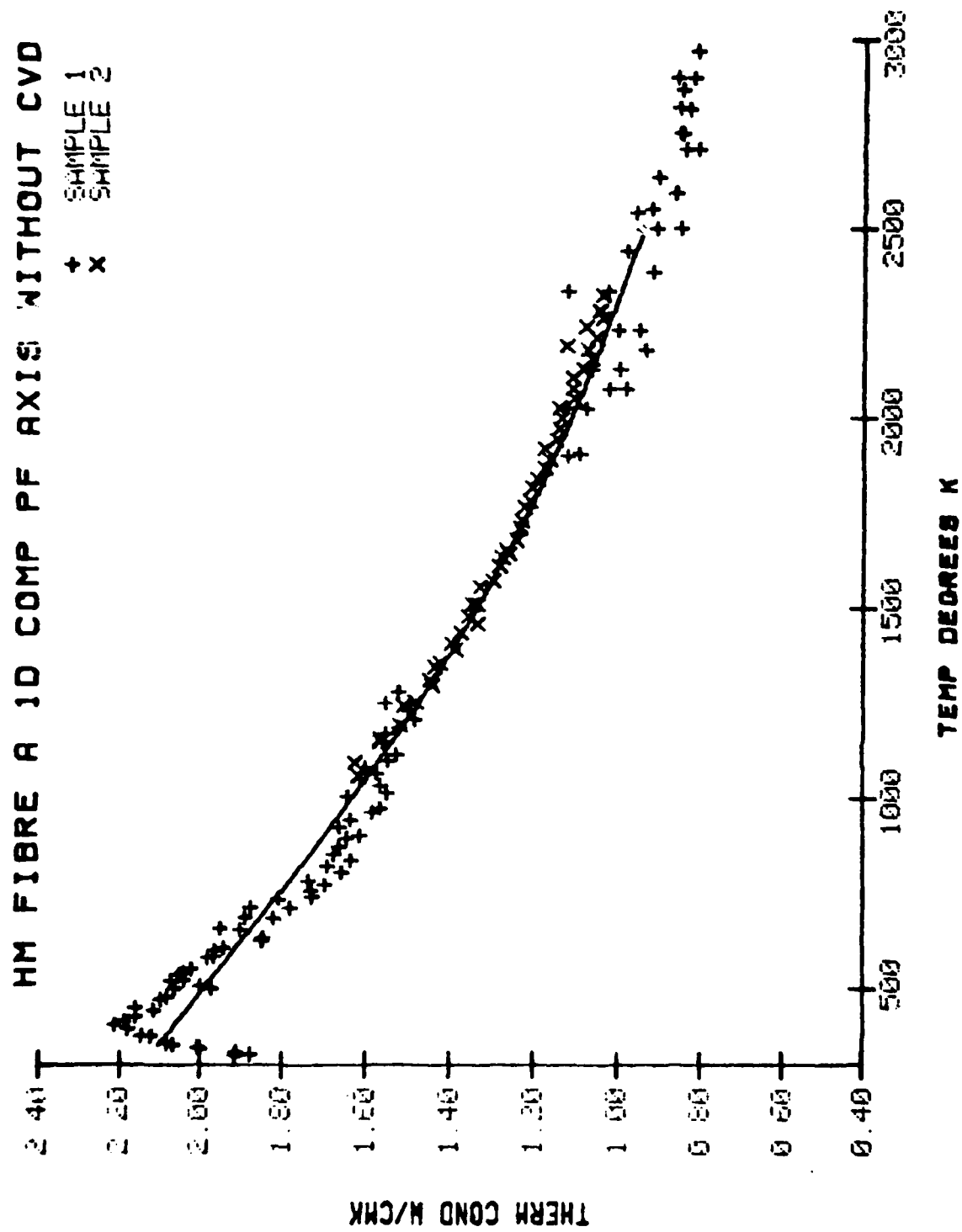


Figure 29

HM FIBRE A 1D COMP TF AXIS WITH OUT CVD

+ SAMPLE 1
 x SAMPLE 2
 □ SAMPLE 3

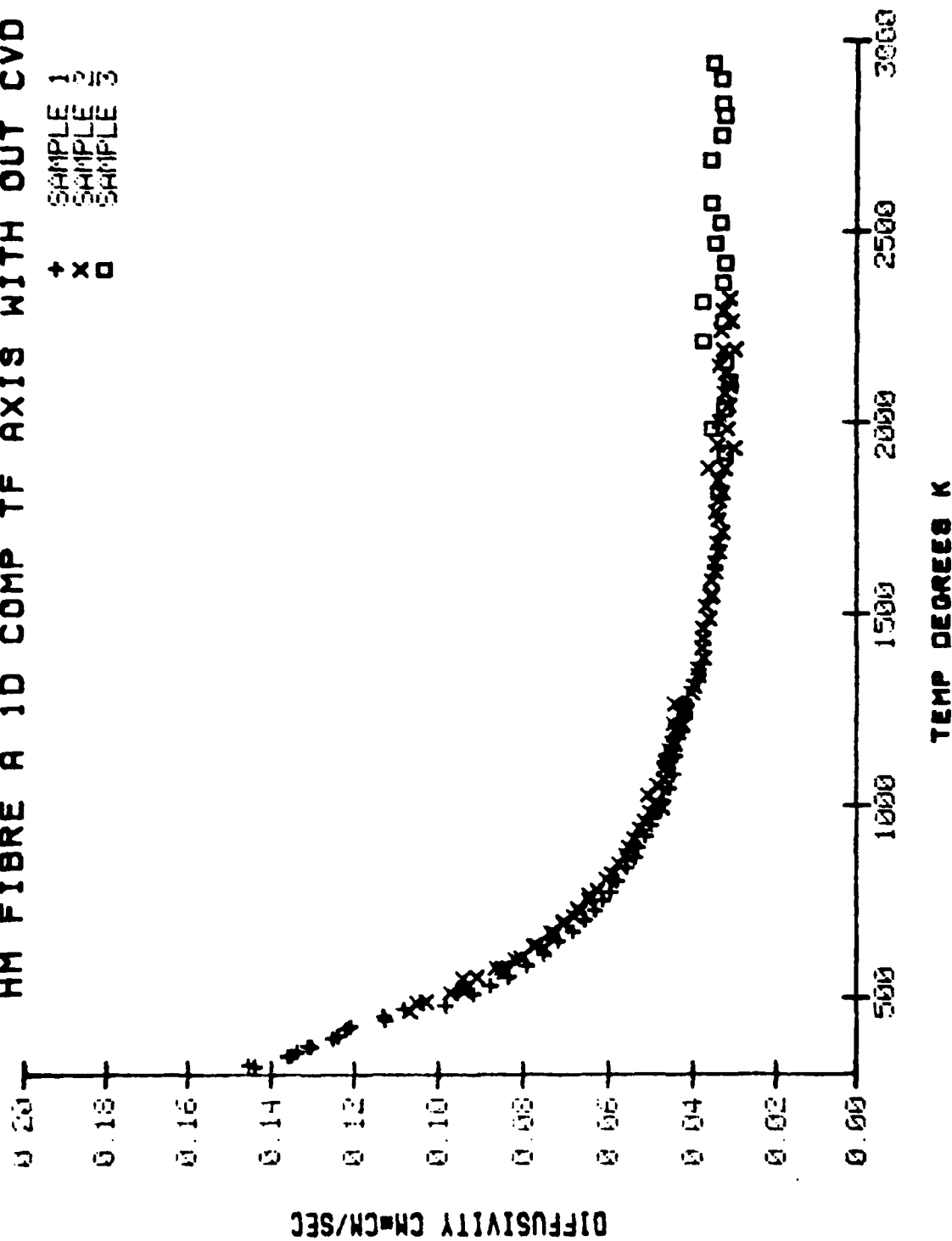


Figure 30

HM FIBRE A 1D COMP TF AXIS WITH OUT CVD

+ SAMPLE 1
 x SAMPLE 2
 o SAMPLE 3

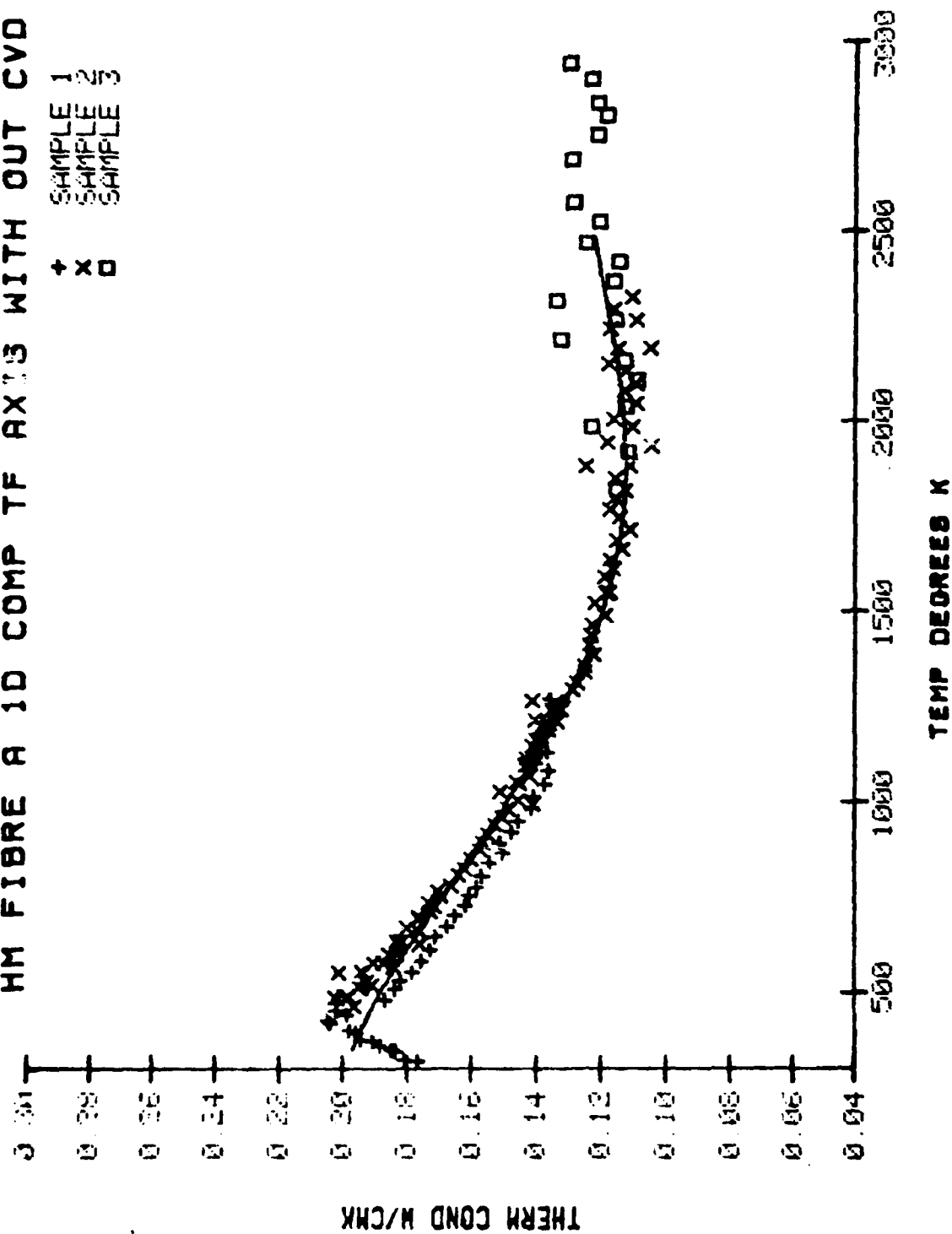


Figure 31

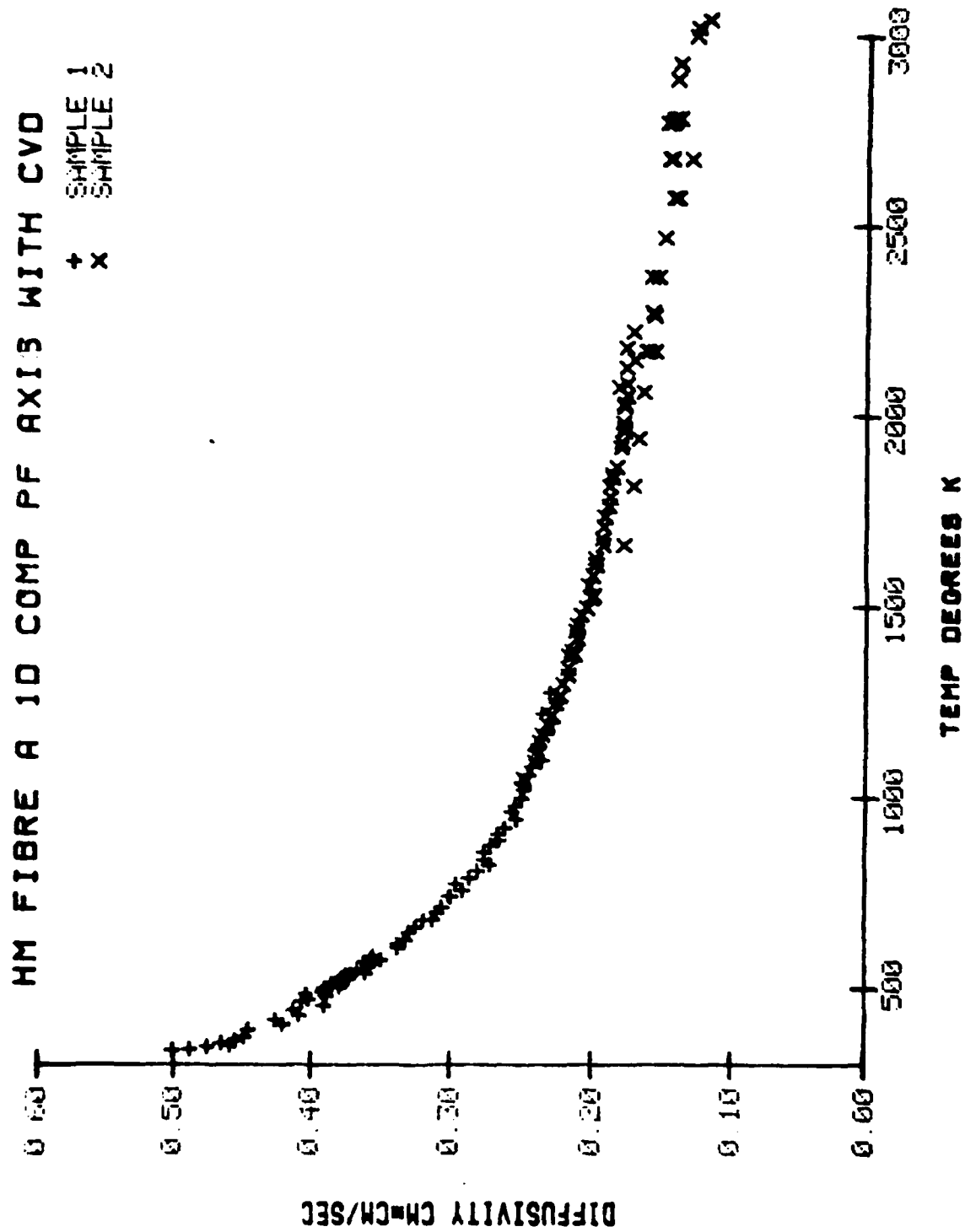


Figure 32

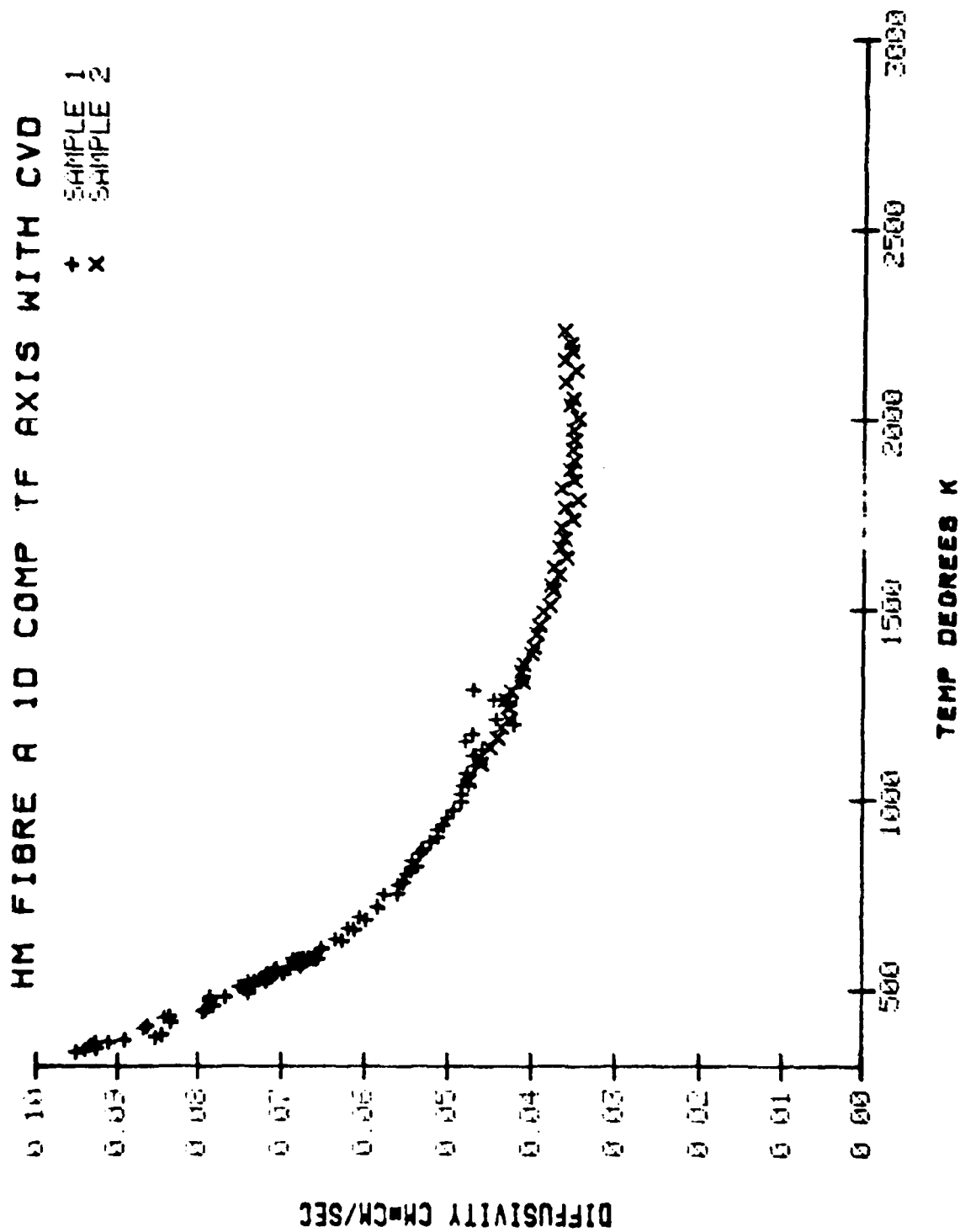
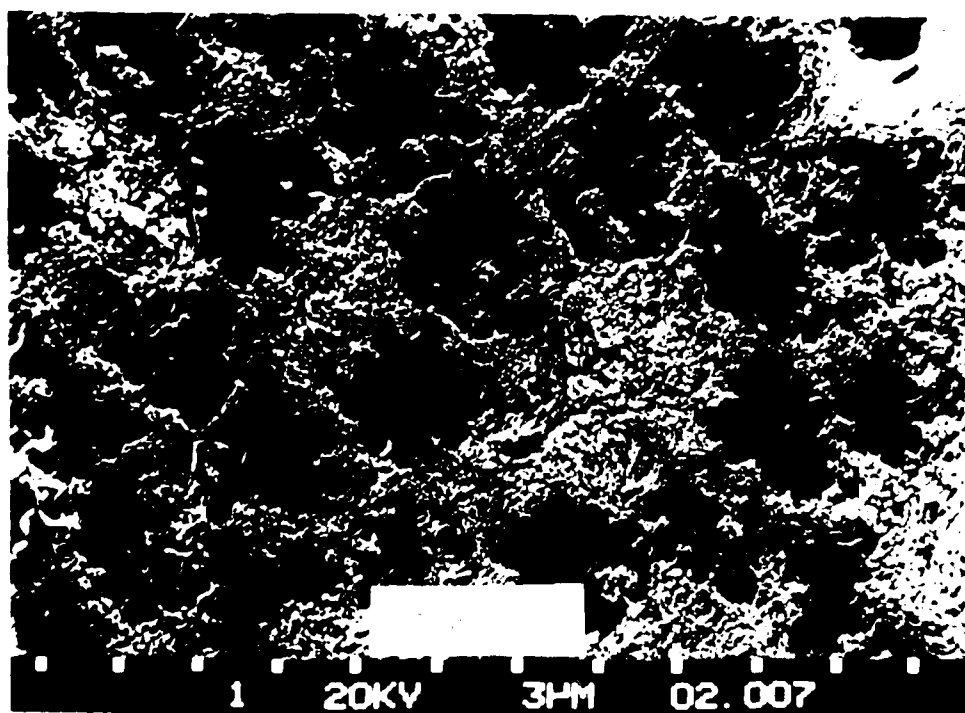
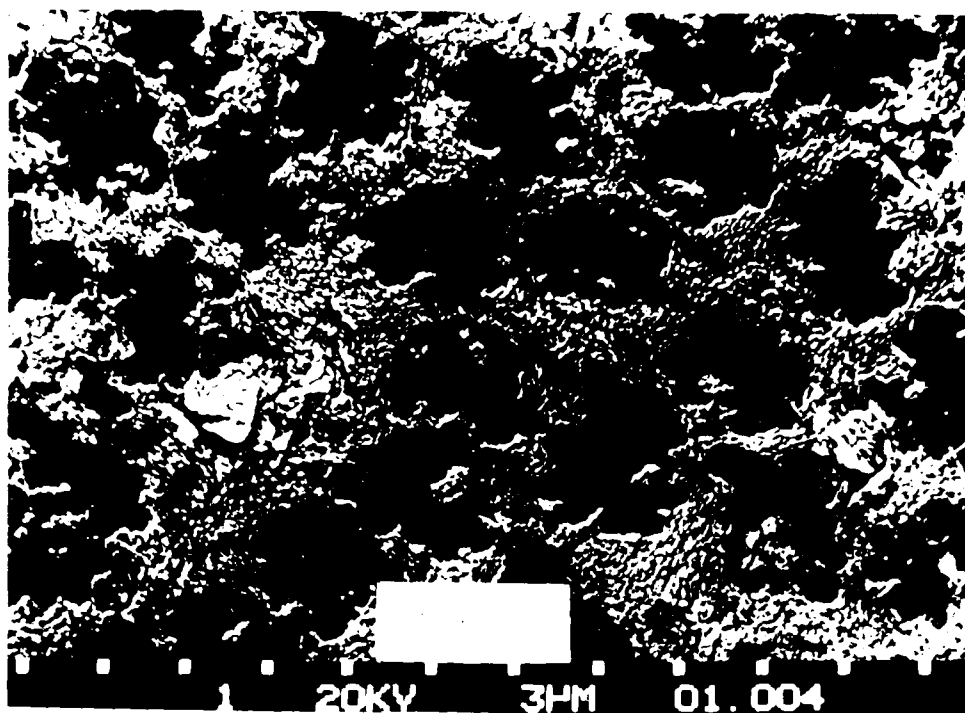
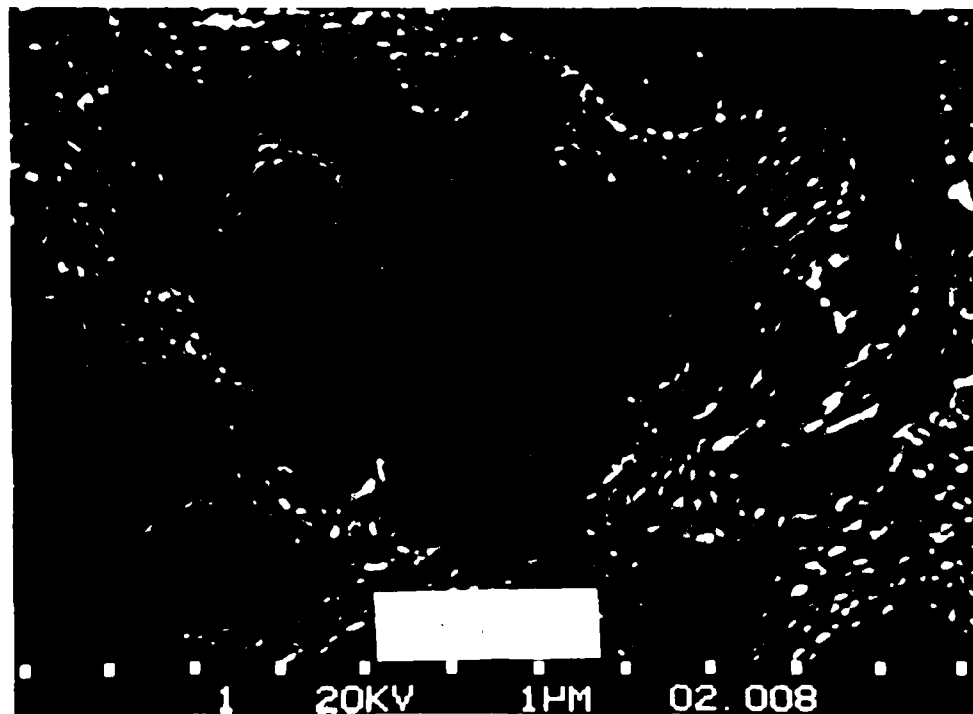
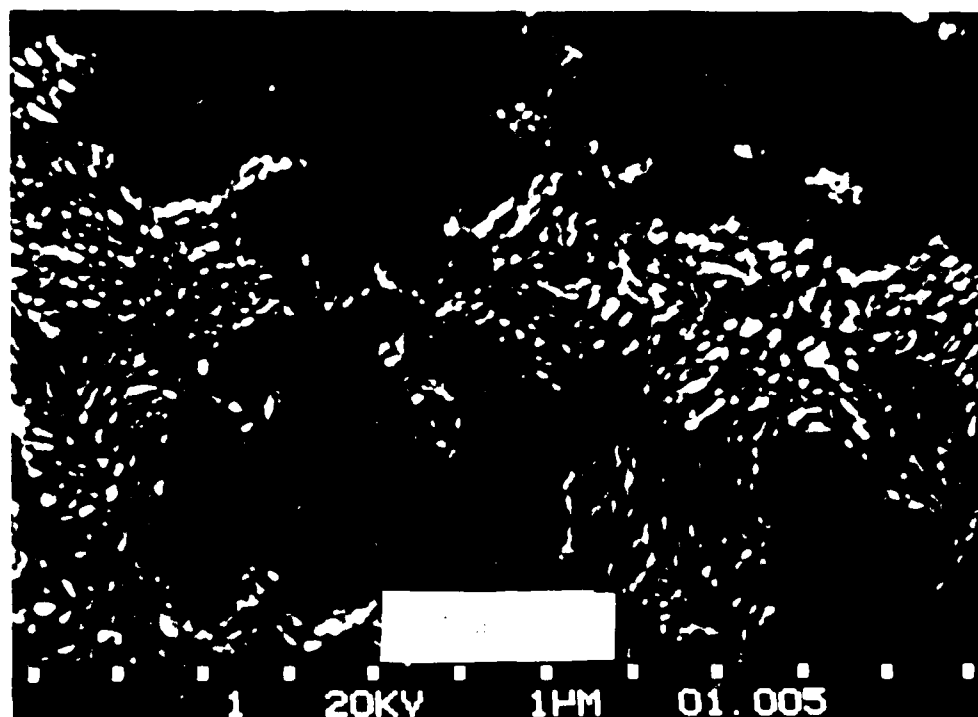
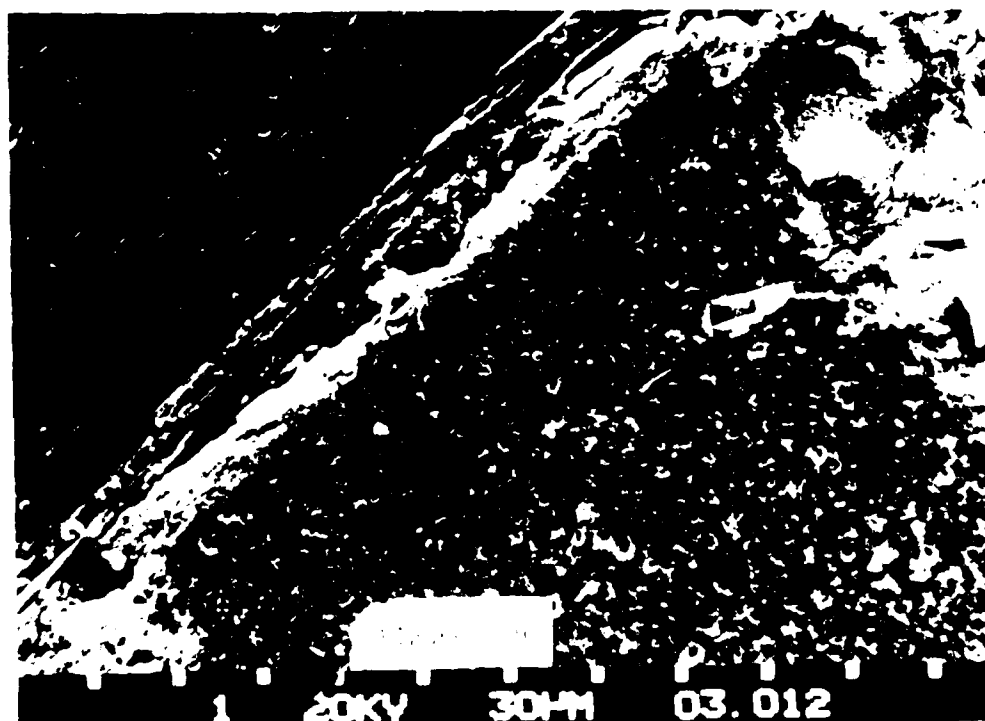
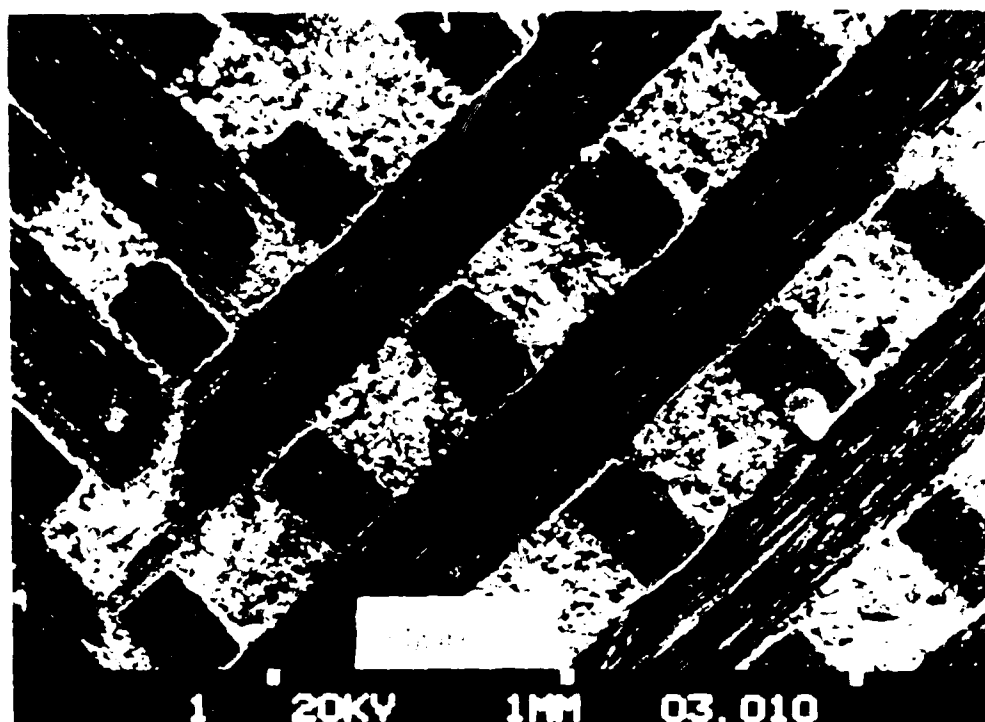


Figure 33







AD-A102 994

MANCHESTER UNIV/UNIV OF MANCHESTER INST OF SCIENCE AN--ETC F/8 11/4
MEASUREMENT OF THE THERMAL DIFFUSIVITY OF CARBON/CARBON FIBRE C--ETC(U)
JAN 81 R TAYLOR, R N PROCTER AFOSR-77-3449

UNCLASSIFIED

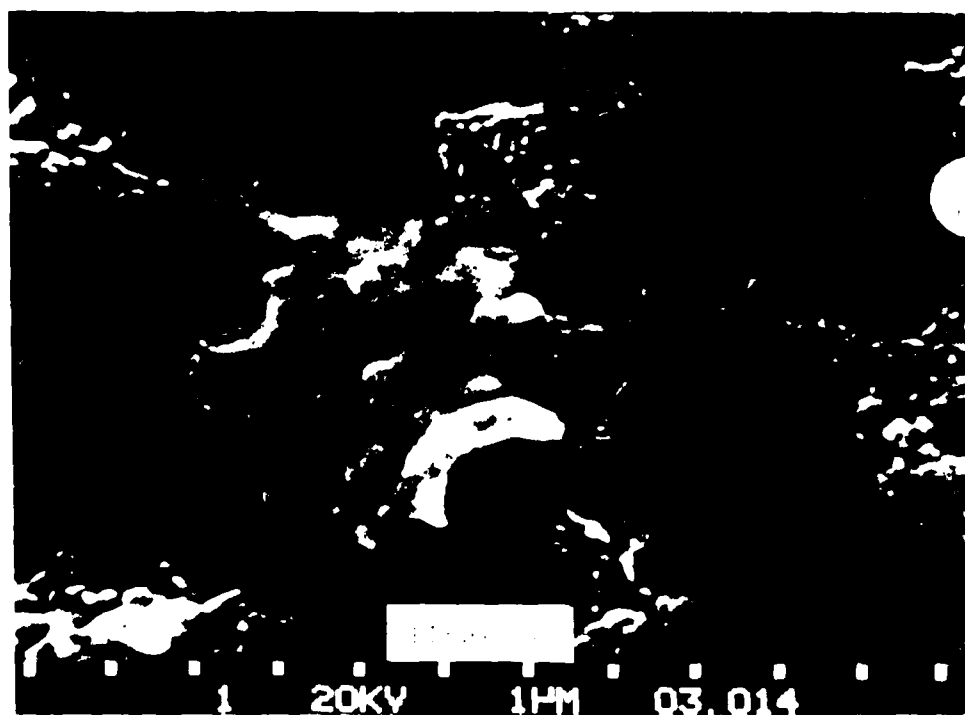
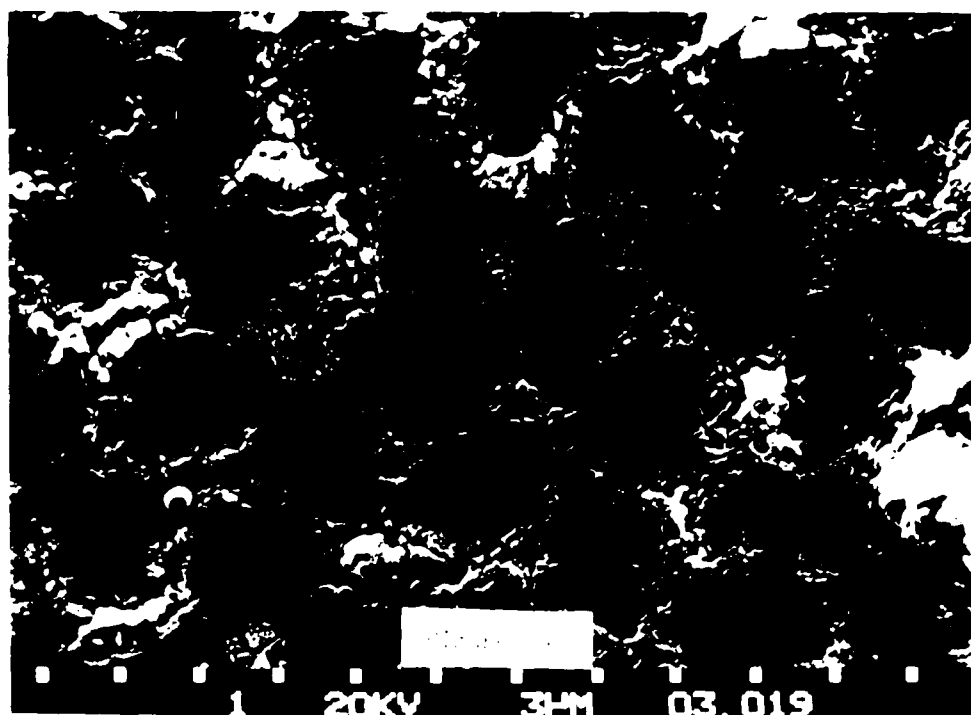
AFOSR-TR-81-0638

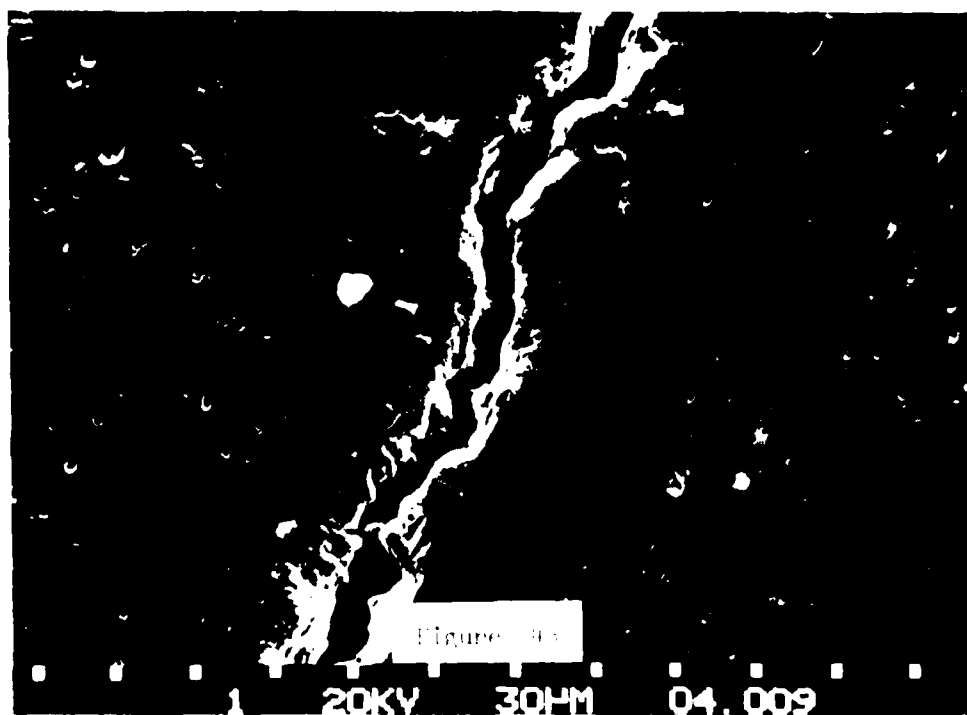
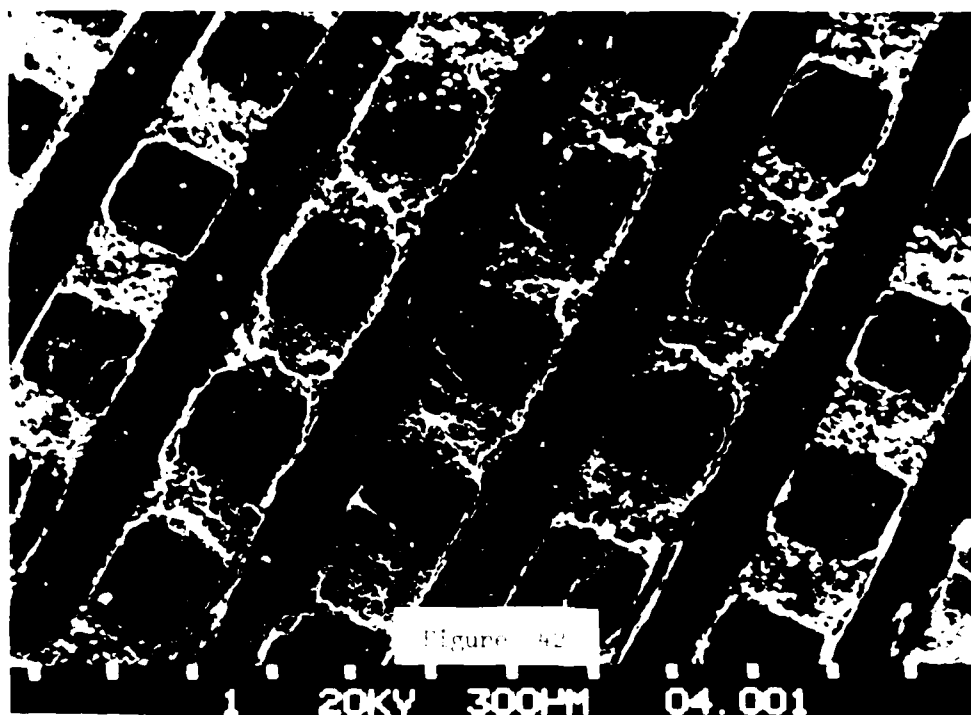
NL

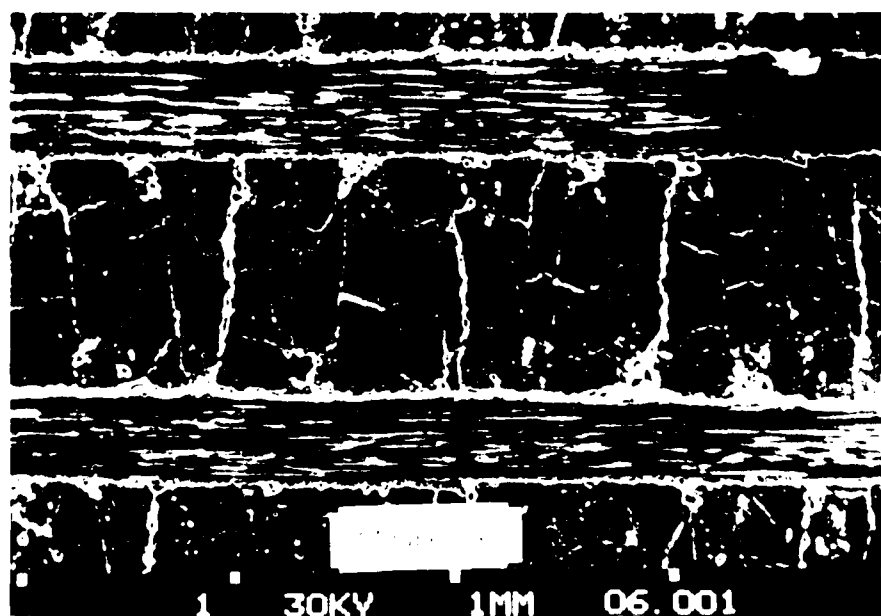
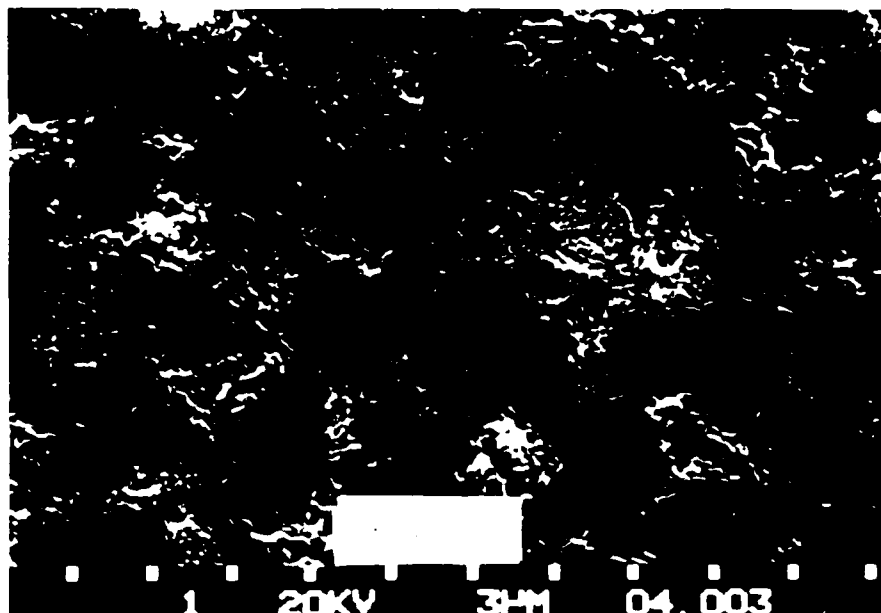
2 of 2
2 DEC 1981

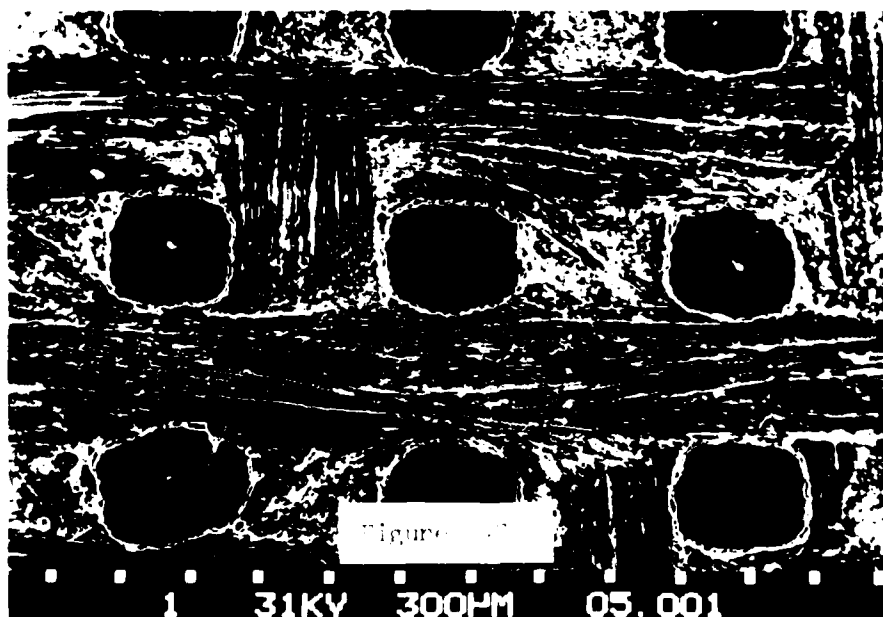
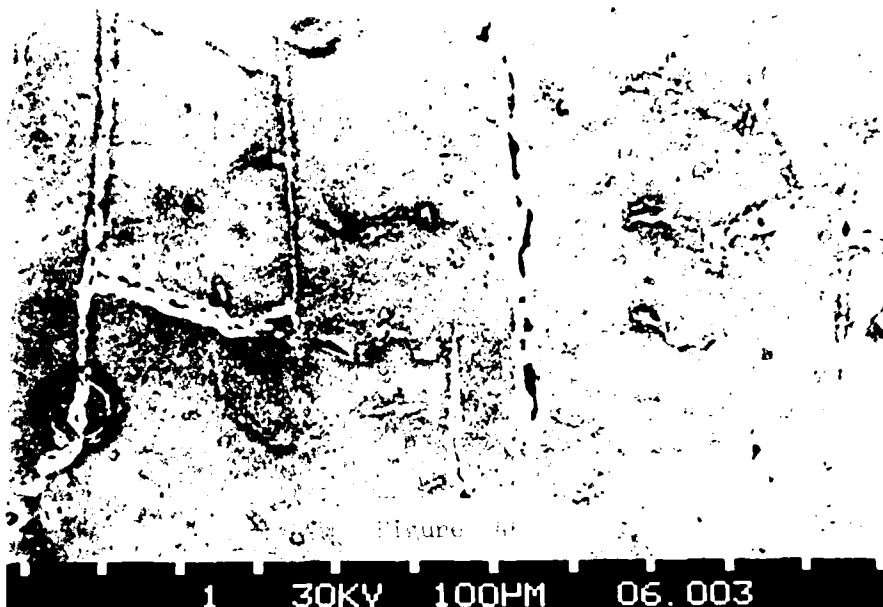


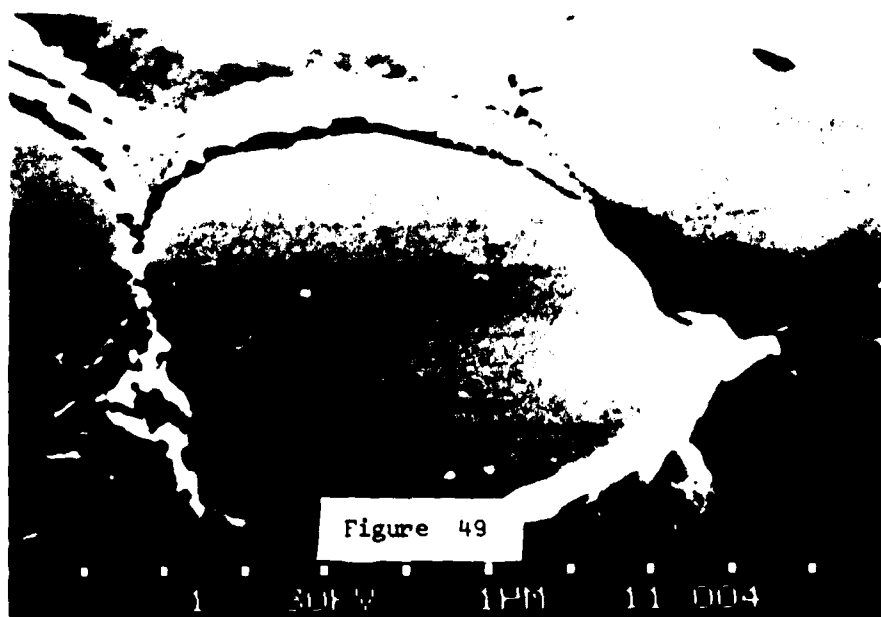
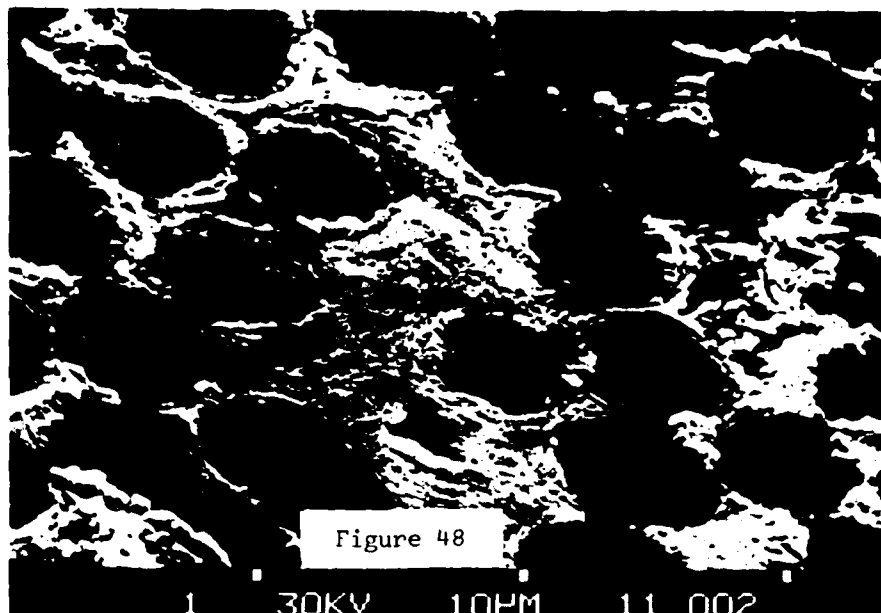
END
DATE
FILMED
9-81
DTIC

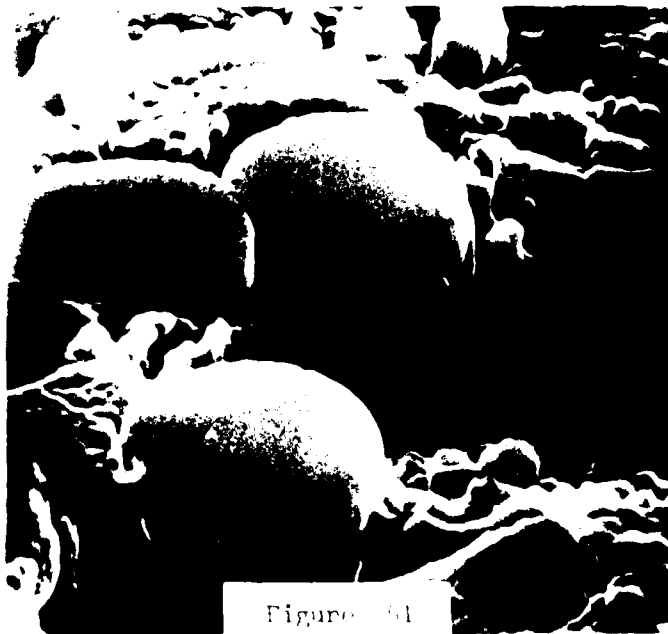
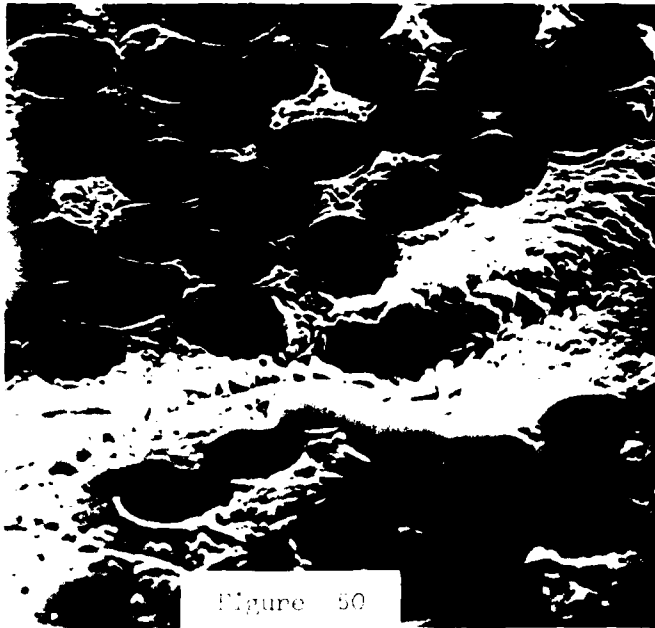












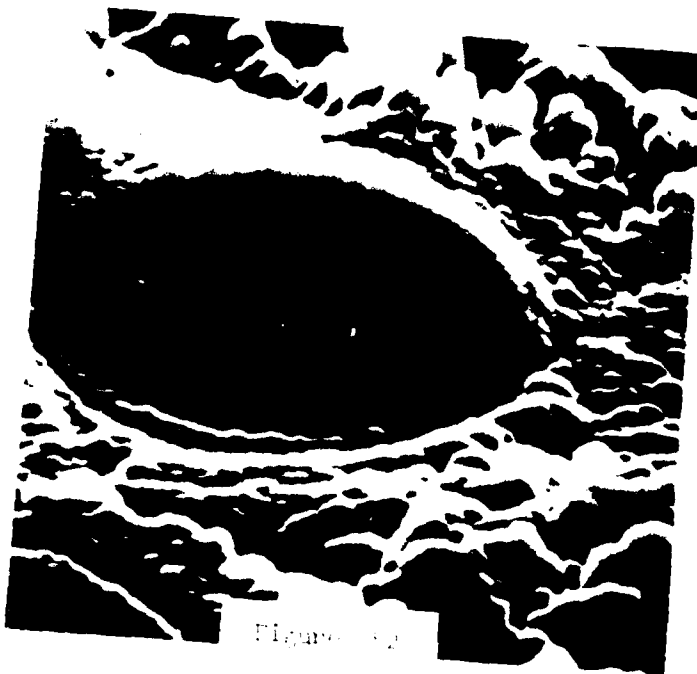
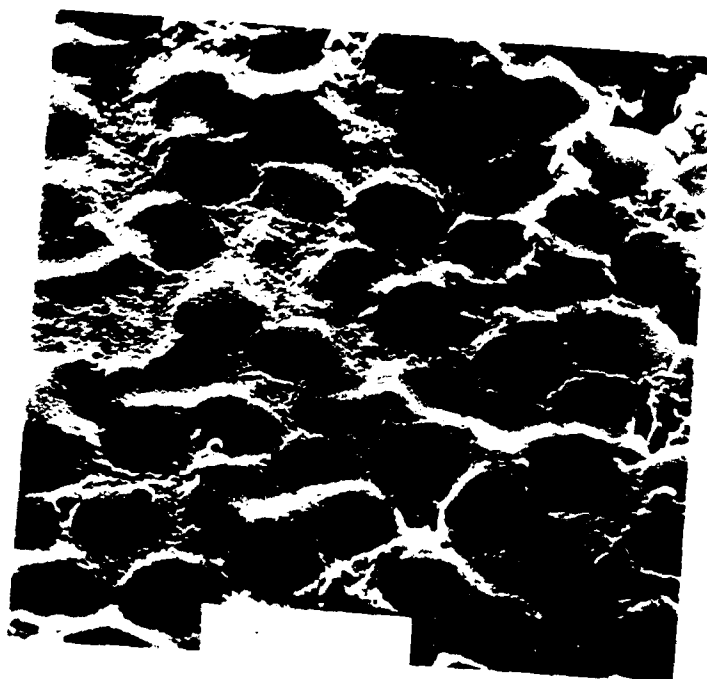
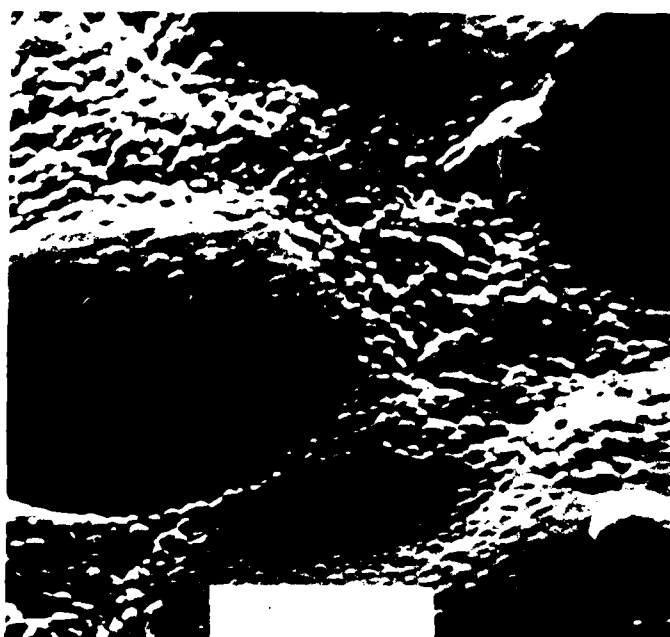
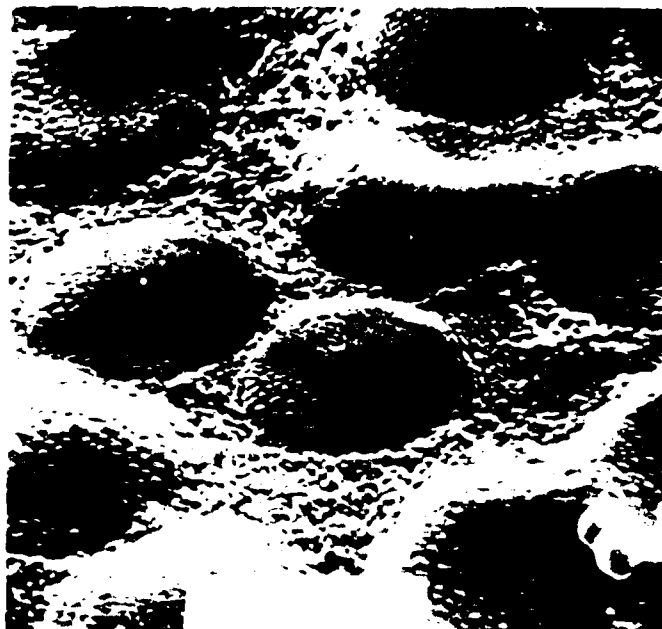
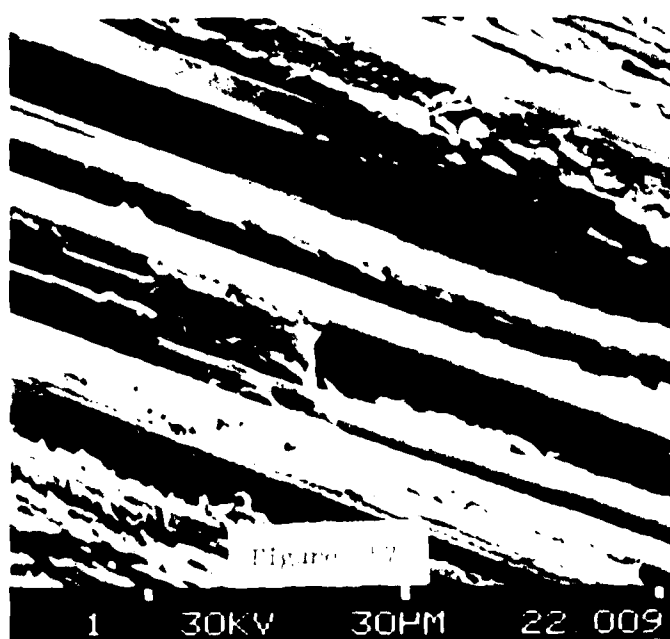
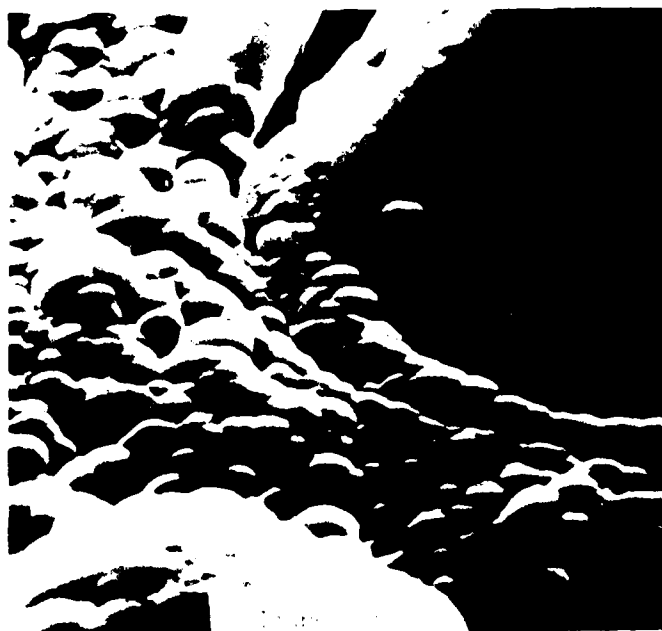
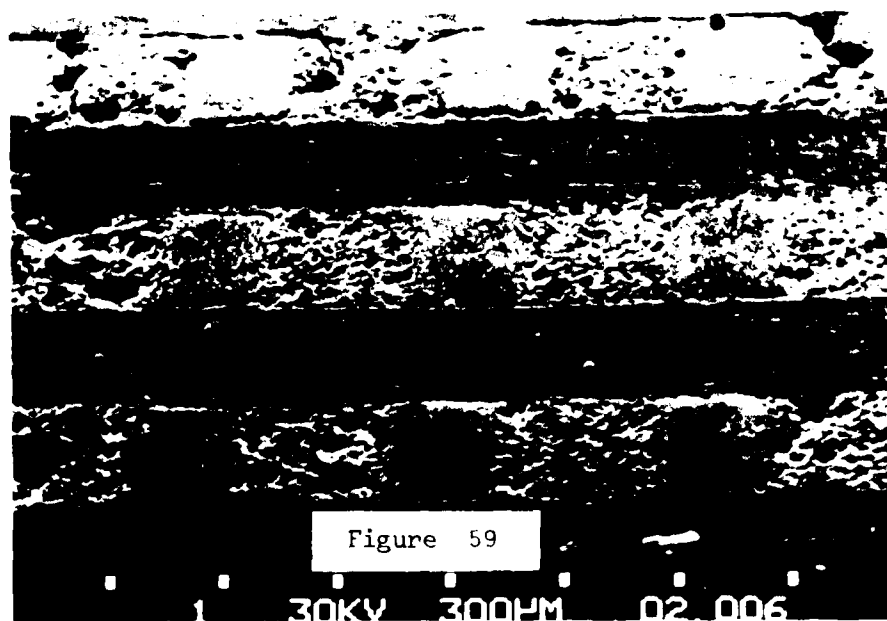
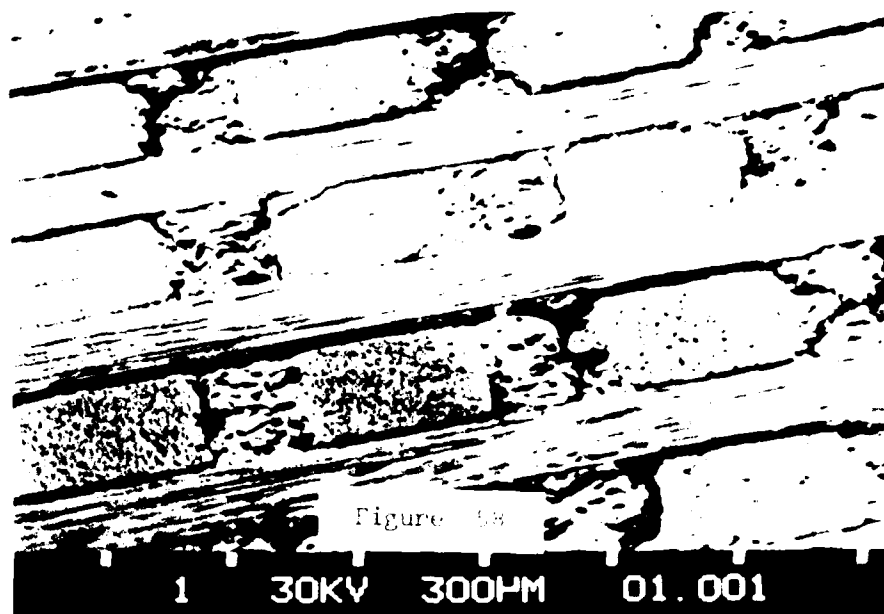


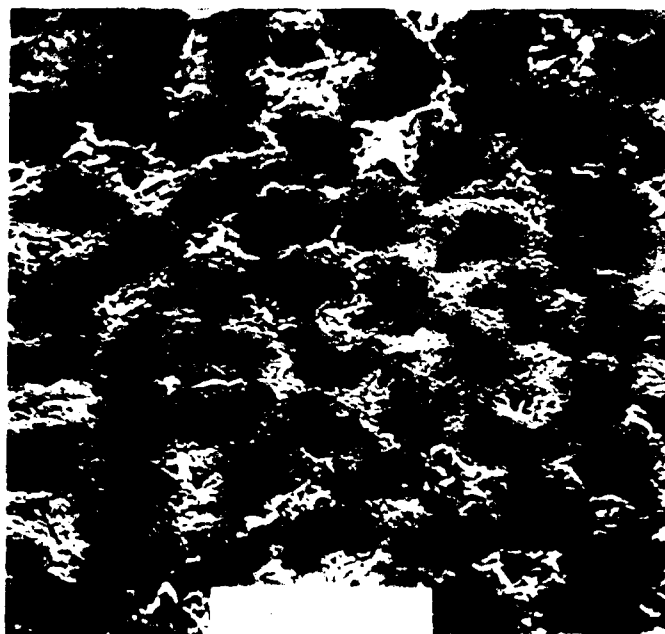
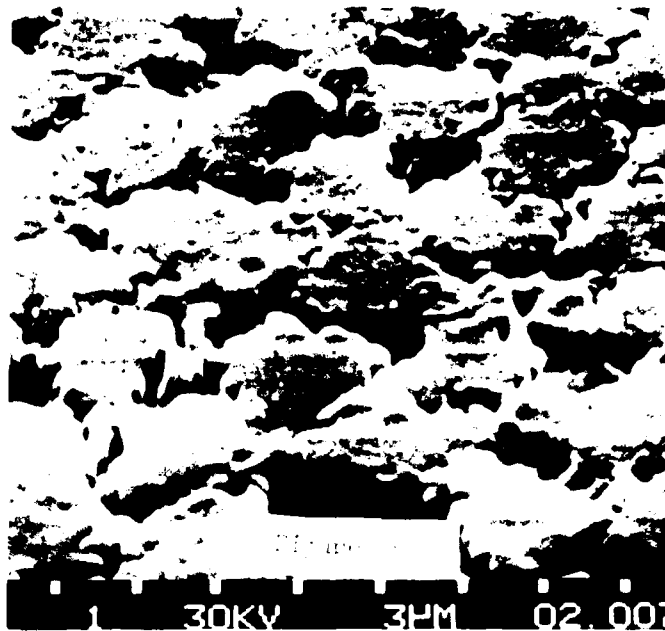
Figure 12

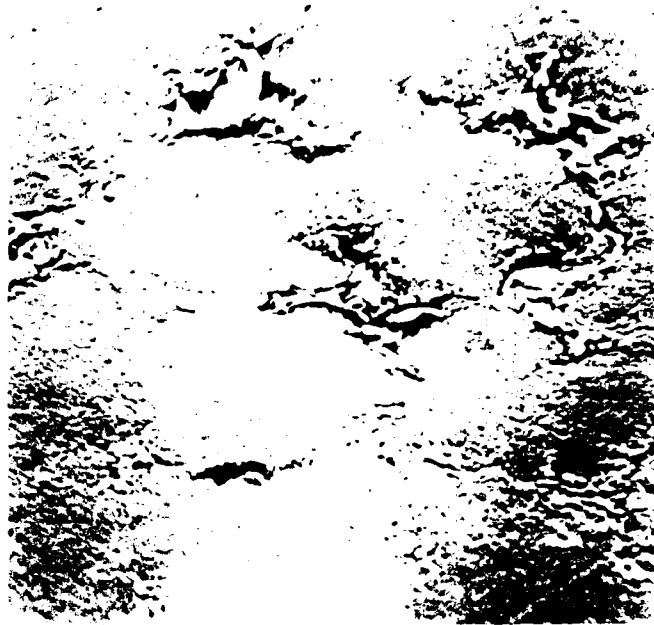


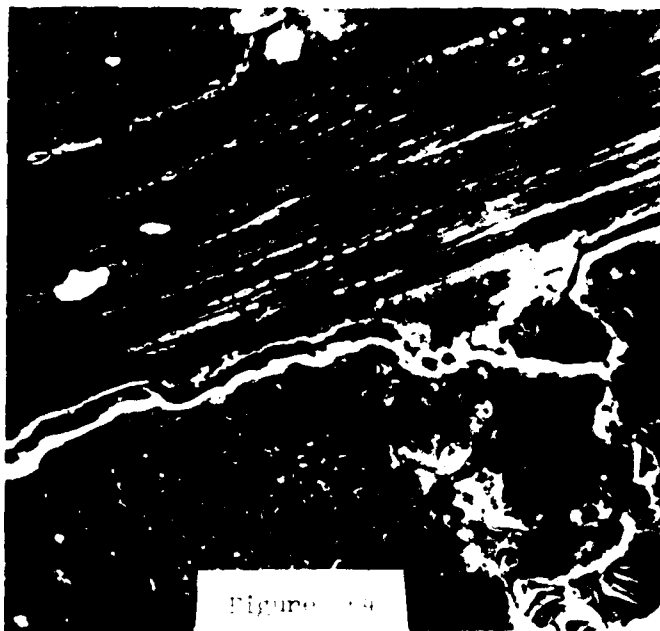












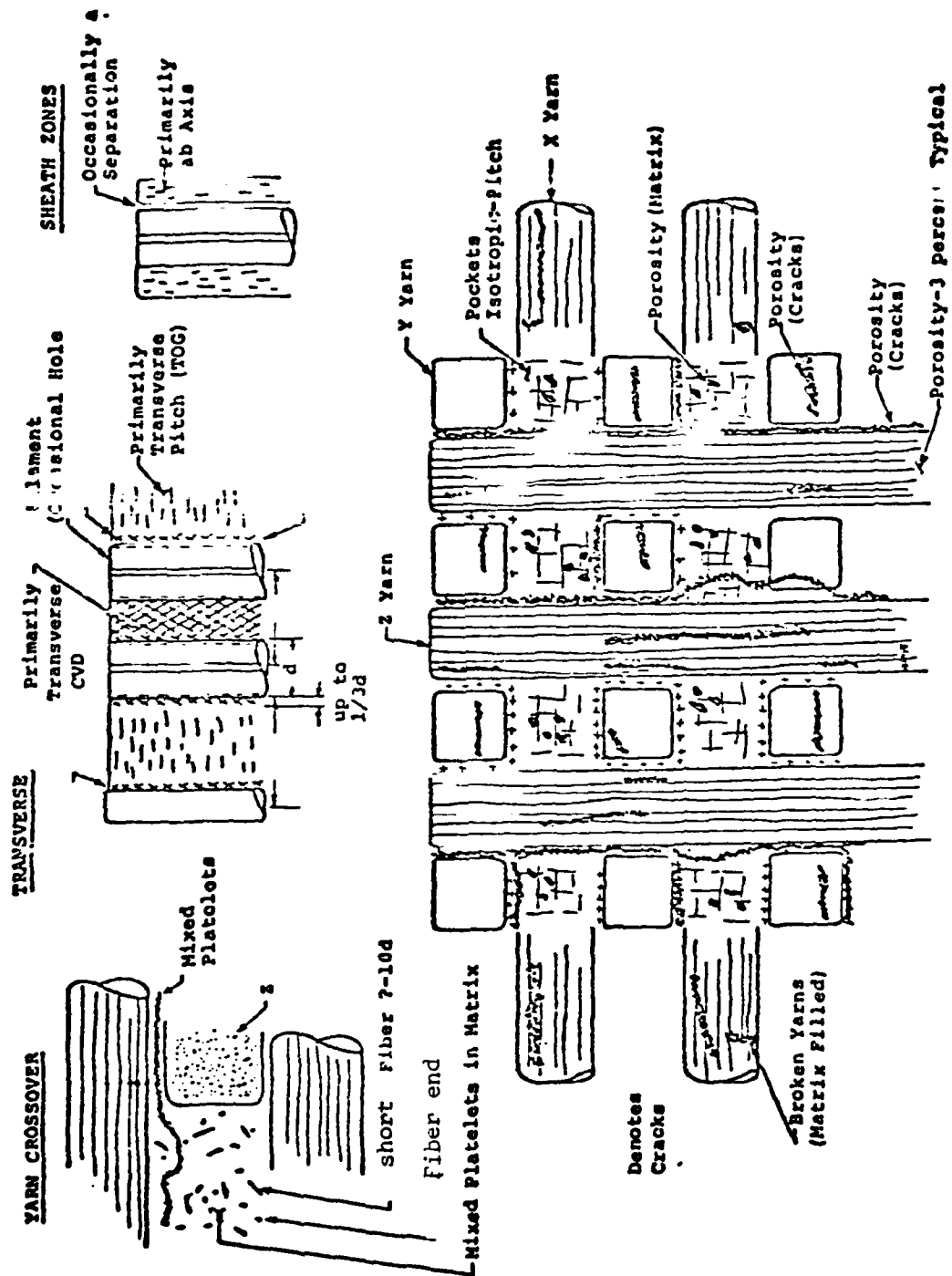


Figure 65. Schematic of the Typical Structure of composite "A" after AFML-TR-77-26)

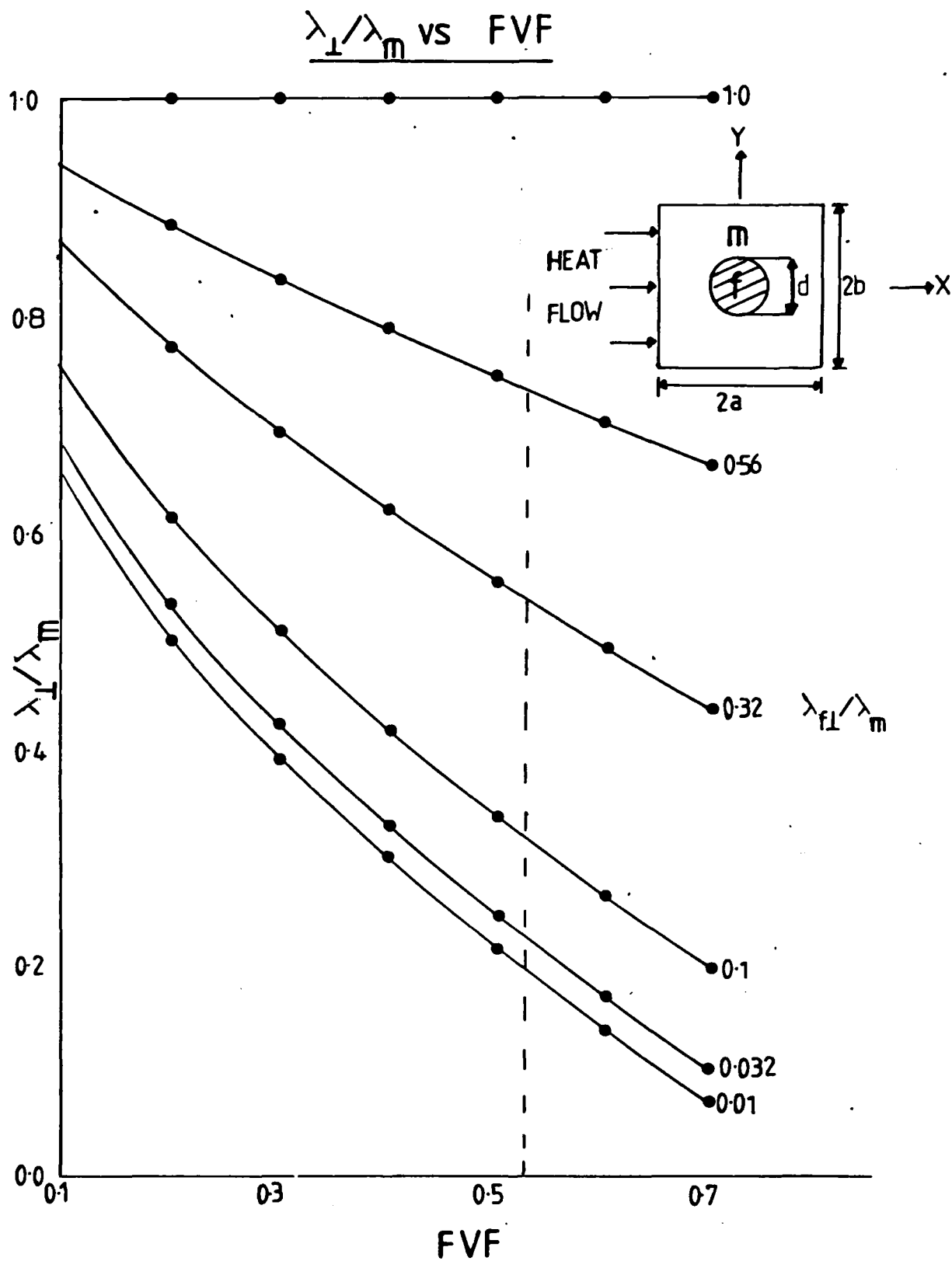


Figure 66

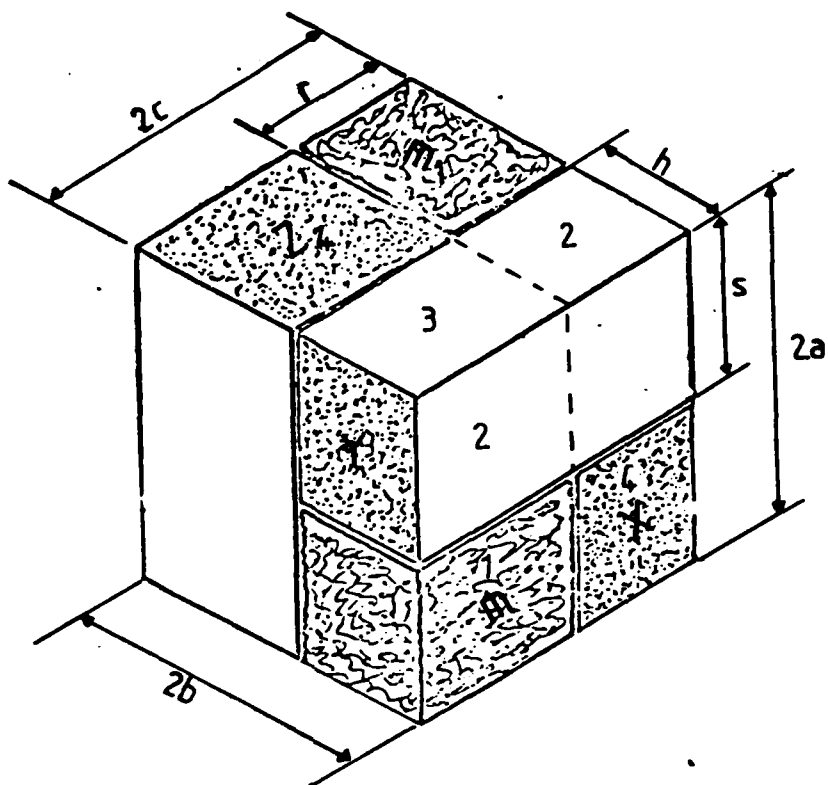


Figure 67

END

DATE
FILMED

9-81

DTIC